

2 mup

X-661-74-130

PREPRINT

NASA X-70673

# PROCEEDINGS OF THE WORKSHOP ON ELECTRON CONTAMINATION IN X-RAY ASTRONOMY EXPERIMENTS

STEPHEN S. HOLT

(NASA-TM-X-70673)	PROCESSINGS OF THE	N74-28246
WORKSHOP ON ELECTRON CONTAMINATION IN 179	X-RAY ASTRONOMY EXPERIMENTS (NASA)	THRU
HC \$11.50	468 p	N74-28257
	CSSL 03A	Unclas
		41596

G3/29

MAY 1974



**GODDARD SPACE FLIGHT CENTER**  
**GREENBELT, MARYLAND**

**For information concerning availability  
of this document contact:**

**Technical Information Division, Code 250  
Goddard Space Flight Center  
Greenbelt, Maryland 20771**

**(Telephone 301-982-4488)**

N74-2829

Proceedings of the Workshop  
on Electron Contamination in  
X-Ray Astronomy Experiments

26 April 1974

Edited by  
Stephen S. Holt

## Forward

A working group of interested x-ray astronomy experimenters was assembled at NASA headquarters on 26 April 1974 to discuss the problem of particle contamination of x-ray astronomical data. Present, as well, were two auroral particle experimenters (R. A. Hoffman and J. D. Winningham), who were kind enough to support the working group with their data and insights.

The text of this document represents the material discussed in the working group by those in attendance, in the form of informal unedited manuscripts. In addition, papers were thoughtfully submitted by several colleagues who could not attend the meeting.

Special thanks are due A. Opp for the conception of this working group, F. Seward for the pioneering investigation of this problem, and T. J. Rosenberg for a manuscript to complement the particle data present at the meeting.

Attendees

E. Boldt	NASA-GSFC
T. Chubb	NRL
C. J. Crannell	MIT
P. J. N. Davison	MSSL
R. Doxsey	MIT
R. Hill	LLL
R. A. Hoffman	NASA-GSFC
S. S. Holt	NASA-GSFC
H. Kestenbaum	Columbia U.
A. Levine	MIT
S. Naranan	NRL
A. Opp	NASA Hq.
T. Palmieri	LLL
J. Rosendhal	NASA Hq.
R. Rothschild	NASA-GSFC
E. Schreier	SAO/HCO
D. Schwartz	SAO/HCO
S. Shulman	NRL
F. Seward	LLL
J. D. Winningham	U. T. Dallas
D. Venkatesan	U. Calgary

## Contents

As the manuscripts received have not been retyped for this compendium, there is no overall page numbering or uniformity of style. To aid the reader in locating specific material, an off-colored title page precedes each manuscript. The contents have been ordered as follows:

1. Electrons at Low Altitudes: A Difficult Problem for Soft X-Ray Astronomy.....F. D. Seward, R. J. Grader, A. Toor, G. A. Burginyon and R. W. Hill
2. The Geographical Distribution of  $\sim 100$ -keV Electrons Above the Earth's Atmosphere.....F. D. Seward
3. Quasitrapped Electrons in the Low L Region. Preliminary Results of a Rocket Observation on Jan. 22, 1974.....S. Hayakawa, T. Kohno, F. Nagase and Y. Tanaka
4. Low Energy (10eV to 10 keV) Equatorial Particle Fluxes..... J. D. Winningham (including Soft Particle Fluxes near the Equator .....W. J. Heikkila)
5. AE-LEE Measurements at Low and Mid Latitude.....R. A. Hoffman, J. L. Burch and R. J. Janetzke
6. Midlatitude Electron Precipitation: A Possible Source of Contamination of Galactic X- and  $\gamma$ -Ray Measurements.....T. J. Rosenberg
7. Electron Contamination in a Mid-Latitude Soft X-Ray Astronomy Experiment During an Intense Magnetic Storm .....S. Naranan, H. Friedman, G. Fritz, R. C. Henry and S. Shulman
8. Soft X-Ray Bremsstrahlung and Fluorescent Line Production in the Atmosphere by Low Energy Electrons.....W. Kraushaar
9. Geomagnetic Background Events Observed by UHURU.....D. Schwartz
10. The Particle Background Observed by the X-Ray Detectors Onboard Copernicus.....P. J. N. Davison
11. A Survey of Trapped Low Energy Electrons Near the Inner Boundary of the Inner Radiation Zone from the OSO-7.....J. E. Neighbors and G. W. Clark

1. Electrons at Low Altitudes: A Difficult Problem for Soft X-Ray Astronomy....F. D. Seward, R. J. Grader, A. Toor, G. A. Burginyon and R. W. Hill

**ELECTRONS AT LOW ALTITUDES:  
A DIFFICULT BACKGROUND PROBLEM  
FOR SOFT X-RAY ASTRONOMY**

F. D. Seward  
R. J. Grader  
A. Toor  
G. A. Burginyon  
R. W. Hill

October 24, 1973

# Contents

Abstract . . . . .	1
Introduction . . . . .	1
Acquisition and Analysis of the Electron Data . . . . .	3
Spatial Distribution . . . . .	3
Altitude Dependence . . . . .	7
Energy Distribution . . . . .	8
Flux Variation with Solar Activity . . . . .	10
Results in Relation to the Geophysical Environment . . . . .	12
Electron-Rejecting Collimators to Reduce the Background . . . . .	14
Theory . . . . .	15
Flight Tests . . . . .	17
Laboratory Tests . . . . .	18
Recommendations for a Good Collimator . . . . .	22
Predicting the Electron-Induced Background . . . . .	24
References . . . . .	25

# ELECTRONS AT LOW ALTITUDES: A DIFFICULT BACKGROUND PROBLEM FOR SOFT X-RAY ASTRONOMY

## Abstract

Quasi-trapped and precipitating electrons have been observed with rocket-borne x-ray astronomy detectors in the altitude range 150 to 500 km. Because the flights occurred at low magnetic latitudes the electrons were unexpected. Data from many flights

are combined to derive altitude dependence, an average electron spectrum, and variation with solar activity. Development of electron-rejecting collimators is discussed, and laboratory and flight data on these collimators are presented.

## Introduction

Our x-ray astronomy observations made with rocket-borne instruments have repeatedly shown a strong background due to electrons. The existence of these electrons surprised us, since the rocket flights were at low latitudes and at altitudes supposedly well below the radiation belts. No electron detectors were carried on the rockets, but we have been able to derive a considerable amount of data on the electrons from the x-ray detector observations. In this report we summarize 14 observations of such electrons and describe our continuing efforts to make an efficient x-ray collimator that rejects electrons completely, which has turned out to be a difficult problem.

The salient facts about these electrons are as follows:

- Counters with very thin windows ( $<70 \mu\text{g}/\text{cm}^2$ ) are needed to observe the electrons clearly—the thinner the win-

dow, the larger the electron-induced counting rate. Such counters are a fairly recent development.

- The flux of electrons shows a definite dependence on direction.
- The flux is dependent on solar activity.

The detectors we use for x-ray observations have thin windows and large area, making them highly sensitive to the low fluxes of low-energy electrons encountered on the rocket flights. Slat-type collimators with smooth metal vanes produce a narrow x-ray field of view for the counters. These collimators easily scatter into the counters any electrons that arrive at nearly normal incidence, since small-angle electron scattering is very efficient. The collimators do exclude electrons arriving at large angles to the normal, and therefore it is possible to measure from the counter data the

direction of electron flux. Analysis of the electron spectrum is difficult, however, because a large but unknown proportion of the electron events in the counter represents electrons that have been scattered from the collimator.

Figure 1 shows some unpublished data, from a rocket-borne detector with a very thin window, to illustrate the electron problem. Two prominent x-ray sources can be seen between regions of strong electron-induced background whose level is 2.5 times that of the normal background from cosmic rays and diffuse

x rays. This strong electron background is present in spite of a collimator designed to reject electrons by means of a magnetic field.

To obtain useful electron information from our x-ray astronomy data, we have combined data from flights at three geographical locations in the Pacific: Kauai (one of the Hawaiian Islands), Johnston Island, and a site at 27°N 125°W. The basic geophysical features are similar for these three locations, although magnetic field conditions are slightly different. We have derived a consistent set of

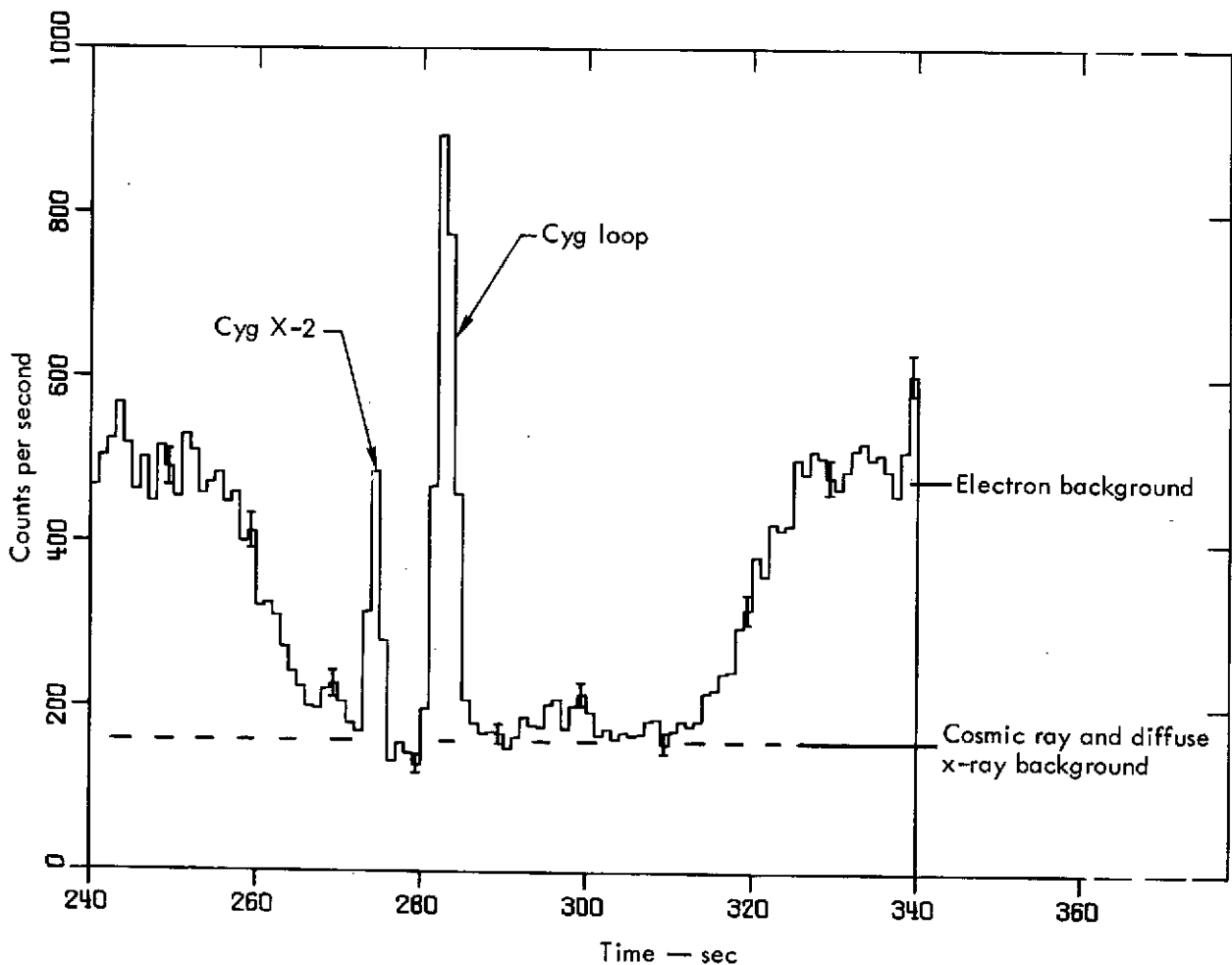


Fig. 1. X-ray detector data from a slow scan through the Cygnus region, made during a flight on May 20, 1972. Electron background is 2.5 times the normal background due to cosmic rays and diffuse x rays. Counts shown are events depositing 0.2-4.0 keV in the counter.

electron data in this way, obtaining an electron spectrum above the atmosphere, the altitude dependence of the electron flux, and the variation of the electron flux with solar activity. These results are valid for the Kauai Range and probably also for other similar locations. The expected variation of electron flux with geographic location is discussed elsewhere.<sup>1</sup>

In this report we first derive data on the observed electrons and then discuss our efforts to shield the x-ray detectors from the electrons. Our goal for the

past two years has been to make an efficient x-ray collimator that rejects electrons completely. It has been quite difficult to eliminate electron events from the x-ray astronomy data. Our hopes have been falsely encouraged by misleading data from early flights and laboratory measurements. We have now reanalyzed all flight data and made new laboratory measurements of the efficiency with which various collimators reject electrons. This report summarizes our present understanding of the problem.

## Acquisition and Analysis of the Electron Data

Table 1 summarizes the basic information about our rocket flights on which electrons have been observed. The detectors were in all cases proportional counters. To be detected, an electron had to pass through the counter window and deposit sufficient energy in the counter gas to create a pulse larger than the discriminator setting. Two discriminators were used: an upper level discriminator (ULD) and a lower level discriminator (LLD).

Counting rate data from these flights is shown in Figs. 1-5 and also in Figs. 14 and 15 (later in the report).

### SPATIAL DISTRIBUTION

Many of the flights had an attitude control system (ACS). On such flights, maneuvers were set up to scan particular astronomical regions of interest. These maneuvers were not planned for electron measurements, and thus the electron data are usually incomplete as regards distri-

bution relative to the magnetic field lines. Nevertheless, some flights have produced a fairly complete magnetic scan, and electron angular distributions around the magnetic field lines have been derived.

We find it helpful to think in terms of two separate electron distributions: (1) "Perpendicular" electrons, which move perpendicular to the field lines and consequently mirror in the vicinity of the rocket. These are at best "quasi-trapped" since they cannot drift completely around the earth on the L-shell in which they move. (2) "Parallel" electrons, whose distribution is very broad and is centered in a direction parallel to the field line. These parallel electrons come down the field line and directly into the atmosphere below the rocket. We have analyzed our data assuming only these two electron distributions are present.

A good example of perpendicular electrons is given in Fig. 2, which shows data from a spinning rocket that carried two

Table 1. Summary of information on rocket flights on which electrons have been observed.

Date	Launch site	Rocket orientation <sup>a</sup>	Apogee (km)	Collimator					Energy thresholds (keV)			5-day sum of A <sub>p</sub>
				Field of view (FWHM)	Material	Electron rejection	No-scattering cutoff energy (keV)	Window material and thickness (mg/cm <sup>2</sup> )	LLD	ULD	Back counter	
5/15/68	Kauai	Spinning	163	5° × 30°	Painted brass	None	—	Formvar (0.06)	3.5	11	—	79
11/3/68	27N, 125W	Spinning	225	2.5° × 30°	Painted aluminum	None	—	Mylar (0.53)	—	19	—	368
11/7/68	Johnston Is.	ACS	314	1.5° × 30°	Aluminum	None	—	Formvar (0.06)	3.5	5.5	—	157
5/17/69	Kauai	Spinning	159	5° × 32°	Painted brass	None	—	Formvar (0.06)	3.5	11	—	271
5/12/70	Kauai	ACS	300	1.3° × 20°	Copper	Electrostatic	33	Formvar (0.07)	4.0	5.5	60	19
9/24/70	Johnston Is.	ACS	500	1.8° × 15.5°	Aluminum	Pulse shape discriminator	—	Mylar (3.5)	—	45	—	74
5/26/71	Kauai	ACS	300	1.3° × 20°	Copper	Electrostatic	33	Formvar (0.07)	4.0	5.5	60	34
10/23/71	Kauai	ACS	300	1.3° × 20°	Copper	Electrostatic	50	Formvar (0.06)	3.5	5.5	60	22
11/17/71	27N, 125W	Spinning	267	3° × 20°	Brass	Magnetic	78	Formvar (0.07)	—	—	—	9
5/20/72	Kauai	ACS	321	2° × 12°	Aluminum	Magnetic	53	Formvar (0.035)	2.5	5.5	—	79
10/20/72	Kauai	ACS	310	1.3° × 20°	Chemically blackened Cu	Magnetic	200	Formvar (0.09)	5.0	6.0	60	67
10/21/72	Kauai	ACS	325	2° × 15°	Copper	Electrostatic	11	Formvar (0.027)	2.0	3.5	—	73
4/25/73	27N, 125W	Spinning	280	6° × 7°	Painted aluminum	None and magnetic	0 41	Formvar (0.06)	3.5	5.0	—	139
6/23/73	Kauai	ACS	300	1.1° × 15°	EDM aluminum	Magnetic	600	Formvar (0.06)	3.5	5.0	60	75

<sup>a</sup>ACS = attitude control system.

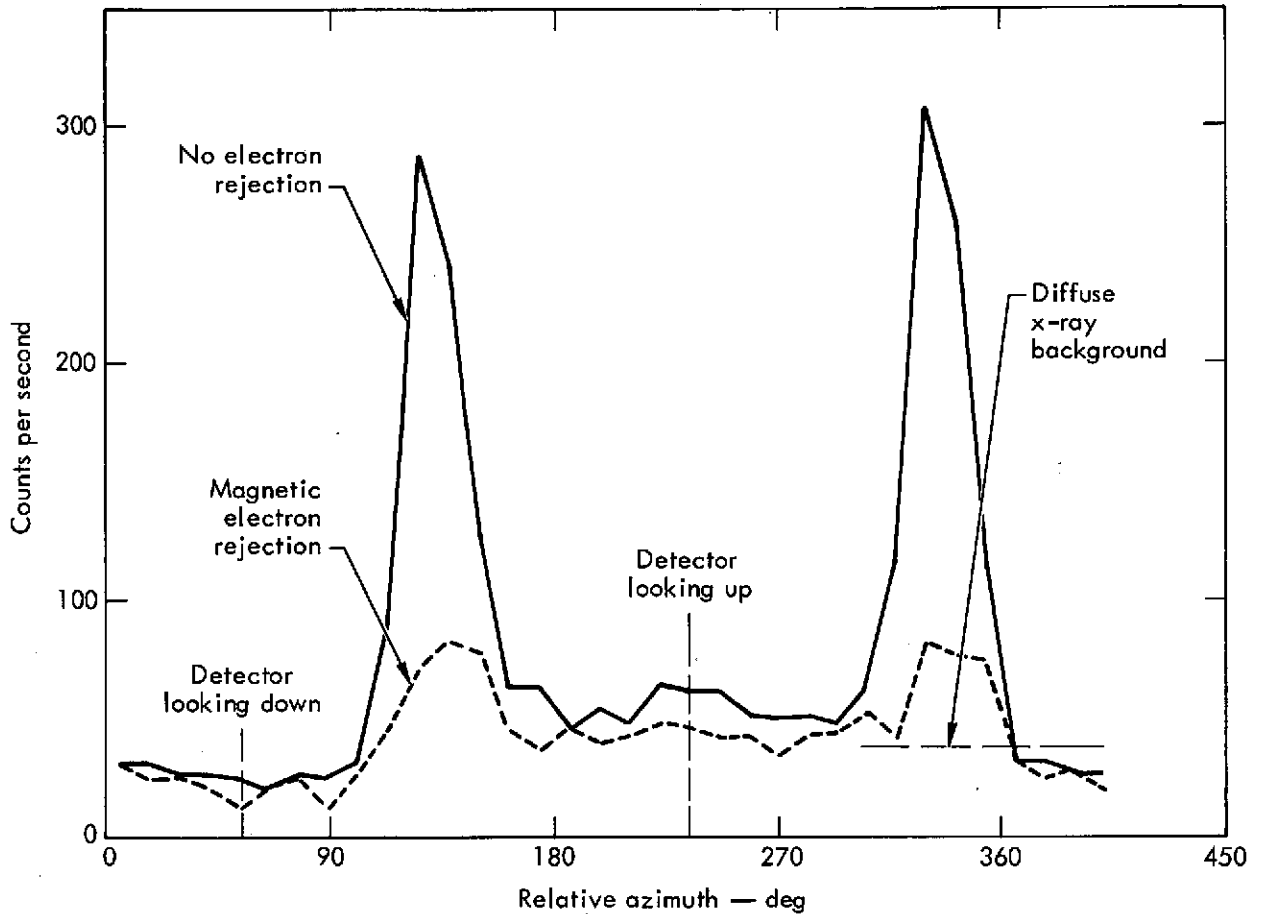


Fig. 2. Perpendicular electrons (i.e., electrons moving perpendicular to the magnetic field lines) observed during a flight on April 25, 1973. Altitude was 280 km, electron threshold  $\sim 5$  keV (ULD).

identical counters. Both counters were collimated to give the same field of view ( $6^\circ \times 7^\circ$  FWHM), but one collimator had a magnetic field to reject electrons while the other collimator had no magnetic field. The difference between the two counting rates shows the electron flux. Maximum flux is seen twice per revolution when the detector points perpendicular to the earth's magnetic field lines. A smaller parallel electron flux appears almost isotropically when the detector is looking up from the atmosphere.

Figure 3 shows a pure parallel electron distribution observed from a spinning rocket at lower altitude. Two strong

x-ray sources appear superposed on the electron-induced background.

Figures 4 and 5 show data from two attitude-controlled flights. They illustrate the appearance of electrons in typical flight data and show how well these data may be fitted by assuming the two electron distributions. In both these figures the histogram is the counting rate above the upper level discriminator of a methane-filled counter. The entire flight, from launch to reentry, is shown. Solid and dashed curves are respectively the contributions of perpendicular and parallel electrons. The flux and spatial width of these two populations have been

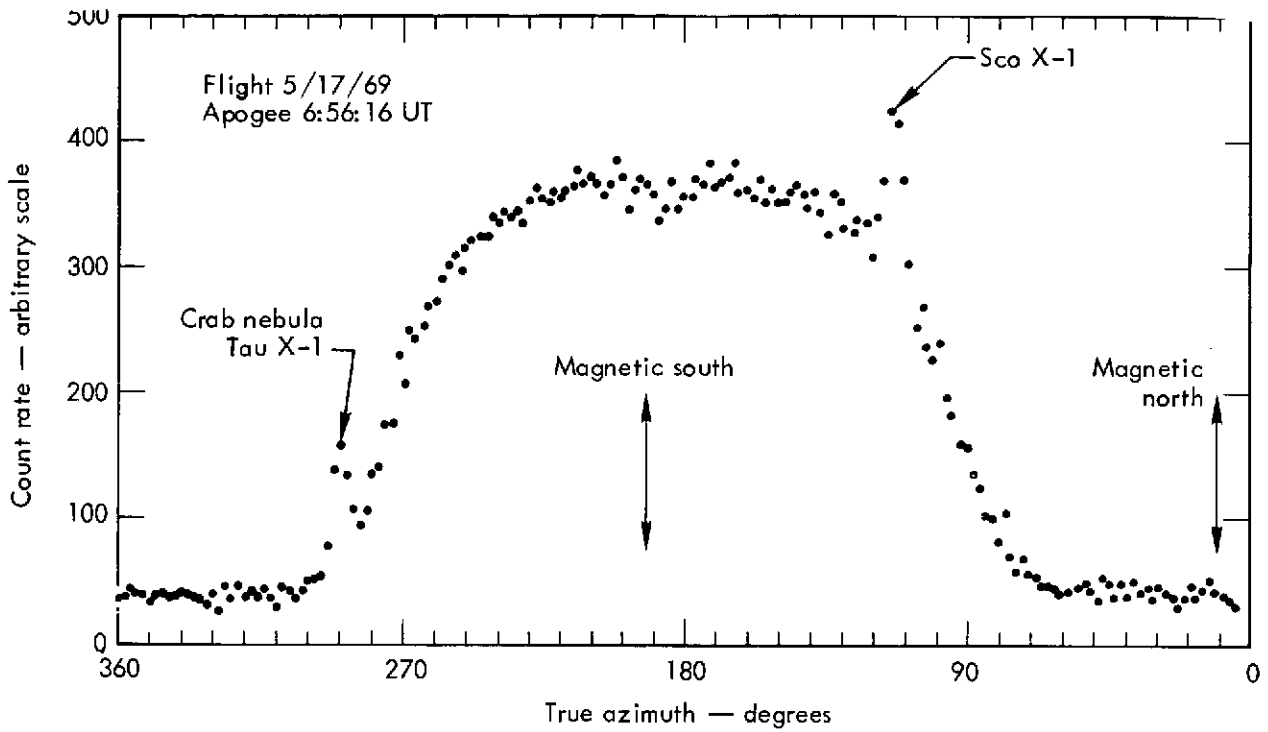


Fig. 3. Parallel electrons (i.e., electrons moving parallel to the magnetic field lines) observed during a flight on May 17, 1969. Altitude ~150 km, electron threshold 3.5 keV.

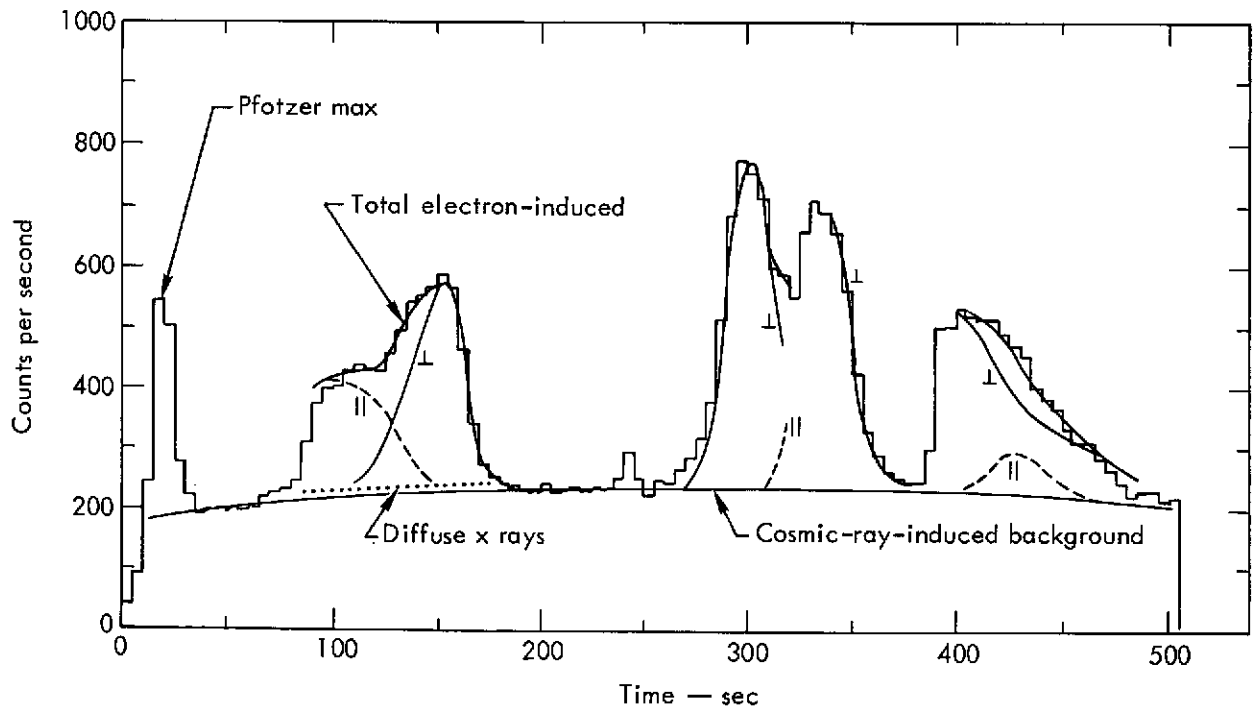


Fig. 4. Electrons observed during a flight on May 26, 1971. Counts above ULD (5.5 keV) vs time.

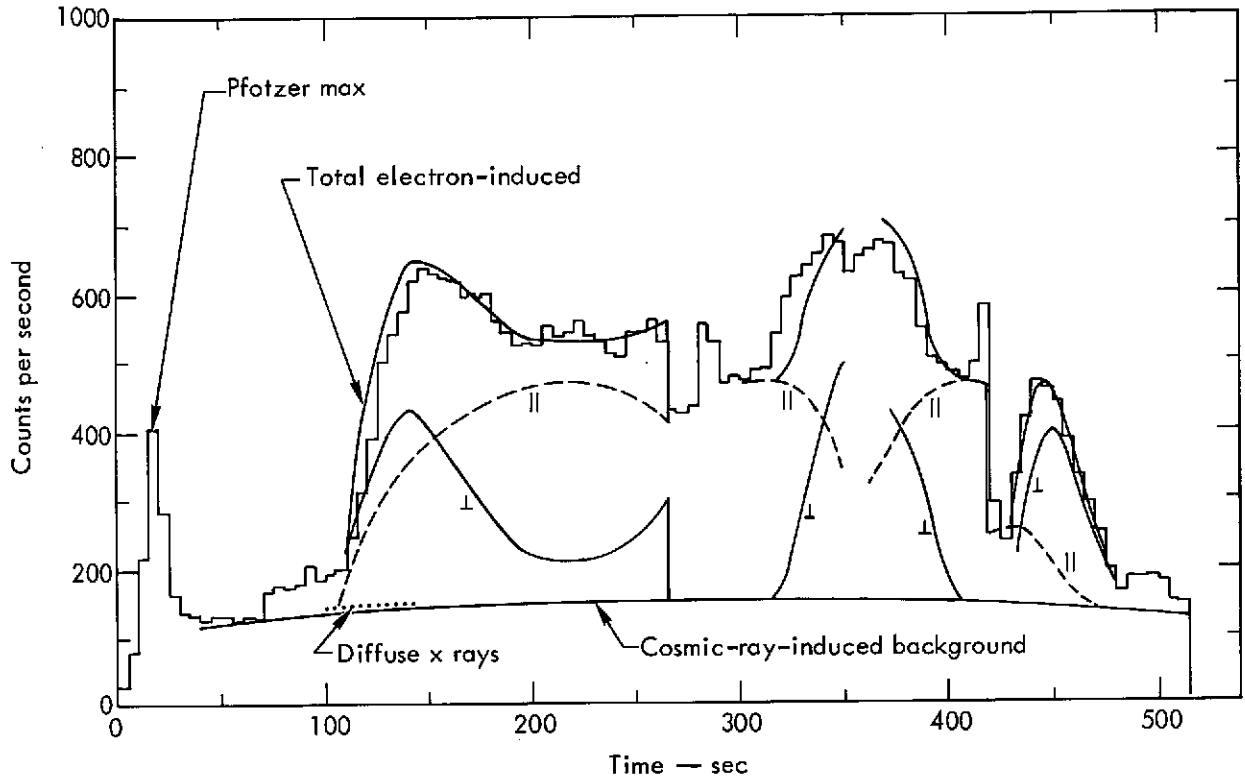


Fig. 5. Electrons observed during a flight on October 20, 1972. Counts above ULD (6.0 keV) vs time.

adjusted to give a good fit to the data. The altitude dependence of each group has been derived from these data. Gaps in the calculated curves correspond to times when the payload was maneuvering to set up the next slow scan. During some of these maneuvers the motion is too rapid to determine the position well.

The most electron-free observations occur when the detector is looking down the magnetic field line toward the atmosphere. Electron flux in this hemisphere is a minimum and the part that is not occulted by the earth is suitable for x-ray observations.

#### ALTITUDE DEPENDENCE

The altitude dependence of perpendicular electrons has been derived from

spinning rockets which sampled the directional flux throughout the flight and from a few suitable ACS flights. These data are shown in Fig. 6. The solid curves, normalized to each set of data points, vary inversely as the square root of the atmospheric density. The variation in flux from flight to flight is due to the different energy thresholds of the detectors and to changing solar activity. The data from any one flight, however, are reasonably well fitted by the curves shown.

To calculate atmospheric density the appropriate CIRA atmosphere was used.<sup>2</sup> Thus, fluctuations of atmospheric density with solar activity and time of day have been somewhat compensated for.

Figure 7 shows the measured fluxes of parallel electrons. This flux at any one

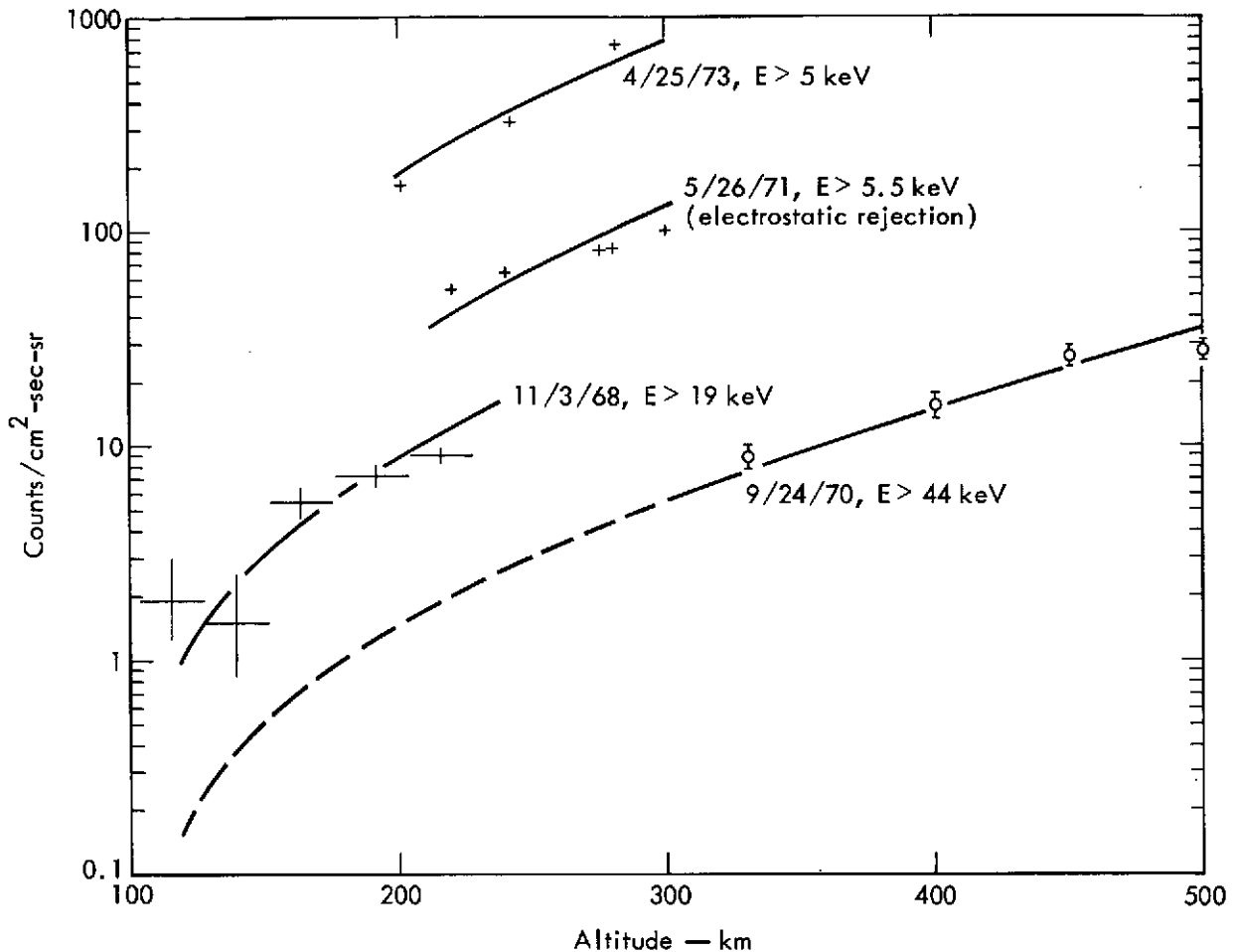


Fig. 6. Altitude dependence of perpendicular electrons as observed on four flights (ULD data).

time is fairly constant above 200 km. There is a great variation from flight to flight which is mostly due to changing solar activity.

The energy thresholds determined by the window have been listed for those experiments carrying electrostatic collimators. These collimators were run at about 250 V potential; as we will show later, this had little effect on the measured electron flux.

LLD data have been used for two early flights since the ULD was set very high on these detectors. The solid lines in Fig. 7 are smooth curves drawn through the data points of a given flight.

#### ENERGY DISTRIBUTION

Most of our detector systems have two discriminators. The LLD is set at the minimum x-ray energy of interest, and the ULD at the maximum x-ray energy acceptable in the counter. Typical settings are 0.2 and 2.5 keV. Virtually all background events caused by high energy particles such as cosmic rays traversing the detector appear above the upper level discriminator. In the absence of electrons, the in-flight background observed above the ULD is quite constant, varying only slightly with altitude. This is the data channel where electrons are seen

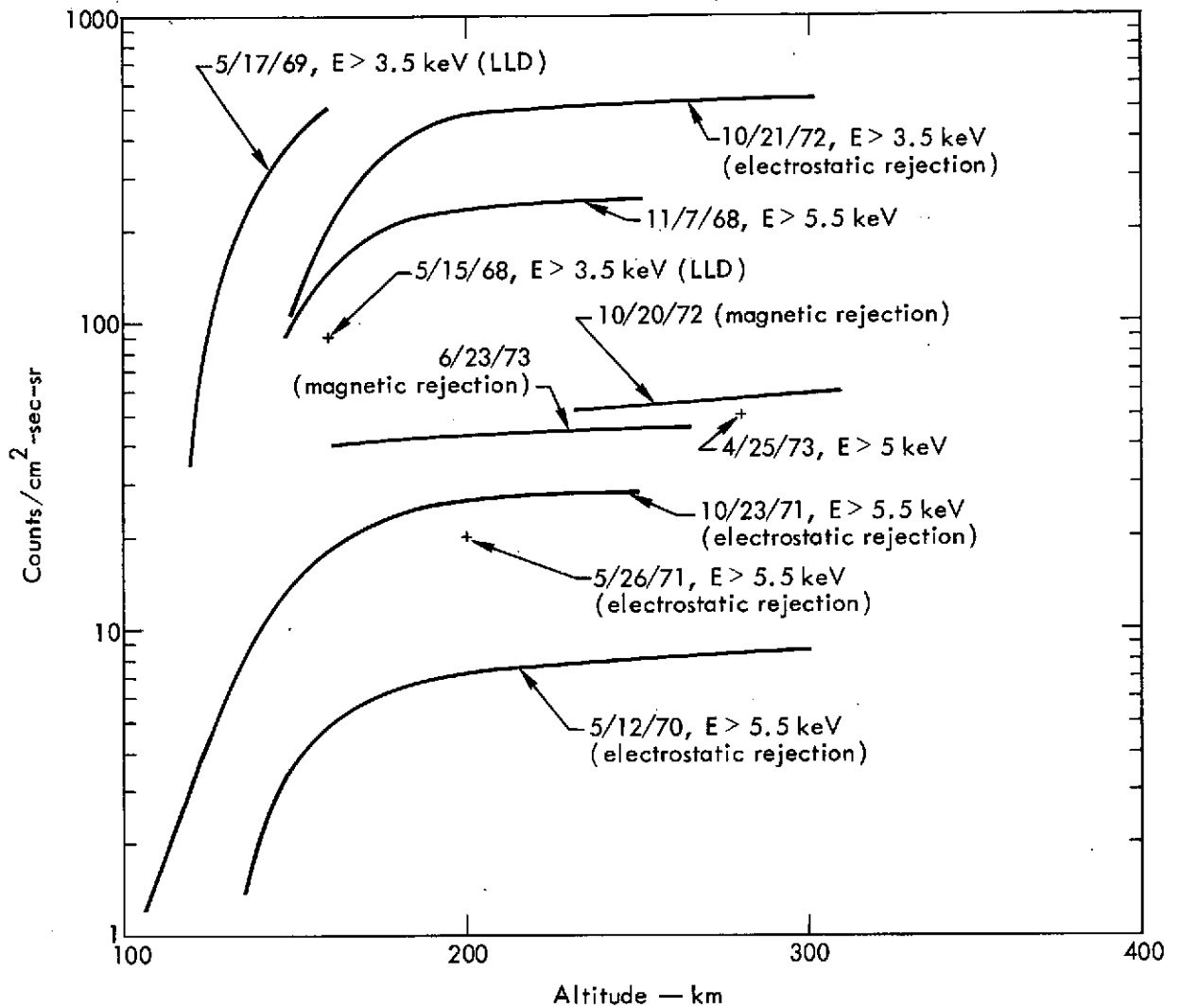


Fig. 7. Altitude dependence of parallel electrons as observed on ten flights (ULD data except where marked LLD).

most clearly. Electrons between the LLD and the ULD are sometimes difficult to see in the rapidly varying x-ray counting rate.

To determine the energy spectrum of the incident electrons we consider each rocket to give an integral energy spectrum measurement. The counter only detects electrons with energies above a threshold determined by the thickness of the window and the discriminator energy threshold. We used the range-energy

relations of Kanter<sup>3</sup> and Nelms<sup>4</sup> to calculate these energy thresholds. The material was usually carbon since counter windows were Formvar and front counters were filled with methane or propane. Some of our detectors were multilayer counters, and the effective window for the back counter was a layer of Formvar, methane, and Mylar.

The range-energy curves we used are shown in Fig. 8. The energy defined by these range curves is close to the onset

of detector window transmission. The counters are barely able to detect electrons at this threshold energy. If electron energy is increased by a factor of about 1.5 above this threshold, the counter efficiency becomes about 50%.

To derive an energy spectrum, we have plotted in Fig. 9 the maximum observed electron counting rate as a function of threshold energy for several rocket flights. Only perpendicular electron fluxes are shown. These data were obtained with collimators having no electron rejection. Most of the points were obtained at times of high solar activity. Consequently the flux represented is high. Some of the data points have been corrected to 300 km using the altitude dependence discussed previously.

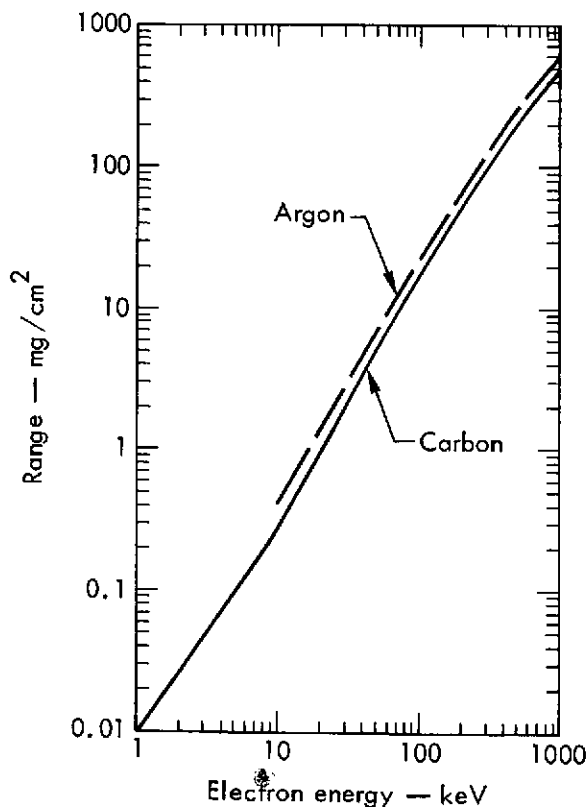


Fig. 8. Range-energy curves used in the electron energy calculations.

The line drawn through the points is described by

$$N(E > E_t) = 1.6 \times 10^4 E^{-2.1} \text{ counts/cm}^2\text{-sec-sr},$$

where  $N$  is the number of counts in the detector, and  $E$  and  $E_t$  are respectively the electron energy and the threshold energy in keV. To convert this to electron flux, one must divide by the counter efficiency, which is not well known. In the absence of more definite information the number 0.5 is recommended.

#### FLUX VARIATION WITH SOLAR ACTIVITY

Several hours after a large solar flare, the ejected solar plasma strikes the earth's magnetosphere. The earth's magnetic field is consequently compressed, which shows as a sudden increase in the

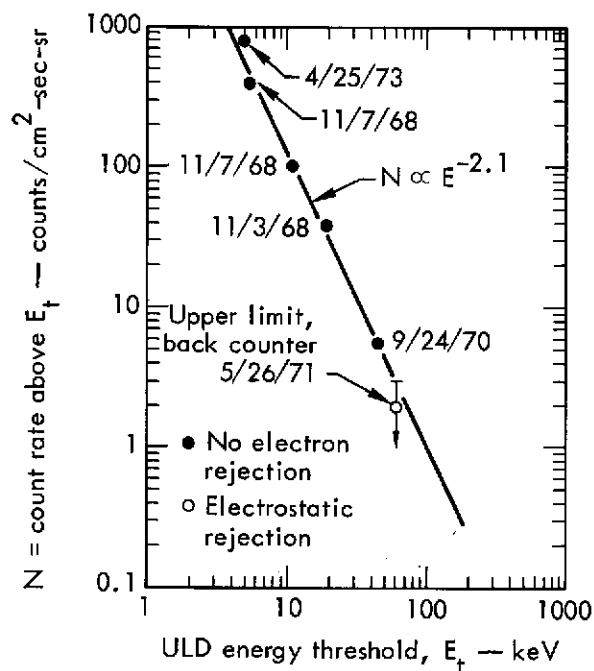


Fig. 9. Derived energy spectrum for perpendicular electrons at 300 km.

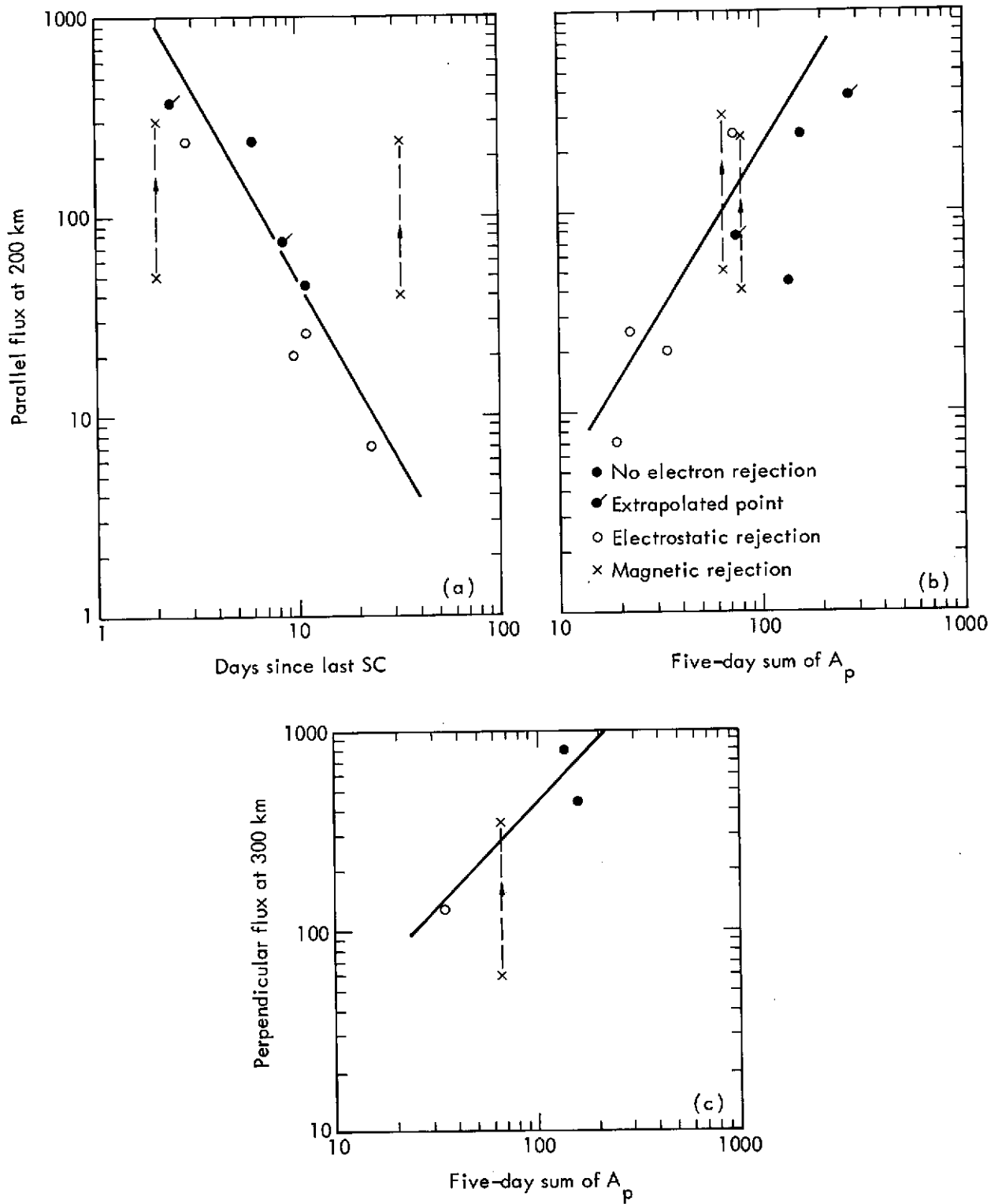


Fig. 10. Variation of electron flux with magnetic storms caused by solar flares.  
 $E > 5$  keV.

earth's magnetic field at sea level. This "sudden commencement" (or SC) signals the beginning of a magnetic storm, a period lasting a week during which the disturbed particle currents in the magnetosphere cause additional fluctuations in the field measured at sea level.

There is a correlation of the electron flux with solar activity. This is illustrated in Fig. 10 by comparing the observed flux with magnetic activity. Straight lines have been drawn to roughly show the effect.

Figure 10(a) shows our parallel electron data plotted as a function of the elapsed time between the rocket flight and the last sudden commencement. The most intense parallel electron fluxes are observed during the first few days of the magnetic storm. These electrons are precipitating into the earth's atmosphere. Figure 10(a) shows parallel electron flux ( $E > 5$  keV) at 200 km altitude. Two lower altitude flights have been extrapolated to 200 km using the observed altitude dependence. The electrostatic collimator points can probably be compared directly with those points taken with collimators having no electron rejection.

Two data points taken with magnetic collimators have been increased by a factor of 6 since this is our estimate of the minimum rejection efficiency of this collimator. Thus many of the data points have been adjusted. Since varying geomagnetic phenomena are in any case imprecise, we feel this procedure is justified.

Figure 10(b) displays these data in a different fashion. The observed parallel electron flux has been plotted as a function of magnetic activity. The average daily planetary magnetic field index,  $A_p$ , has been summed for the five days preceding the launch. The observed data has been plotted as a function of this five-day sum of  $A_p$ . Since  $A_p$  is large immediately following a sudden commencement, the two plots are almost equivalent.

The perpendicular electron flux also varies with magnetic activity. Figure 10(c) shows the few perpendicular electron measurements that we have. The flux increase with magnetic activity is apparently not as great for perpendicular electrons as for parallel electrons.

## Results in Relation to the Geophysical Environment

This section is a discussion of particle motion over the Kauai Range. Data in this report were taken from three launch sites: Kauai, Johnston Island, and a site located at 27°N 125°W. Although magnetic field conditions are slightly different, basic features are similar for all three locations.

At great altitudes, electrons are constrained to move about magnetic field

lines. An electron moving parallel to the field plunges directly into the earth's atmosphere, loses its energy, and is stopped. An electron having a velocity vector making a large angle with the magnetic field vector and traveling down toward the earth will "mirror" as the magnetic field strength increases; i.e., it will be reflected back up the field line. The motion of such an electron consists

of a fairly rapid bouncing between mirror points, back and forth along the field line, coupled with a slow drift to the east. If the mirroring altitude is high enough, this eastward drift will carry the electron completely around the earth. During this drift, although moving from one field line to another, the electron is constrained to remain in a specific magnetic shell characterized by the parameter  $L$ . ( $L$  in a pure dipole field is the maximum distance a field line extends from the center of the earth, measured in earth radii.) The motion of an electron in the earth's magnetic field is completely determined by the  $L$ -value of the magnetic shell and the value of the magnetic field,  $B$ , at its mirror points. These two items can be treated as invariants of motion.

At an altitude of 300 km above the Kauai Range the magnetic coordinates are  $L = 1.20$ ,  $B = 0.32$  G. An electron mirroring at 300 km altitude above Kauai mirrors at an altitude of 500 km at the southern hemisphere conjugate point and has an altitude of 1200 km as it travels (along the field line) through the magnetic equator. These electrons cannot drift all the way around the earth on this  $L$  shell. The mirror point altitude as the electron goes east decreases and descends into the dense atmosphere. Thus, electrons observed mirroring (moving perpendicular to the field line) at 300 km above Kauai cannot be permanently trapped in the earth's field but are at most quasi-trapped.

The times for an electron to bounce between mirror points and to drift around the world have been calculated by Hamlin et al.<sup>5</sup> and by Lew.<sup>6</sup> A 100-keV electron mirroring at 300 km above Kauai has a

bounce period of 0.16 sec and a drift period of 5 hr (if it were possible to drift around the earth without descending into the atmosphere). At the mirror point the electron has a trajectory with a radius of curvature of 33 m and takes  $1.3 \mu\text{sec}$  to make a revolution around the field line.

The presence of the atmosphere greatly modifies the behavior of electrons in this region. Electrons scatter and lose energy in the atmosphere. When a mirroring electron is scattered it assumes a trajectory that lowers the mirror point to a region where the atmosphere is denser; thus further scattering is more probable, the mirror point lowering is accelerated, and the electron is soon on a trajectory where it descends deep enough to be lost. Over the Kauai Range the chance of scattering is determined by the atmospheric density over Kauai, since this mirror point is lower than the corresponding mirror point in the southern hemisphere. Atmospheric density varies greatly with solar activity and time of day. We have calculated the densities for an atmosphere with average solar activity (CIRA No. 5)<sup>2</sup> at 22:00 local time. Deviations from these values are expected to be on the order of a factor of

If an electron has traversed an amount of material equal to  $1/100$  of its range it will have been scattered through an angle of about  $10^\circ$ . We have calculated the altitude at which an electron of given energy, mirroring at that altitude, might be expected to encounter this amount of material. Curves have been drawn in Fig. 11 to illustrate the expected behavior. The highest curve corresponds to an energy where it takes 100 bounces between mirror points to traverse this

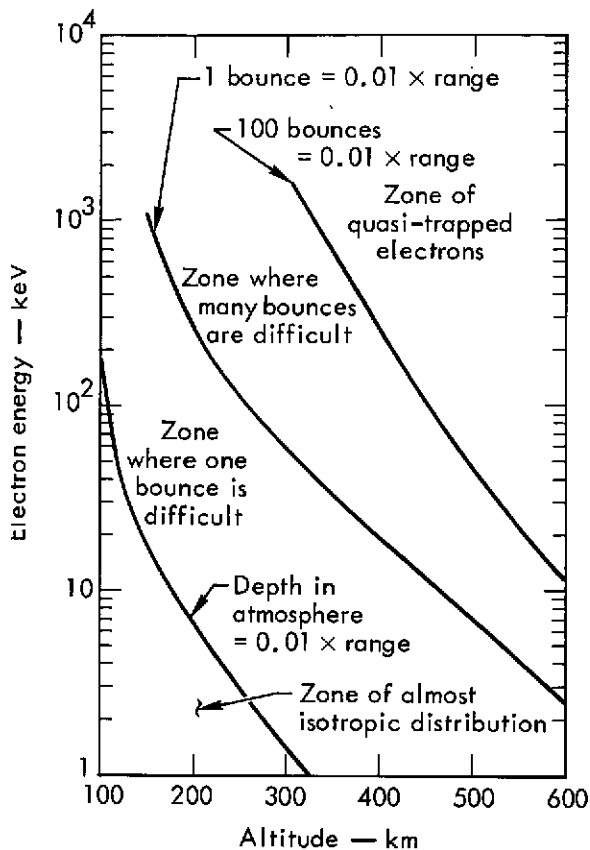


Fig. 11. Expected electron behavior over Kauai. Electron energy is plotted vs altitude for various effective depths in the atmosphere.

amount of atmosphere. Thus, the mirror notion should be relatively stable at altitudes above or at energies higher than his curve. The next lower curve shows the energies where the electron is ex-

pected to be scattered a few degrees in only one bounce. Mirroring electrons should not persist below this curve. The bottom curve shows altitudes at which electrons moving parallel to the field lines have traveled through an atmospheric thickness of 1/100 of their range. Below this curve the electron flux should be almost isotropic.

As an illustration, at 300 km altitude, electrons having energies of ~1 MeV are able to mirror many times without much scattering. As the energy is decreased to below ~100 keV, electrons are appreciably scattered during one mirror oscillation, and thus mirroring electrons should not be observed strongly below this energy.

When mirroring electrons are observed at low altitude they appear as a distribution peaked at a direction corresponding to velocities perpendicular to the field line. We have observed distributions like this in several flights in the altitude range 200 to 300 km. Figure 11 indicates that these electrons must have energies of ~100 keV or more. Our measured in-flight collimator transmission of 4/25/73 also implies an effective electron energy of >100 keV, which is in agreement with this analysis.

## Electron-Rejecting Collimators to Reduce the Background

We have so far discussed the number of electrons penetrating into the counter by referring to the counting rate above the ULD. Thus, the rates shown in Figs. 4-10 are all from ULD data. Electron-induced counts also appear between the LLD and the ULD. These counts are due to events which deposit

only a small amount of energy in the counter gas. Such events are not caused by high energy electrons passing through the detector. They are probably due to low energy electrons scattered from the collimator into the counter or to x rays generated by electrons striking the collimator.

The pulse height spectrum of events induced by low energy electrons always has approximately the same form,  $dN/dE \propto E^{-1}$ , which is illustrated in Fig. 12. The expected primary electron spectrum is more like  $dN/dE \propto E^{-3}$  (derived from data of Fig. 9). Thus, we consider the low energy spectrum to contain little information about the primary electron spectrum. The low energy events, however, are the ones we want to eliminate. If all electron events were to appear only above the ULD there would be no background problem.

Table 2 lists some flight data in which we have been able to clearly distinguish electron-induced events in the x-ray data. The table shows the electron-induced background at 1 keV relative to the total number of electron counts depositing more than 5 keV in the detector. Specifically, we define the relative number of low energy events to be

$$\frac{\text{Electron-induced counts/sec-keV at 1 keV}}{\text{Electron-induced counts/sec above ULD } (\geq 5 \text{ keV})}$$

Table 2. Relative number of low-energy electron events observed on eight flights with various collimator vane materials and electron rejection schemes.

Flight date	Collimator vanes	Electron rejection	Relative number of low energy events
5/15/68	Painted	None	0.24
11/7/68	Aluminum	None	0.84
5/17/69	Painted	None	0.25
5/26/71	Copper	Electrostatic	0.16
5/20/72	Aluminum	Magnetic	0.66
10/20/72	Blackened copper	Magnetic	0.30
10/21/72	Copper	Electrostatic	0.14
6/23/73	EDM aluminum <sup>a</sup>	Magnetic	<0.10

<sup>a</sup>EDM = electric-discharge-machined.

The relative induced background in Table 2 varies according to the type of collimator used. A plain aluminum surface seems to give the highest relative background. Plain copper is lower and rough paint or rough EDM (electric-discharge-machined) aluminum are also low. Laboratory measurements of electron rejection show a similar dependence on collimator material. There is no structure in the electron-induced low energy spectrum that might indicate characteristic x rays from the collimator. Thus, the most likely source of these low energy events is low-energy scattered electrons.

## THEORY

We have used both electrostatic and magnetic fields to sweep electrons into the collimator walls. The fields were applied so that electrons were swept into the walls across the narrowest collimator dimension. If we assume that electrons entering the collimator are eliminated after one collision with a wall, i.e., that

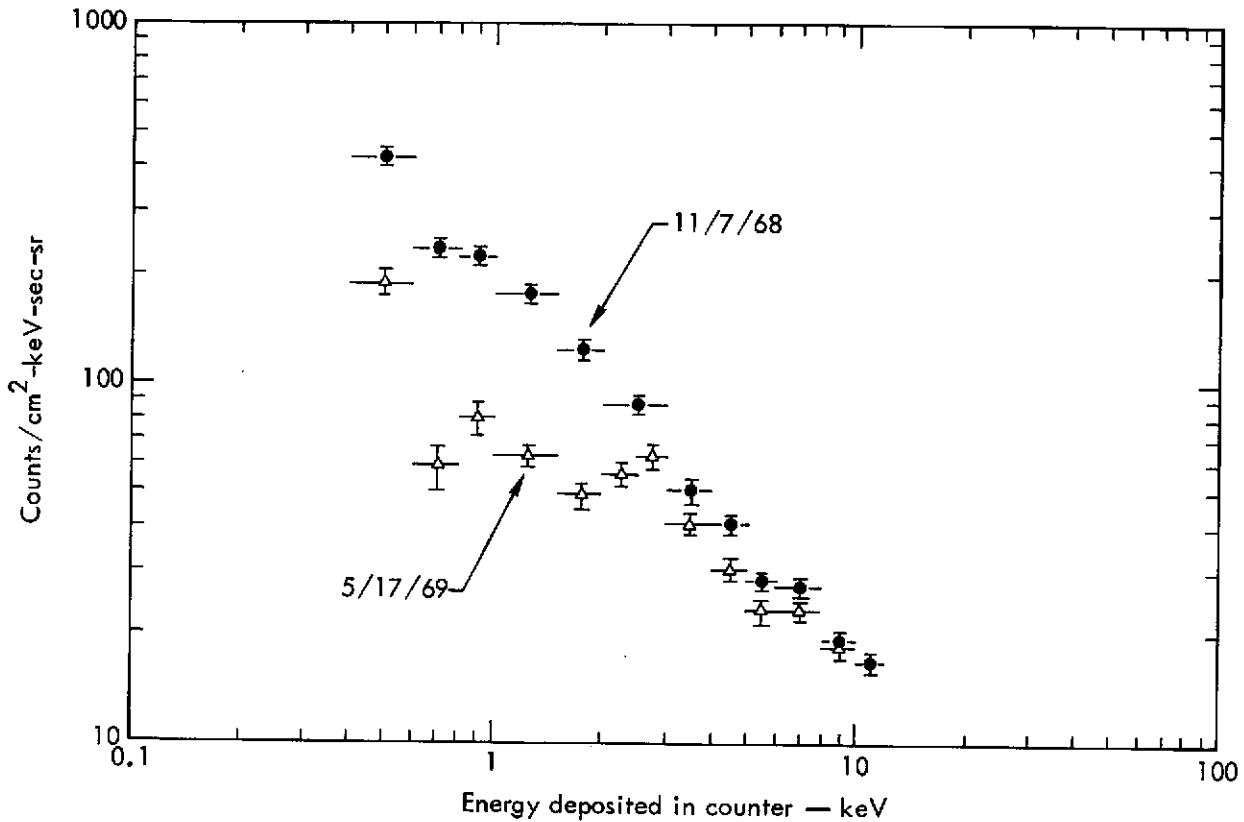


Fig. 12. Pulse height spectrum of events induced by low energy electrons.

there is no scattering, then a collimator section of length  $\ell$  cm and width  $d$  cm will reject all electrons with energies less than a cutoff energy,  $E_c$ .

Electrostatic electron rejection. The applied potential in volts is

$$V = \frac{16d^2 E_c}{\ell^2 + 16d^2},$$

where  $E_c$  is in eV.

Magnetic electron rejection. The critical radius of curvature is

$$\rho_c = \frac{4d^2 + \ell^2}{8d},$$

and

$$B\rho_c = 3336 (E_c^2 + 1.02E_c)^{1/2},$$

where  $B$  is in gauss (G),  $\rho_c$  in cm, and  $E_c$  in MeV.

We know, however, that these considerations are too simple in assuming no scattering. The angles of incidence are only 1 or 2°, so electrons scatter easily from the collimator walls. Therefore, to be pessimistic, the cutoff energy can be calculated allowing a single scattering in which energy loss is negligible. In this case, the cutoff formulae become

$$V = \frac{64d^2 E_c}{64d^2 + \ell^2},$$

$$\rho_c = \frac{16d^2 + l^2}{32d}$$

Using typical collimator dimensions of  $d = 0.10$  in. and  $l = 2.5$  in., we have calculated (Table 3) the required electrostatic and magnetic fields for the no-scattering and single-scattering assumptions (see Fig. 13).

### FLIGHT TESTS

Figures 2, 14, and 15 show flight data taken with electron-rejecting collimators. The collimator of Fig. 2 had a field of view of  $6^\circ \times 7^\circ$  FWHM and contained a magnetic field of about 100 G. Calculated no-scattering and single-scattering cutoffs were at 41 and 3.3 keV, respectively. The in-flight transmission of this collimator for perpendicular electrons was  $\sim 0.15$ . (This can be obtained directly from Fig. 2.)

Figure 14 shows data taken with an electrostatic collimator. The detector was first oriented to point directly up the field line and the collimator voltage was stepped to 0, 200, and 700 V. This was repeated later in the flight with the detec-

tor pointing perpendicular to the earth's magnetic field. (Calculated no-scattering and single-scattering cutoff energies are 0, 11, and 38, and 0, 3, and 10 keV, respectively.) The collimator transmission was 1.0 and 0.8 at the two applied voltages when pointing parallel to the field and 1.0 at both voltages when pointing perpendicular to the field.

With 700 V applied, the counting rate in the x-ray window became high. If the electron potential is above 280 V, carbon K x-rays are generated when ionospheric electrons (density  $10^4 - 10^5/\text{cm}^3$  at thermal energies) are accelerated into the collimator walls. Thus, electrostatic collimators cannot be used with applied fields above 280 V. Since not many electrons are rejected at this potential, the electrostatic collimator is not a good system to use.

Figure 15 (and also Fig. 1) shows data taken on a different flight with the same detector but with a magnetic collimator with calculated cutoffs at 53 and 3.6 keV. The electron background is much lower. If we assume the primary electron flux unchanged (the five-day sums of  $A_p$  are very close), the magnetic collimator transmission was  $\sim 0.20$ .

Table 3. Calculated electrostatic and magnetic fields required for the assumptions of no scattering and single scattering of electrons from the collimator vanes. Vane dimensions are  $d = 0.10$  in. and  $l = 2.5$  in. (see Fig. 13).

Cutoff energy, $E_c$ (keV)	Electrostatic field (V)		Magnetic field (G)	
	With no scattering	With single scattering	With no scattering	With single scattering
10	250	930	17	65
30	750	2800	30	115
100	2500	9300	56	220
300	7500	—	105	410

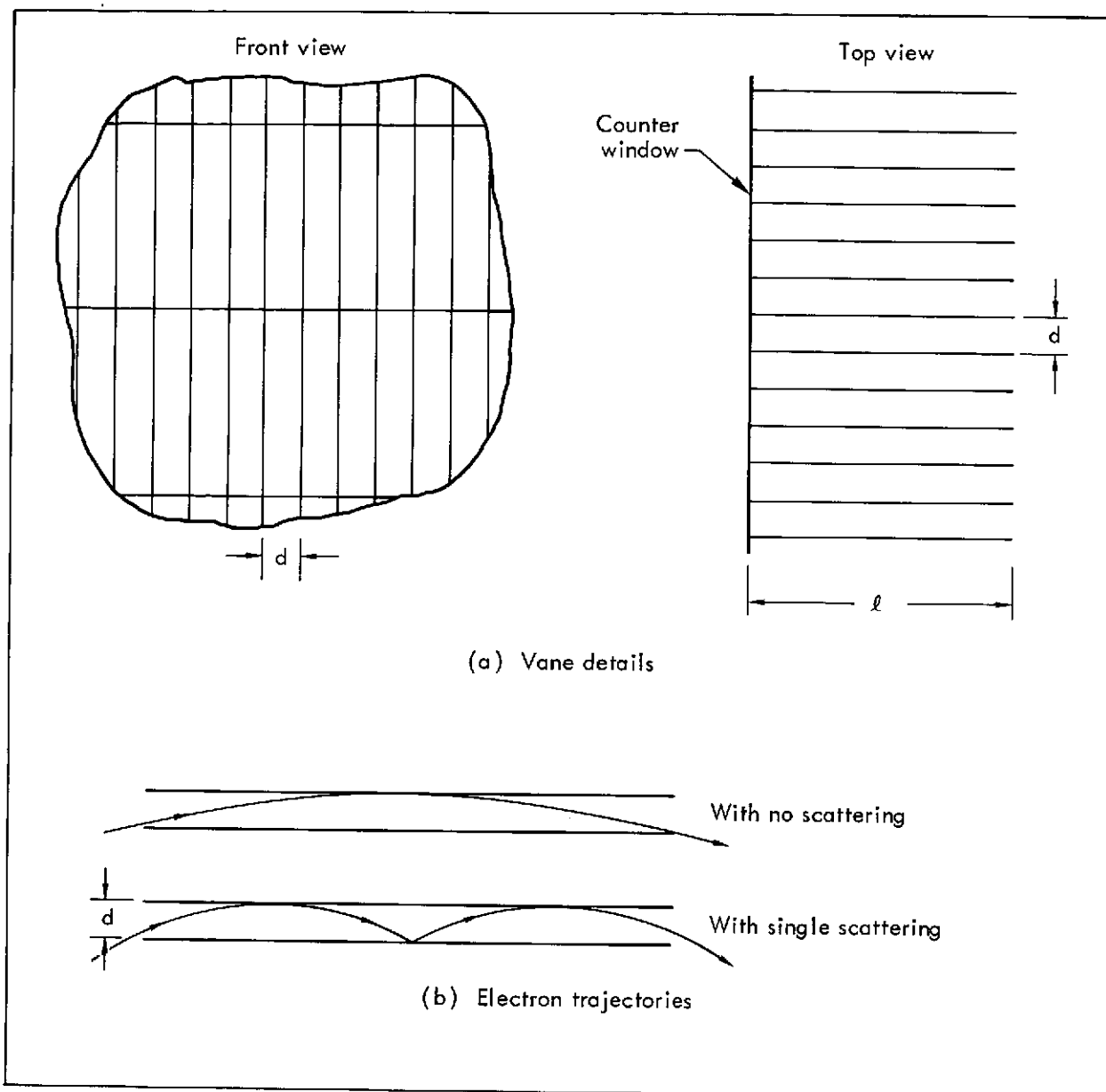


Fig. 13. Vane details of an electron-rejecting collimator. (a) Front and top views of a portion of the vanes. (b) Trajectories through the vanes assumed for an electron of energy  $E_c$  with no scattering and with a single scattering.

#### LABORATORY TESTS

We have measured the electron transmission of collimators in the laboratory. Our goals were first to understand the measured in-flight transmissions and then to study collimators constructed of different materials.

Electron sources used were  $^{63}\text{Ni}$  and  $^{90}\text{Sr}$ . Nickel 63 emits a continuous spectrum of electrons having an end-point energy of 65 keV. The  $^{90}\text{Sr}$  source emits electrons equally from both  $^{90}\text{Sr}$  and  $^{90}\text{Y}$ . The end points of the  $\beta$  spectra are 540 keV and 2.2 MeV.

The experimental apparatus consisted of a small stainless steel proportional

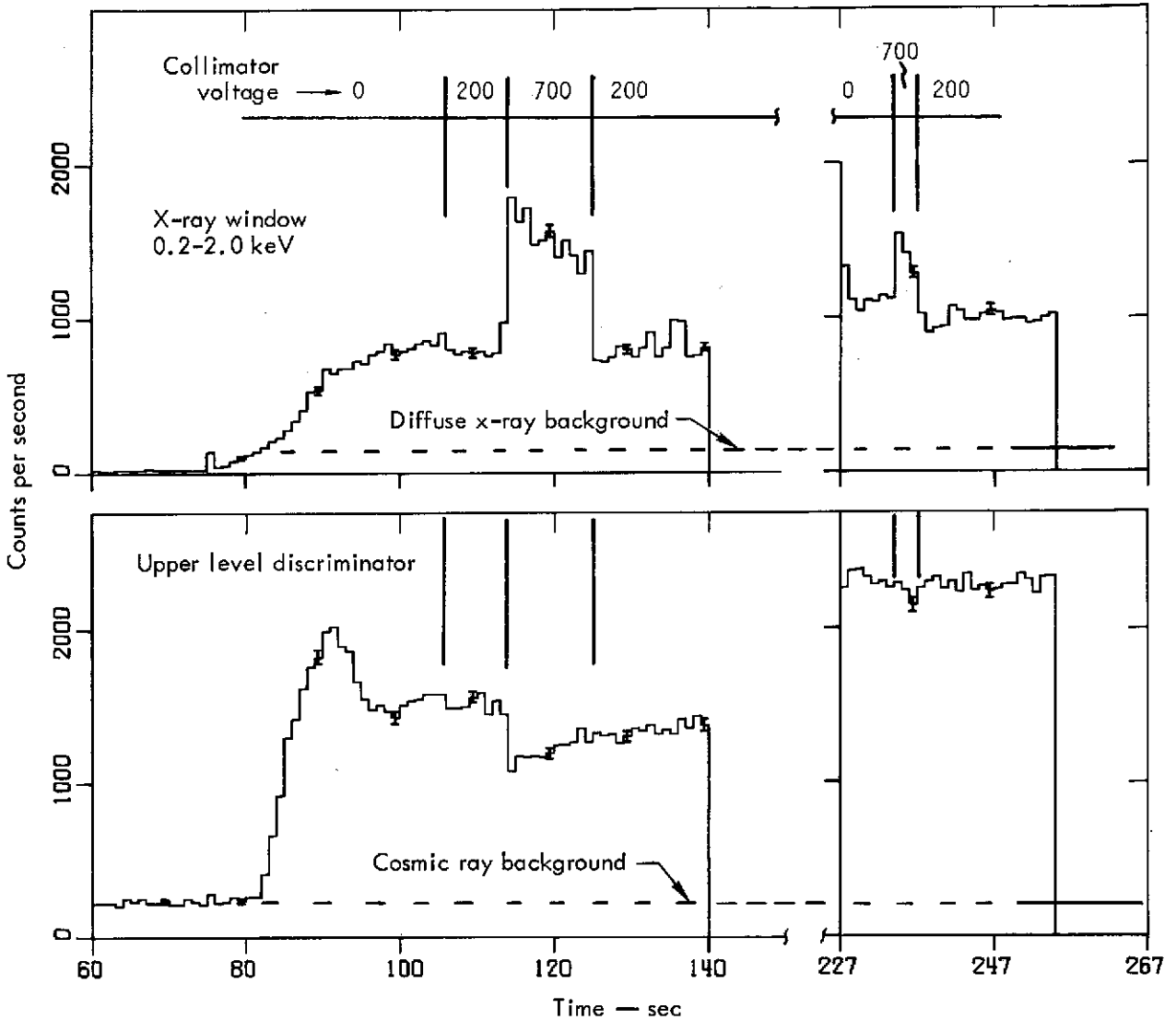


Fig. 14. In-flight test of a collimator with electrostatic electron rejection made on October 21, 1972.

counter with a  $30\text{-}\mu\text{g}/\text{cm}^2$  Formvar window operating with propane gas at 100 mm Hg absolute pressure. The counter was constructed so that selected collimators could be placed over the thin window and tested with ceramic-slab permanent magnets of various strengths. The electrons were collimated to illuminate a region slightly larger than the counter collimator area. High intensity magnets of 800-G field could be placed next to the source-collimator to "shut

off" the electron beam for background measurements. Figure 16 shows a schematic of the experimental geometry. This apparatus was placed in a vacuum tank and operated at  $\sim 10^{-5}$  Torr.

The  $^{63}\text{Ni}$  source was essentially x-ray-free between the nickel L and K edges, enabling us to achieve electron counting rates of 150 times background in the range from 1 keV to counter saturation at 5 keV. The  $^{90}\text{Sr}$  source produced a large x-ray flux below 6 keV which

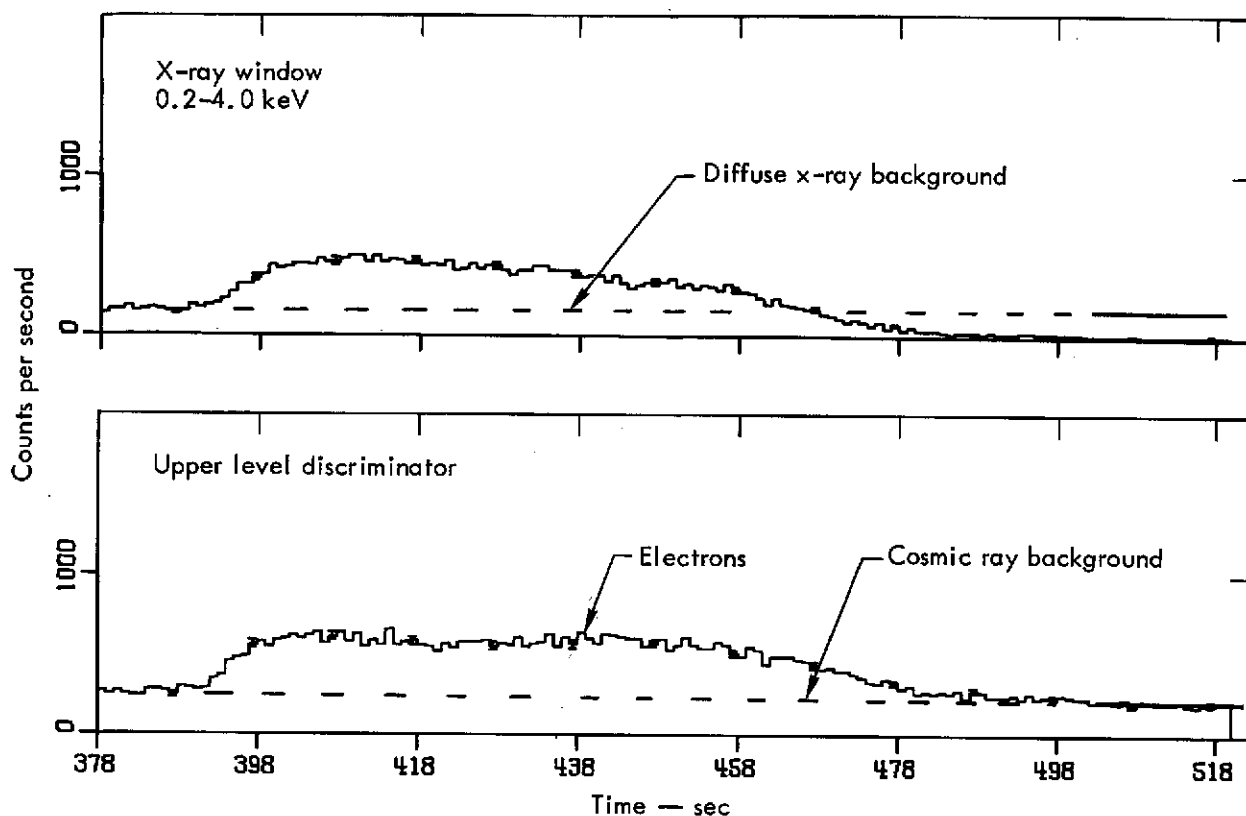


Fig. 15. Data from a detector and collimator with magnetic electron rejection flown May 20, 1972.

masked all low-energy electron events in the counter.

The transmission of each collimator was measured by first taking the initial count rate with no sweep magnets on the collimator or the source-collimator. Next the collimator magnets were installed and the count rate measured for several field strengths. Finally, the source-collimator magnets were used to shut off the electron beam and obtain the background due to natural radioactivity and x rays from the electron source.

The rocket flight of 4/25/73 carried two honeycomb-type collimators. One contained magnets and was electron-rejecting, the other was not. The in-flight measured electron transmission

was 0.15 (this is shown in Fig. 2). The laboratory-measured transmission of this collimator was 0.02 for  $^{63}\text{Ni}$  electrons and 0.45 for  $^{90}\text{Sr}$  electrons. Thus, the  $^{90}\text{Sr}$  electrons, 50% of which have energies above 0.4 MeV, are more energetic than those encountered in flight, while the  $^{63}\text{Ni}$  electrons, with 65 keV maximum energy, are not energetic enough to reproduce the flight environment.

Even though neither source duplicates the natural electron spectrum, they can both be used to measure the relative transmissions of collimators made from different materials. We have made such measurements to find a material which will minimize electron scattering in the

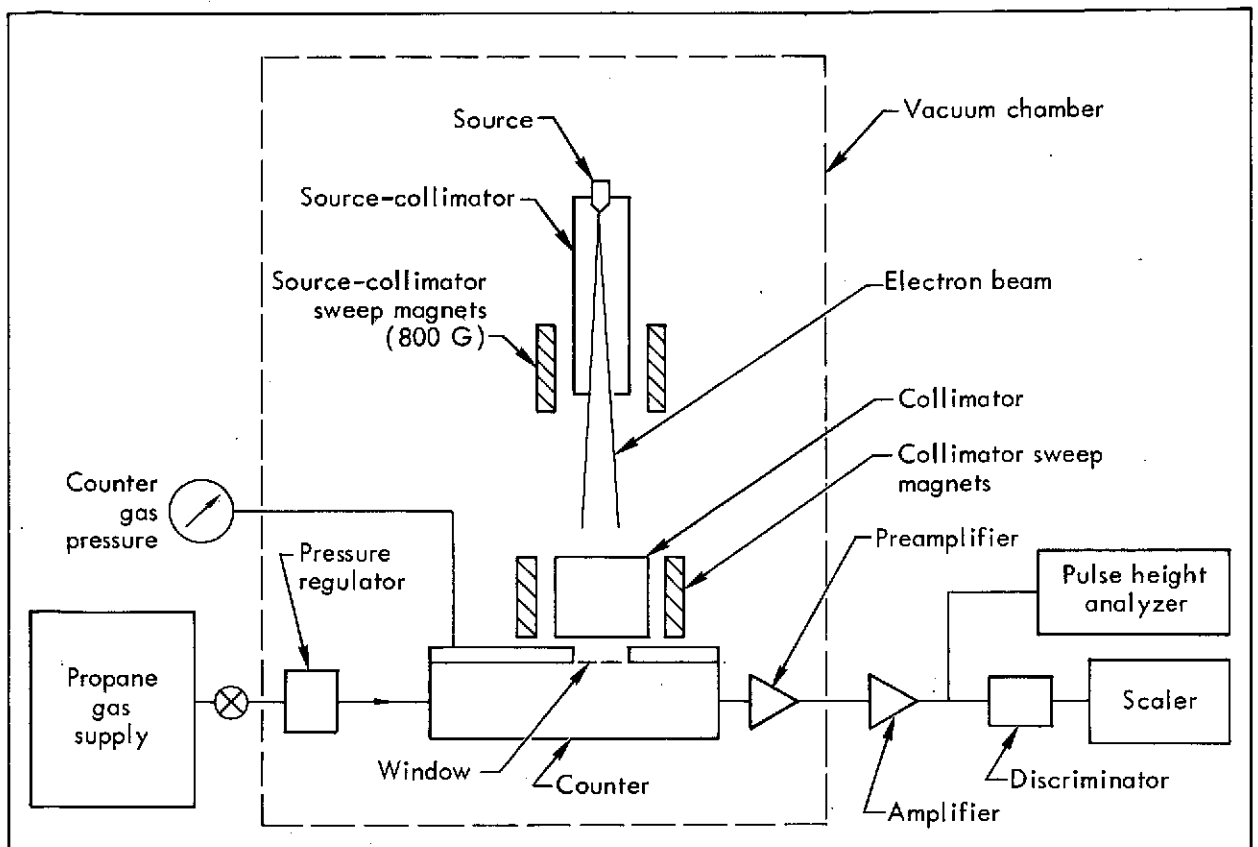


Fig. 16. Schematic of the laboratory apparatus for measuring electron transmission by a collimator.

collimator. For this purpose a series of slat-type collimator samples was constructed. All were of the same dimensions with collimator angle of  $2^\circ \times 12^\circ$  FWHM. The only parameter varied was the surface roughness of the vanes. The vanes were made with polished aluminum, expanded metal (aluminum sheet perforated with 1/8-in. holes), EDM aluminum (electric-discharge-machined), 100-line woven aluminum screen, and copper.

The variation of electron transmission with the strength of the magnetic sweep field is shown in Fig. 17 for  $^{63}\text{Ni}$  and  $^{90}\text{Sr}$  electrons. Here the effect of collimator surface roughness is apparent in the consistently lower transmission for

the EDM and screen collimators. Figure 18 shows the measured transmission of the electrostatic collimator. The vanes of this collimator were of copper-plated Synthane (printed circuit board material).

Figure 19 shows selected laboratory-measured transmissions plotted as a function of calculated no-scattering collimator cutoff energy. Note the appreciable transmission above the end-point energy of the  $^{63}\text{Ni}$  source. These are scattered electrons, as is obvious from the lower transmission with the rough EDM collimator vanes. The flight-measured transmissions are higher, indicating more energetic electrons.

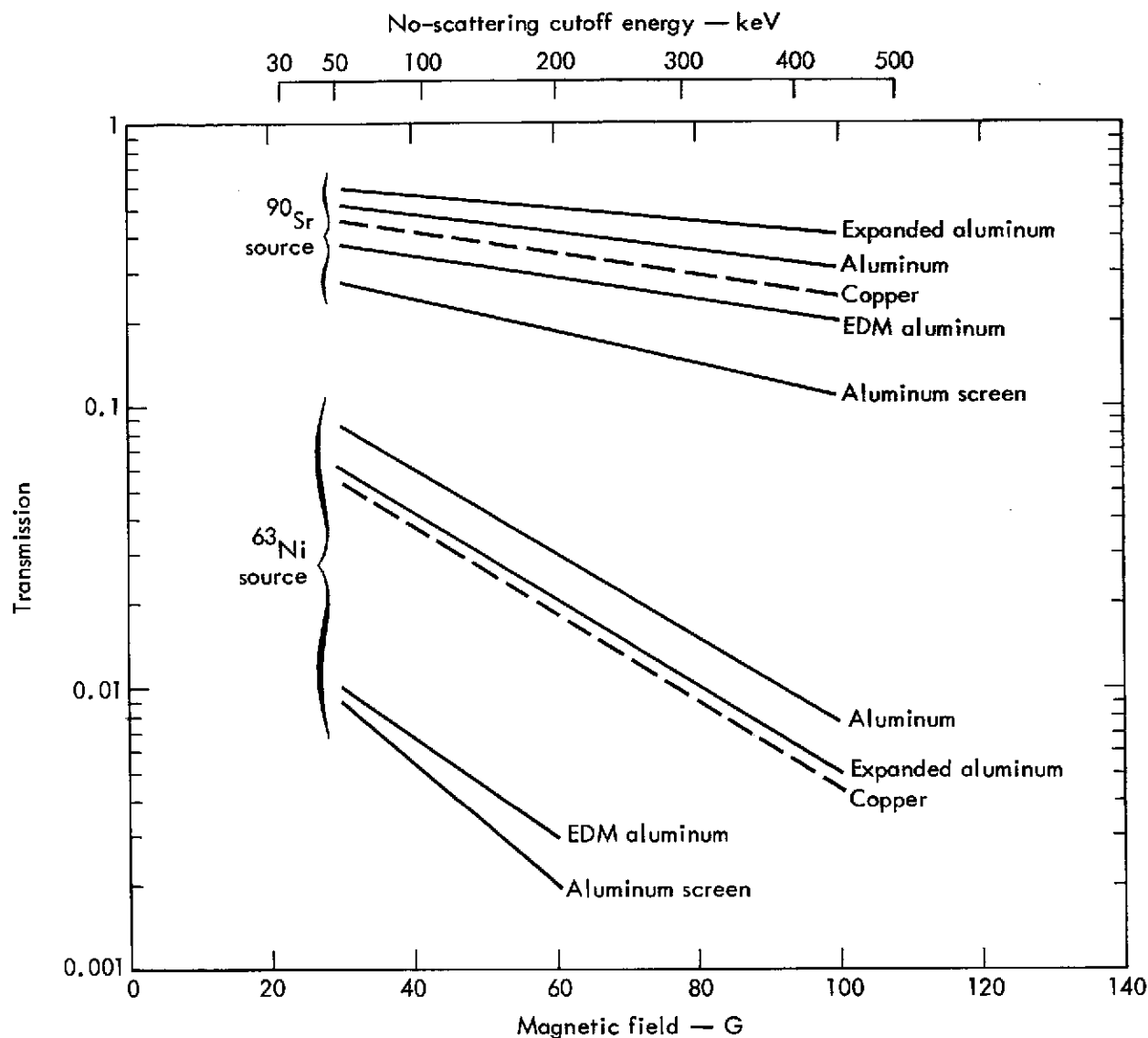


Fig. 17. Laboratory measurements of electron transmission by a collimator with magnetic electron rejection.

#### RECOMMENDATIONS FOR A GOOD COLLIMATOR

We draw the following conclusions concerning electron-rejecting collimators:

1. Electrostatic collimators are impractical. It is a nice feature to be able to turn them off and on in flight; but electron energies are high, requiring a high applied potential, and the consequent generation of soft x rays in the collimator creates more background counts than the collimator rejects.

2. For a magnetic collimator, the field should be as high as possible so electron rejection is at a maximum.

3. Rough-surfaced vanes are necessary to minimize electron scattering and reduce transmission. We found the construction of an aluminum screen collimator too difficult, so we are using EDM collimators for future flights.

4. Collimators with large open areas in the vanes do not reject high-energy

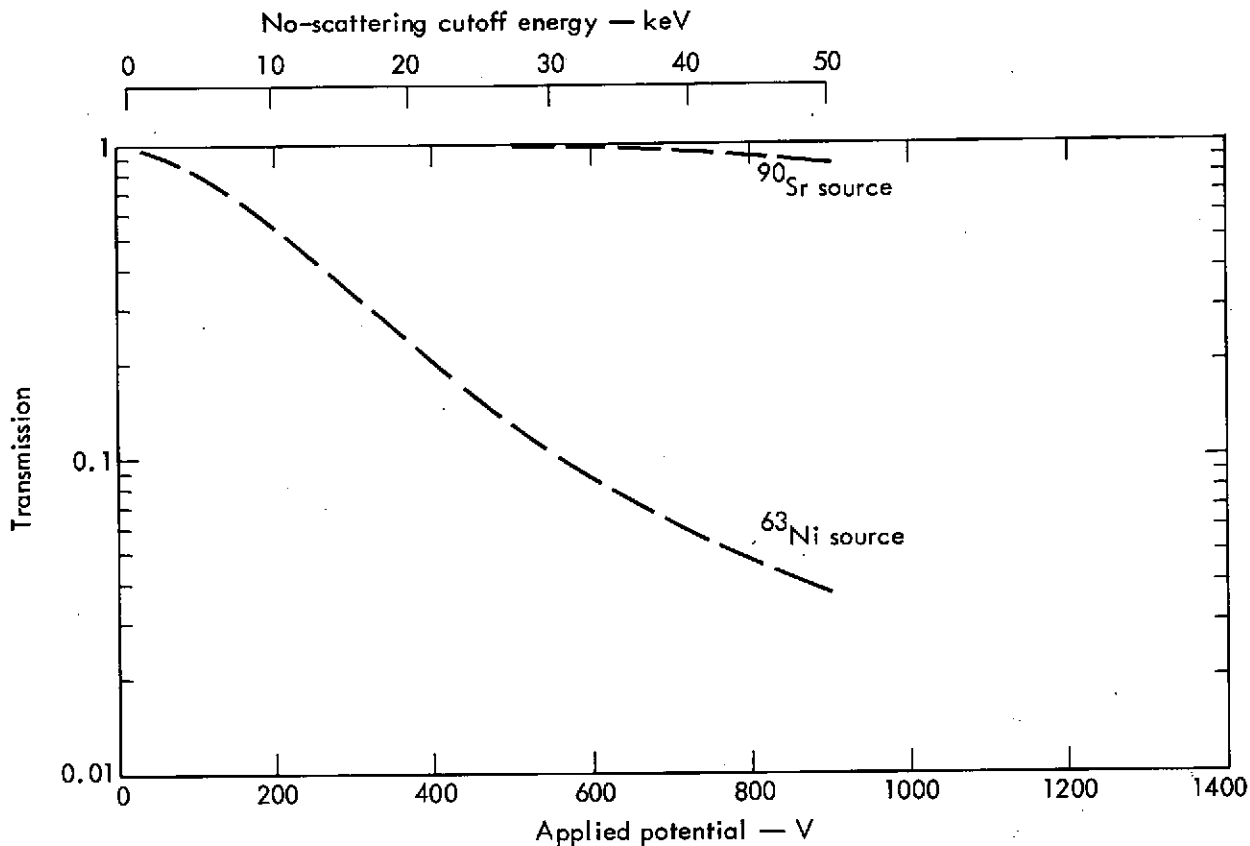


Fig. 18. Laboratory measurements of electron transmission by a collimator with electrostatic electron rejection.

electrons well. The openings permit more scattering than the solid vanes.

The best electron-rejecting collimator is one which will (1) keep the largest fraction of incident electrons out of the counter, and (2) have a low relative number of low energy counts produced by those electrons which do penetrate the collimator. It has been our experience

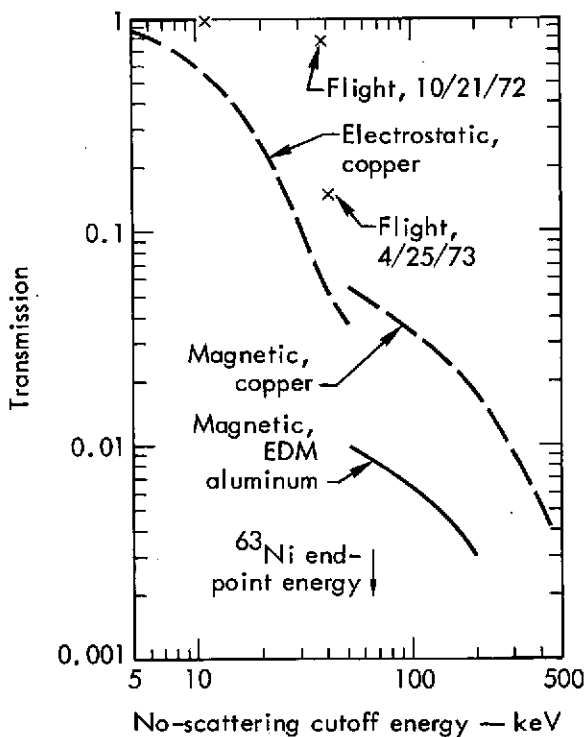


Fig. 19. Comparison of in-flight electron transmission with laboratory transmission measurements made with a  $^{63}\text{Ni}$  electron source.

that magnetic fields produce large rejection efficiencies and that collimator vanes with a rough surface (fine sandpaper texture) increase the rejection by reducing the probability of small-angle electron scattering. A rough surface also produces relatively fewer low energy events.

Our laboratory measurements and flight data lead us to believe that the electrons above the atmosphere can be

treated as having an average energy of  $\sim 100$  keV. If a collimator could be built to reject electrons of 100-150 keV in the laboratory (transmission  $< 10^{-3}$ ), the electron transmissions in flight would be negligible compared with the diffuse background. We think we can achieve this performance using a magnetic collimator constructed from EDM aluminum and with a field of  $\sim 200$  G.

## Predicting the Electron-Induced Background

This report summarizes data taken with different detectors, with a variety of collimators, at different places, and at different times. We have derived, as best we could, the average characteristics of the electron flux above the atmosphere and its effect on our detectors. Our conclusions have been presented in a form hopefully useful to x-ray astronomers, and they may be used to predict background rates on past and future observations. This naturally will not be a precise prediction, but a factor-of-2 accuracy might be expected. Our data applies to Kauai and may be taken as typical for mid-latitudes. Variation with location is expected and is given very approximately by Seward.<sup>1</sup>

The total electron-produced counting rate in a large-area proportional counter with an ordinary (non-electron-rejecting) collimator may be predicted as follows: First, the counter threshold is calculated using the window thickness, the range-energy curve of Fig. 8, and the discriminator setting. Figure 9 then gives the maximum expected rate at 300 km. The

variation of flux with altitude may be predicted from Figs. 6 and 7, and the variation with solar activity from Fig. 10, if these refinements are desirable.

To calculate the electron-induced background in the x-ray window, one obtains the electron rate at 1 keV by multiplying the predicted number of ULD events by an appropriate coefficient selected from Table 2. This coefficient will be between 0.1 and 0.8 depending on the collimator used. The spectrum induced by low energy electrons has the form  $dN/dE \propto E^{-1}$ , where E is energy deposited in the counter. This can be used to predict background levels throughout the x-ray window.

If an electron-rejecting collimator is used, the electron background will be reduced. The in-flight rejection efficiency will not be as good as the laboratory measurements shown in Fig. 19. The nonscattering cutoff energy of the collimator must be calculated to make this comparison, and a transmission intermediate between our  $^{63}\text{Ni}$  and  $^{90}\text{Sr}$  measurements can be expected.

## References

1. F. D. Seward, The Geographical Distribution of ~100-keV Electrons Above the Earth's Atmosphere, Lawrence Livermore Laboratory, Rept. UCRL-51456 (1973).
2. COSPAR International Reference Atmosphere 1965 (North-Holland Publishing Co., Amsterdam, 1965).
3. H. Kanter, Phys. Rev. 121, 461 (1961).
4. A. Nelms, Energy Loss and Range of Electrons and Positrons, NBS Circular No. 577 (1956).
5. D. Hamlin, R. Karplus, R. Vik, and K. Watson, J. Geophys. Res. 66, 1 (1961).
6. J. S. Lew, J. Geophys. Res. 66, 2681 (1961).

2. The Geographical Distribution of  
~ 100-keV Electrons Above the  
Earth's Atmosphere....F. D. Seward

N74-28248

UCRL-51456

**THE GEOGRAPHICAL DISTRIBUTION OF ~100-keV  
ELECTRONS ABOVE THE EARTH'S ATMOSPHERE**

F. D. Seward

October 3, 1973

This work was performed under the auspices of the U.S. Atomic Energy Commission

# THE GEOGRAPHICAL DISTRIBUTION OF ~100-keV ELECTRONS ABOVE THE EARTH'S ATMOSPHERE

## Abstract

Previously unpublished satellite data is used to show the distribution of ~100-keV electrons above the earth's atmosphere. Specific regions of high counting rate are

mapped at altitudes of 300 to 400 km. These regions are used to predict the suitability of various launch sites for rocket-borne x-ray astronomical experiments.

## The Problem

Modern soft x-ray astronomical observations are made with large-area proportional counters that have very thin plastic windows. The counters are consequently very sensitive to low energy electrons. An electron with only a few keV of energy can penetrate a typical window, and a flux of ~100 electrons/cm<sup>2</sup>-sec-ster can double the background counting rate during a typical observation.

Thus, these electrons produce an undesirable effect which, in the

observations we have made, is impossible to distinguish from x-ray data. Consequently, an electron-free region is needed for accurate astronomical observations.

We have derived geographical regions of weak electron flux from low altitude satellite data. These regions can be compared with the locations of rocket launching sites. The best sites should be those farthest from electron regions and can be selected from Figs. 1 and 2.

## Satellite Data

In late 1961 we flew particle detectors on four polar-orbiting satellites.<sup>1,2</sup> One detector consisted of a thin, 5 cm<sup>2</sup> cesium-iodide scintillator, covered by 0.002 in. of Be, with a 1-ster field-of-view. The satellite was in near-polar orbit so most of the surface of the earth was covered. The detector counting rates were sampled once a second, tape recorded, and read out once each orbit. The data analyzed were taken September 18 and 19, 1961, a geomagnetic quiet time. Satellite apogee

was 410 km at 32°S, perigee was 240 km, at 32°N.

The cosmic ray background in the detectors varied with latitude during the flight in a very consistent fashion. The times when the detectors counted at a rate above the cosmic ray background were noted to occur in specific geographic locations. These were placed on a map and contours of constant counting rate were drawn. Figures 1 and 2 are polar maps with the observed regions of higher

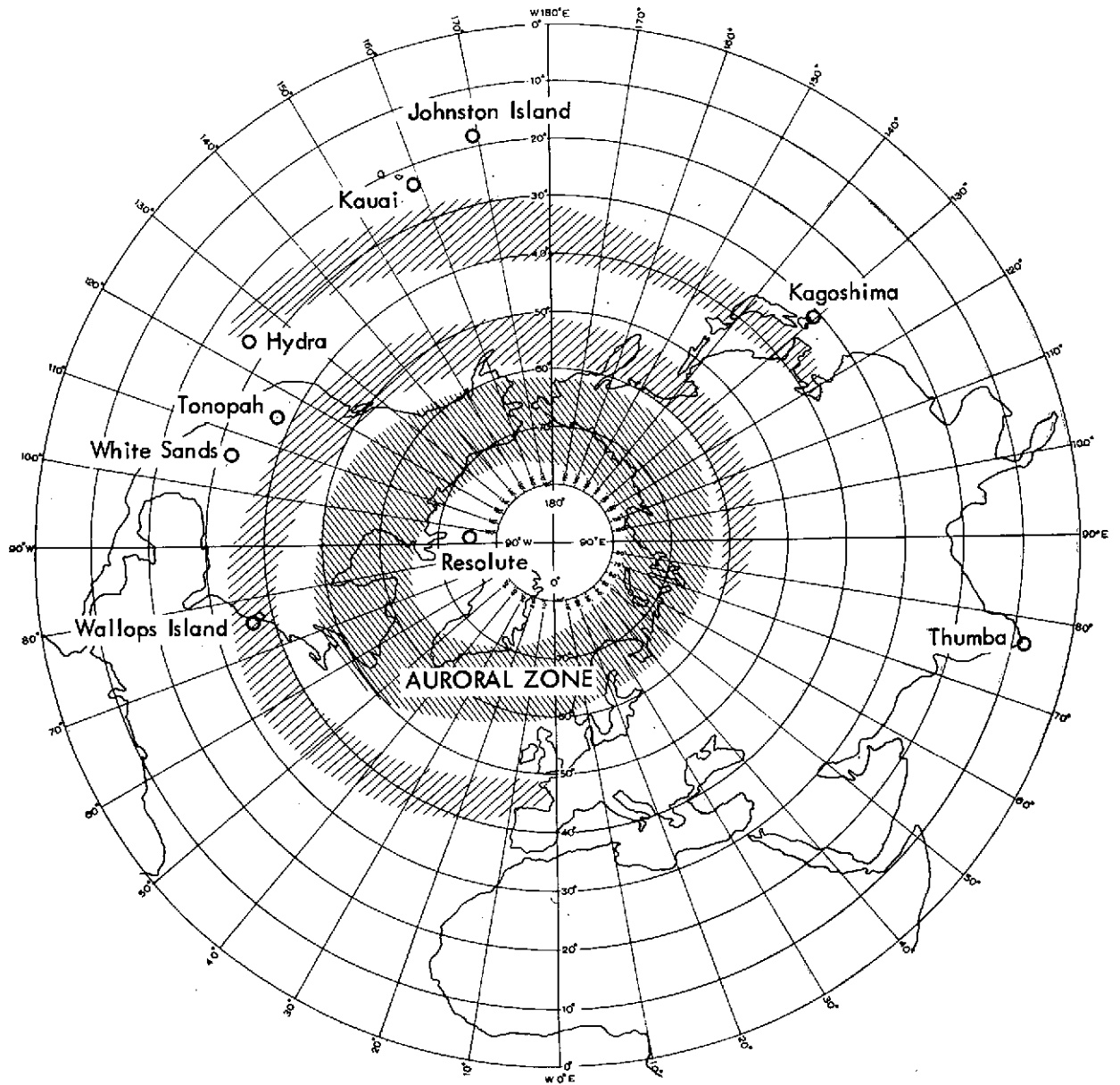


Fig. 1. Regions of high electron flux—northern hemisphere.

counting rate superimposed. The counting rates at a given spot varied with time. Nevertheless, the figures show fairly accurately locations at which particles other than cosmic rays were present. These particles were, in all probability, electrons with energies greater than the

threshold of the detector. Counting rates were highest over the South Atlantic and in the auroral zones. Obviously, these regions are the worst choices for low background experiments and they should be avoided. We wish to direct attention to other low latitude regions of weak

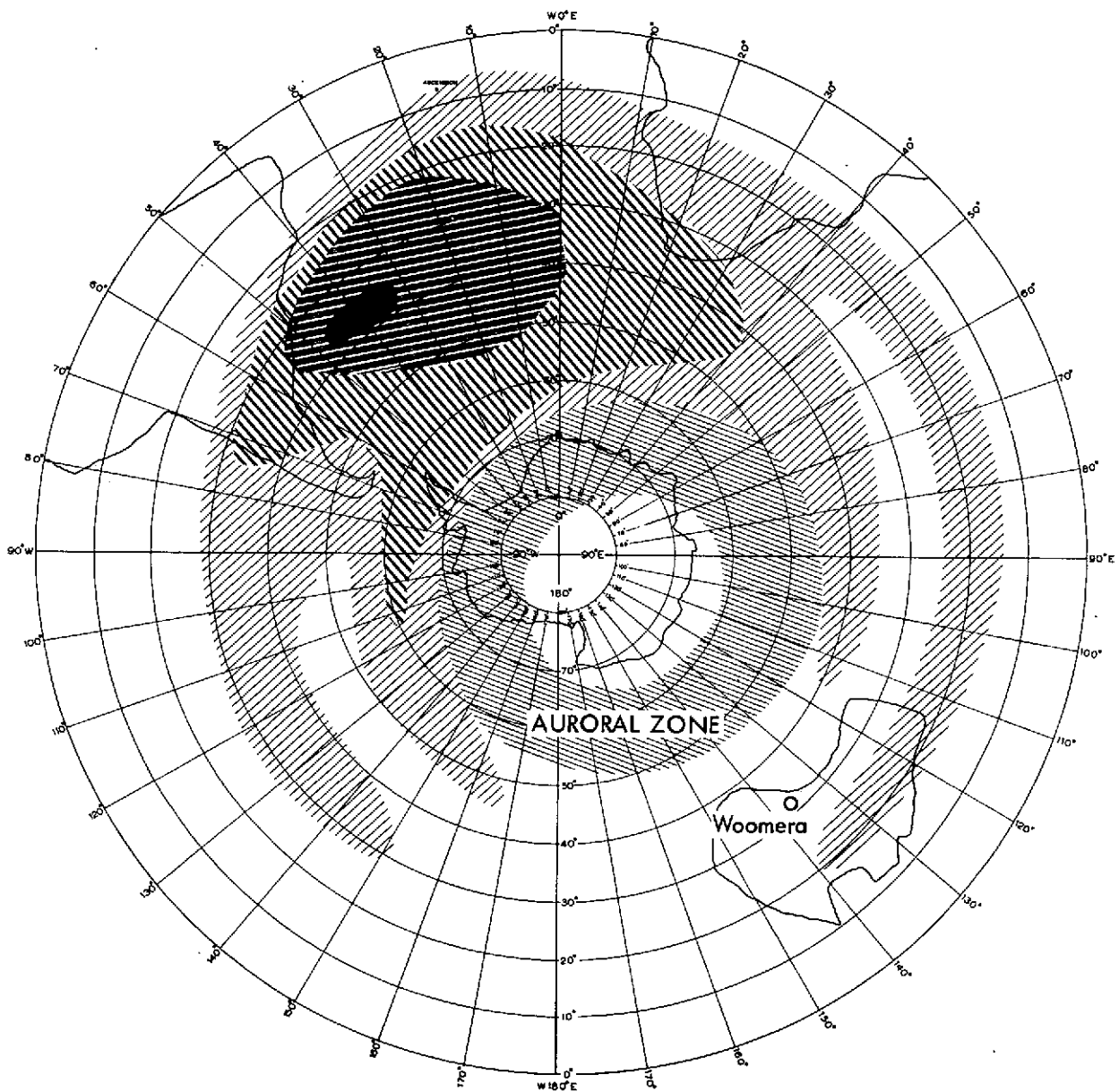


Fig. 2. Regions of high electron flux—southern hemisphere.

electron flux that have not been studied previously.

The observed counting rates were transformed to omnidirectional flux and contours of constant counting rate were plotted in geomagnetic coordinates.<sup>3</sup> Figure 3 shows this plot. Since the

observed electron flux was variable, the flux levels assigned to these contours were not very accurate. There are three regions of high flux distinguishable in Fig. 3.

Since the electron spectrum is steep and energy thresholds of x-ray detectors

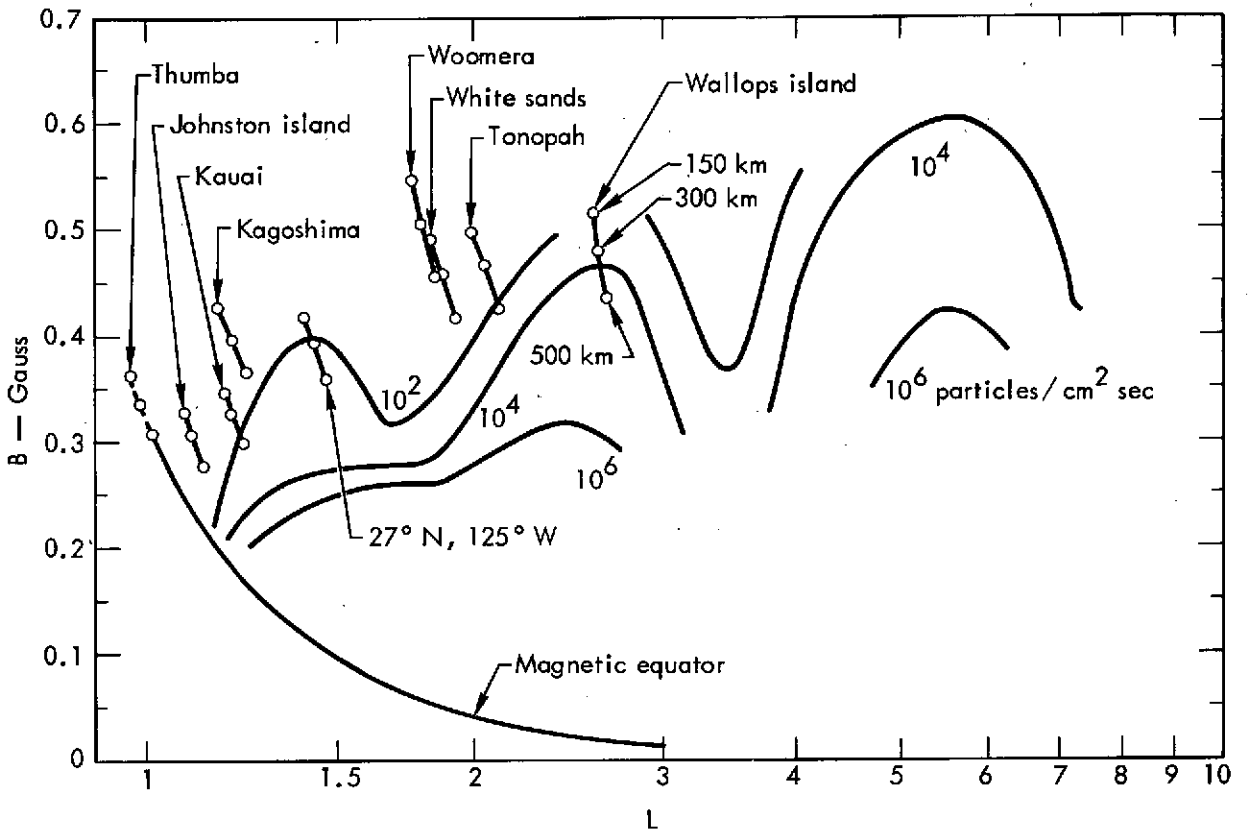


Fig. 3. Data from satellite 1961  $\alpha\beta$  showing omnidirectional flux of electrons with energies  $> 100$  keV.

are less than 100 keV, counting rates will be higher than the rates predicted from the contours of Fig. 3. If the detector threshold were  $\sim 100$  keV for electrons,  $10^2$  particles/cm<sup>2</sup>-sec omni-

directional flux would transform to  $\sim 50$  counts/cm<sup>2</sup>-sec-ster in the detector. (Our collimator geometry and the observed electron pitch-angle distribution have been used to make this comparison.)

## Launching Sites

Figures 1 and 2 show geographic locations of several sites that have been used for x-ray astronomy flights. A rocket launched straight up from one of these locations will follow the magnetic space trajectory indicated in Fig. 3. Points are given for each site at altitudes of 150, 300, and 500 km. The

Thumba range is right on the magnetic equator. The L values shown for Thumba at low altitudes are inexact. Resolute lies at  $L > 10$  and L varies. It is inside the northern auroral zone and should be free from the high auroral electron flux much of the time. However, this region is directly connected to interplanetary

Table 1. Rocket observations of electrons.

Reference	Range	Altitude (km)	Energy threshold (keV)	Flux (counts/cm <sup>2</sup> -sec-ster)	Magnetic activity
Cladis <i>et al.</i> <sup>4</sup>	Wallops Island	1000	50	~10 <sup>6</sup>	?
Hill <i>et al.</i> <sup>5</sup>	Kauai	160	3.5	~500	high
Hill <i>et al.</i> <sup>5</sup>	Johnston Atoll	300	3.5	~800	high
Turiel and MacGregor <sup>6</sup>	27°N, 125°W	225	20	~10	high
Hayakawa <i>et al.</i> <sup>7</sup>	Kagoshima	800	5	~150	quiet
Tuohy and Harries <sup>8</sup>	Woomera	200	20	~2	high

space and subject to incoming low energy solar particles. We observed

these particles from 1961  $\alpha\beta$  but have not shown them in the figures.

### Comparison with Rocket Data

Several groups have reported detecting electrons over the rocket ranges considered. Table 1 lists their observations. For comparison, maximum electron counting rates have been roughly derived from the data given in the individual papers. These rates must be divided by counter efficiency to get the actual electron flux.

Since the electron spectrum is very steep and flux varies with magnetic activity, it is impossible to predict electron fluxes precisely from Fig. 3. Nevertheless, Fig. 3 shows why high electron fluxes are expected at low altitude over Wallops Island, why electrons are apparently not seen at low altitude over White Sands, and why our launch site at Kauai is intermediate between these two locations.

### Conclusions

The best x-ray astronomy ranges are probably Thumba, White Sands, and Woomera. Wallops Island is one of the worst ranges to use for soft x-ray observations.

As rocket altitude increases, over any range, the number of electrons encountered will also increase.

## References

1. F. Seward and H. Kornblum, Near Earth Charged-Particle Backgrounds Measured with Polar Orbiting Satellites, Lawrence Livermore Laboratory, Rept. UCRL-6693 (1963).
2. F. Seward and H. Kornblum, J. Geophys. Res. 70, 3357 (1965).
3. R. Harrison, K. Hubbard, F. Keller, and J. Vette, Plots of Constant B and Constant L for Various Longitudes, Aerospace Corporation, Los Angeles, Rept. TDR 169 (3510-41) TR4 (1963).
4. J. Claidis, L. Chase, W. Imhof, and D. Knecht, J. Geophys. Res. 66, 2297 (1961).
5. R. Hill, R. Grader, F. Seward, and J. Stoering, J. Geophys. Res. 75, 7267 (1970).
6. I. Turiel and A. MacGregor, An Observation of Mirroring Electrons at Low Altitudes, Lawrence Livermore Laboratory, Rept. UCRL-72615 (1970).
7. S. Hayakawa, T. Kato, T. Kohna, T. Murakami, F. Nagase, K. Nishimura, and Y. Tanaka, J. Geophys. Res. 78, 2341 (1973).
8. I. Tuohy and J. Harries, Observation of Electrons at Midlatitude During a Magnetic Storm, to be published in J. Geophys. Res.

3. Quasitrapped Electrons in the Low L Region. Preliminary Results of a Rocket Observation on Jan. 22, 1974  
....S. Hayakawa, T. Kohno, F. Nagase  
and Y. Tanaka

N74-28249

Quasitrapped Electrons in the Low L Region

Preliminary Results of a Rocket Observation on Jan. 22, 1974

S. Hayakawa, T. Kohno, F. Nagase and Y. Tanaka  
Department of Physics, Nagoya University, Nagoya, Japan

Suprathermal electrons in the energy range 5 - 100 keV were measured with thin-window proportional counters on board a sounding rocket L-3H-8 launched from Kagoshima Space Center at 2000 JST (1100UT) on January 22, 1974. The flux of the electrons was found to increase with altitude in the range 100 - 550 km, corresponding to  $L = 1.15 - 1.22$ , the angular distribution to be peaked in the direction perpendicular to the geomagnetic line of force, and the energy to be represented by a power law. These features are similar to those which were observed in our earlier flights with L-3H-7 (Hayakawa et al 1973) and K-9M-40 (Kohno 1973). But the absolute flux was in between the fluxes observed in the earlier experiments. The results to be presented in what follows are preliminary, since data are not completely analyzed yet.

The payload in the present experiment was similar to the one on board L-3H-7 except for the following points. The axes of the field of view of two proportional counters were perpendicular to the rocket axis and to one another. The thickness of carbon-coated polypropylene window of each counter

was  $45 \mu\text{g}/\text{cm}^2$ . The field of view was  $10.2^\circ(\text{FWHM}) \times 3.1^\circ$  (FWHM), the long dimension being parallel to the rocket axis, and the effective area was  $S = 55 \text{ cm}^2$ , and  $S\Omega = 0.53 \text{ cm}^2\text{sr}$ . No electrostatic field for electron rejection was applied, because it had been found ineffective. The same servocontrolled gas supply system was used as before.

Pulse heights measured with these two counters were telemetered through IRIG channels No.12 and No.14, respectively. Channel 14 was switched off at 200 seconds after launch (altitude 503 km) for making it available for another experiment, and the telemeter malfunctioned at 213 seconds after launch (550 km). Pulses through low and high gain amplifiers were transmitted in a time sharing basis, for 1.08 sec through low gain and 3.24 sec through high gain, and 0.34 sec in the high gain period of channel 12 was used to transmit calibration signals. The energy ranges measured correspond to 7 - 200 keV and 1.5 - 40 keV, respectively.

The nose cone of the rocket was ejected at 85 km altitude. Since signal was noisy during properant burning, data in the altitude range 160 - 235 km were discarded. The spin period after burn-out was measured with a magnetometer to be 826 m sec.

The counting rate measured through a high gain channel of No.12 was  $22\pm 2$  c/s before the nose cone ejection, and

immediately thereafter it increased to  $26\pm 2$  c/s. The former is considered to be due to background caused mainly by cosmic-rays, whereas an increase indicates the contribution of cosmic X-rays. The counting rate at about 300 km altitude is about 100 c/s and is considered to be due mostly to electrons. Around and above this altitude the counting rate vs rocket azimuth showed two peaks at which the field of view crossed directions perpendicular to the geomagnetic line of force. The counting rates at the peaks increased rapidly with altitude, and their values above 500 km were so large that the conventional procedure of dead time correction would give rise large errors. In order to show this dramatic increase, data through channel No.12 are presented.

The directional dependence of the electron flux is obtained by summing up the number of counts  $n$  in a given angular bin for each spin measured in an altitude range and by dividing it by the sum of live times  $t_1$  measured,

$$F = \frac{\sum n}{\sum t_1} \quad (1)$$

A mathematical analysis of random processes with dead time, which was worked out in collaboration with F. Makino, shows that Eq.(1) gives a correct procedure of dead time correction. A statistical error is different from the one in the Poisson

distribution. Since the time corresponding to the angular bin of  $5^\circ$  is 11.6 ms which is only slightly longer than the dead time of 8 ms, such a procedure is important for obtaining the true flux of electrons.

The angular dependences corrected for the dead time effect in five altitude ranges are shown in Fig.1. Azimuth angles  $90^\circ$  and  $270^\circ$  correspond to west and east directions perpendicular to the magnetic line of force, respectively. At  $180^\circ$  the counter axis is southward and closest to the upward line of force. In the angular range between SEE and NWW the field of view is partly covered by the earth.

In the lowest altitude range, 130 - 160 km, the flux shows a broad maximum in the direction nearer to the upward magnetic line of force. This is consistent with the angular dependence observed by Hill et al (1970) in the same altitude range.

As the altitude increases, the southward maximum splits into two peaks at about  $90^\circ$  and  $270^\circ$ . The western peak is higher than the eastern peak below 400 km, and they show essentially the same heights thereabove. The FWHM of the peak is about  $40^\circ$  independent of altitude. Since the FWHM expected from the angular width of the collimator is about  $15^\circ$ , the pitch angle distribution of the electrons has a finite width of about  $20^\circ$ . In the southward valley the flux is about three times higher than the background flux and is essentially independent of altitude.

The flux in the northward valley is negligible below 300 km except for a small hump in NW. The hump grows with altitude in parallel to the peak, and the flux in the NE valley also increases gradually but does not exceed that in the southward valley.

The altitude dependences in these four angular ranges are shown in Fig.2. Only the southward component, which represents the flux streaming downward along the line of force, is independent of altitude. The trapped component represented by two peaks and the northward component show a similar altitude dependence if the background is subtracted.

These components show different energy spectra, as one can see from Fig.3. The spectra of the southward and two northward components are essentially the same above 5 keV not only for their shape but also for the absolute flux. The difference in their flux values arise from the measured energy region below 5 keV, below which the transmission probability of electrons through the counter window begins to decrease. Bending of the spectrum of the NE component toward low energy indicates a higher cut-off of the electron spectrum at about 7 keV. The spectrum of the NW components becomes flat below 3 keV, whereas flattening of the southward component takes place at about 5 keV. A power law of the spectrum applies to

these component between 7 keV and 50 keV. The spectrum above 10 keV is obtained also with a low gain channel, and it agrees with that of high gain in the overlapping region.

The spectrum of the trapped component appears to be somewhat complicated. In comparison with a power law-spectrum, turn-over in the low energy region is observed around 7 keV in the 495-550 km range, whereas a turn-over energy is lower in the 410-490 km range. Steepening at high energy may be due to penetration of particles through the counter gas. Incidentally, the energy loss of a relativistic particle penetrating the counter gas of 2.5 cm is 12 keV, and the electron energy corresponding to the range of 2.5 cm in the counter gas is about 40 keV. Taking into account the oblique incidence and range straggling due mainly to scattering in the gas, we estimate that the energy loss spectrum up to 70 keV approximately represents the energy spectrum of electrons.

The present result can be compared with the results obtained by two earlier experiments since both altitude and energy ranges overlap with each other.

In the L-3H-7 experiment at 2100 on September 3, 1971 the maximum energy measured was 3 keV, and incident electrons with energies 5 - 7 keV were mainly observed after penetrating window film with a small probability. If the intensities are compared in the measured energy range 2 - 3 keV, the electron flux observed by the present experiment was about a half of that by L-3H-7, and the altitude and angular dependences were similar to each other.

By the K-9M-40 experiment we found two components, trapped and precipitating. In the present experiments the existence of these two components was confirmed, but there seem to be the northward component whose low energy flux increases with altitude. In the overlapping altitude range the relative flux values of these two components were similar to each other, but the absolute flux in the present experiment was about twice larger than the earlier value.

In all these three cases both magnetic and solar activities were quiet at the times of launch and during a week before launch.

#### References

- Kohno T., J. Geomag. Geoelectr., 25, 131 (1973).  
Hayakawa, S., Kato, T., Kohno, T., Murakami, T., Nagase, F.,  
Nishimura, K. and Tanaka, Y., J. Geomag. Geoelectr., 25, 113 (1973).  
Hill, R.W., Grader, R.J., Seward, F.D. and Stoering, J.P.,  
J. Geophys. Res., 75, 7267 (1970).

## Figure Captions

Fig.1. The directional dependences of the electron intensity in five altitude ranges. The azimuthal angle in the rocket frame of reference is so chosen that the direction inclined toward south by about  $50^\circ$  with respect to the geomagnetic line of force is  $180^\circ$  and the westward and eastward directions perpendicular to the line of force are  $90^\circ$  and  $180^\circ$ , respectively. The solid line is obtained by the running average of the counting rate corrected for dead time observed through the high gain channel in each  $5^\circ$  bin.

Fig.2. The altitude dependences of the electron intensities in the NW( $0^\circ$ - $50^\circ$ ), NE( $310^\circ$ - $360^\circ$ ), peak ( $70^\circ$ - $110^\circ$ ,  $250^\circ$ - $290^\circ$ ), and southward ( $150^\circ$ - $210^\circ$ ) directions. The counting rate is corrected for dead time, whereas the error bar represents  $\sqrt{N_c}$ , where  $N_c$  is the corrected counts in the given altitude range. A correct variance for 500 c/s is about twice larger than the error bar drawn. The background counting rate represented by a horizontal line is obtained from data before nose cone ejection.

Fig.3. The energy loss spectra in given altitude and azimuth angle ranges as indicated. Points with dotted bars are based on data of the low gain channel. The spectra between 10 and 70 keV are essentially equal to those of electrons, whereas those in the lower energy region are affected by the penetration through window film, and those in the higher energy region by the penetration through counter gas.

Fig. 1

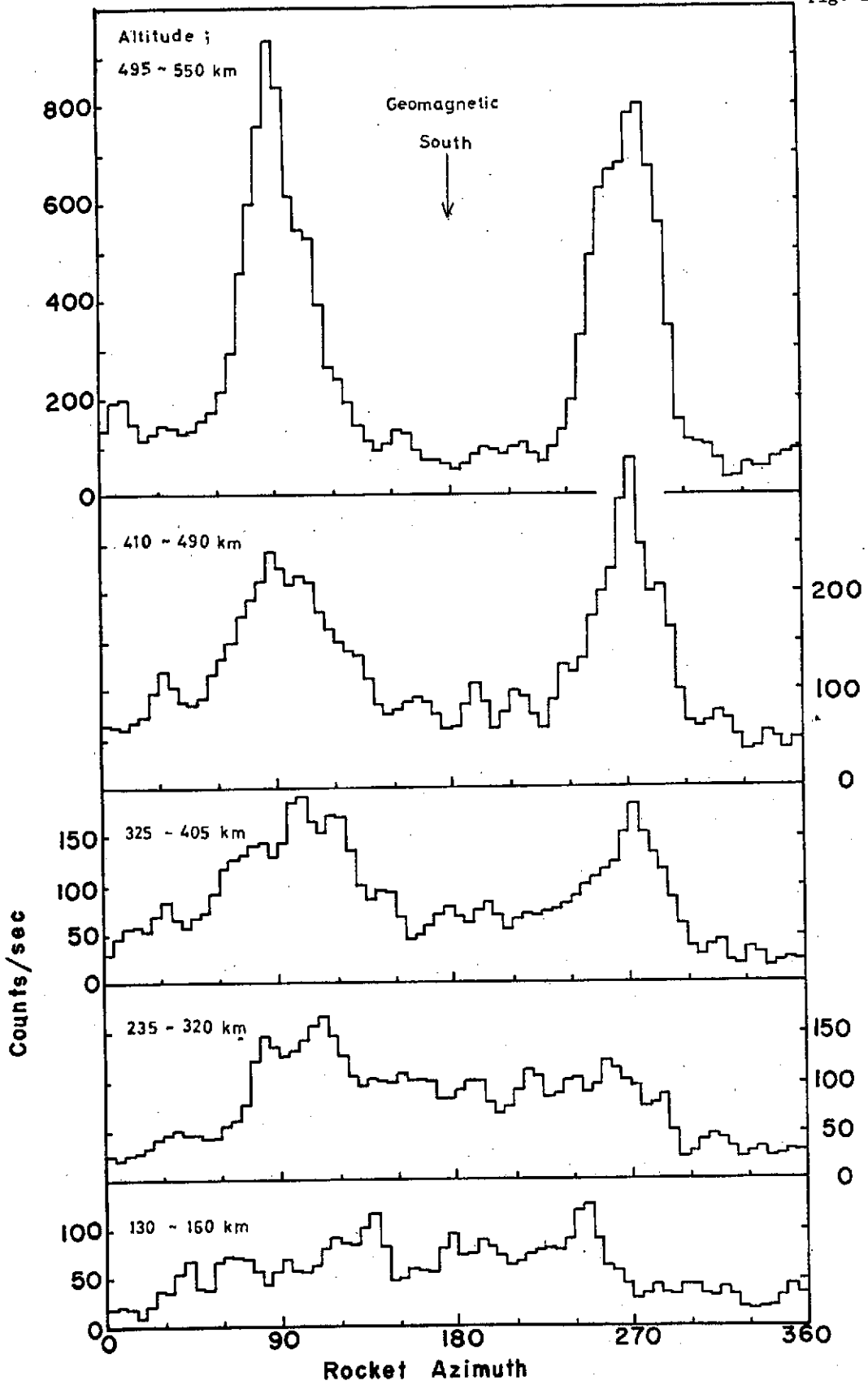


Fig. 2

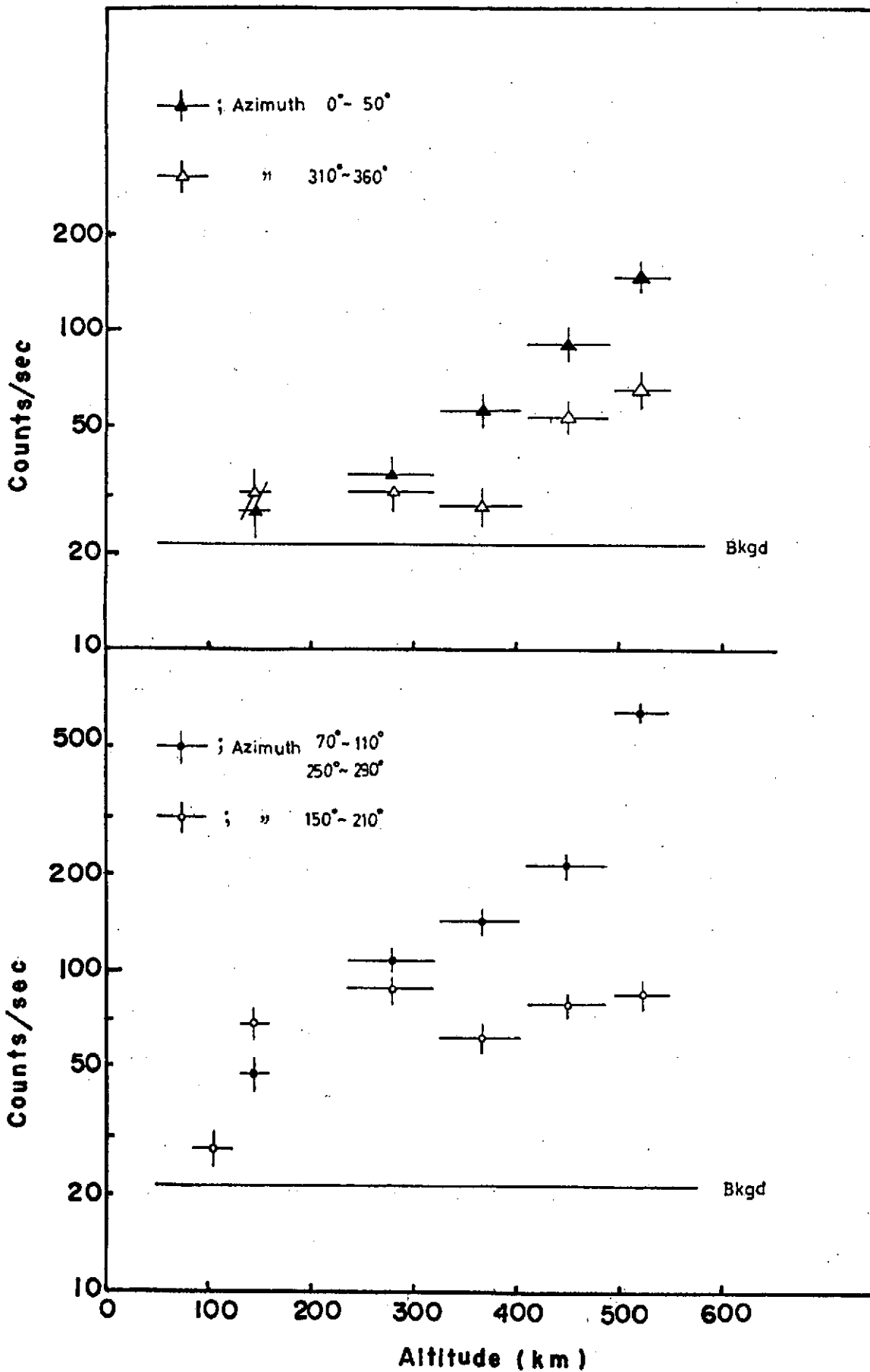


Fig. 3a

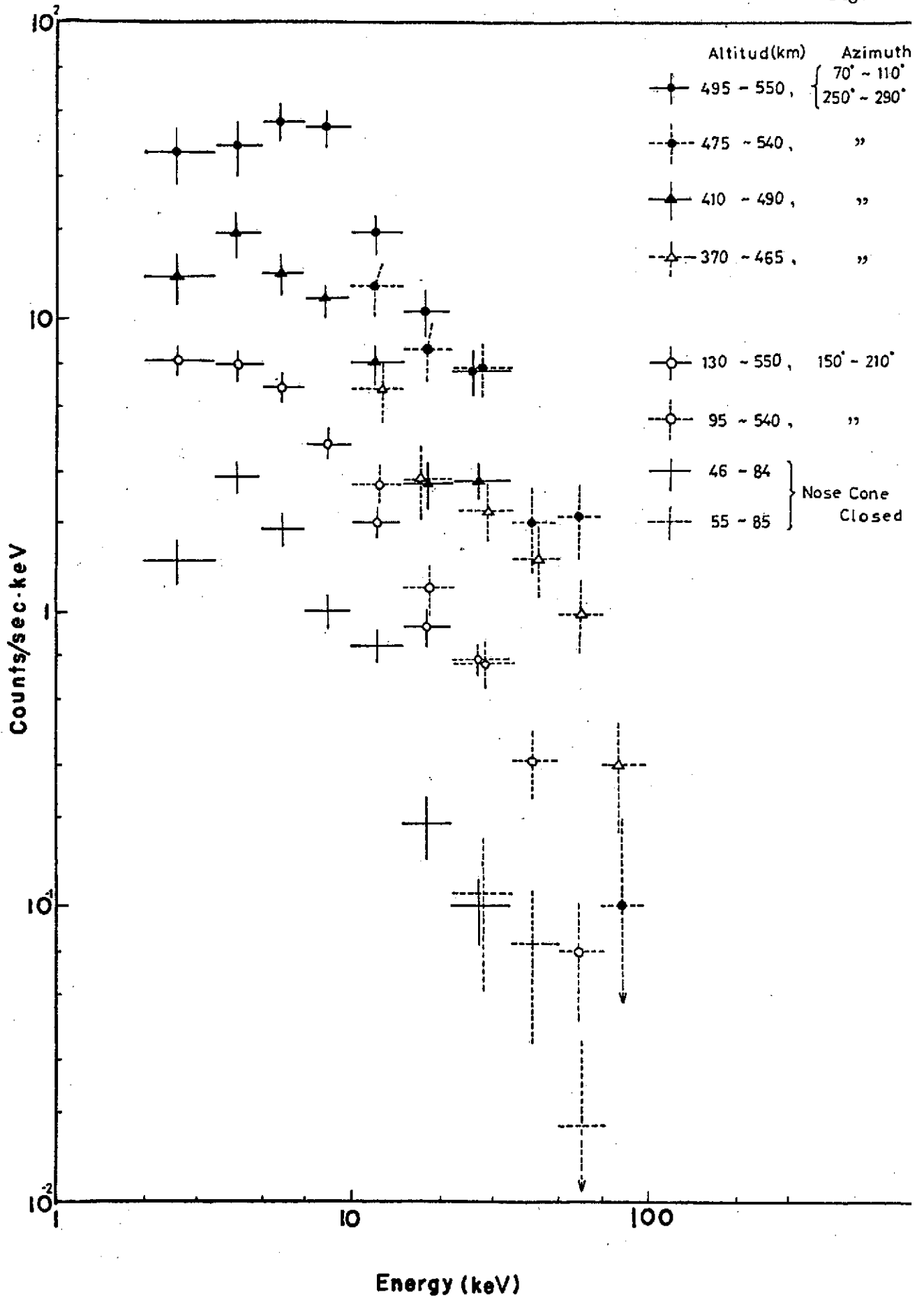
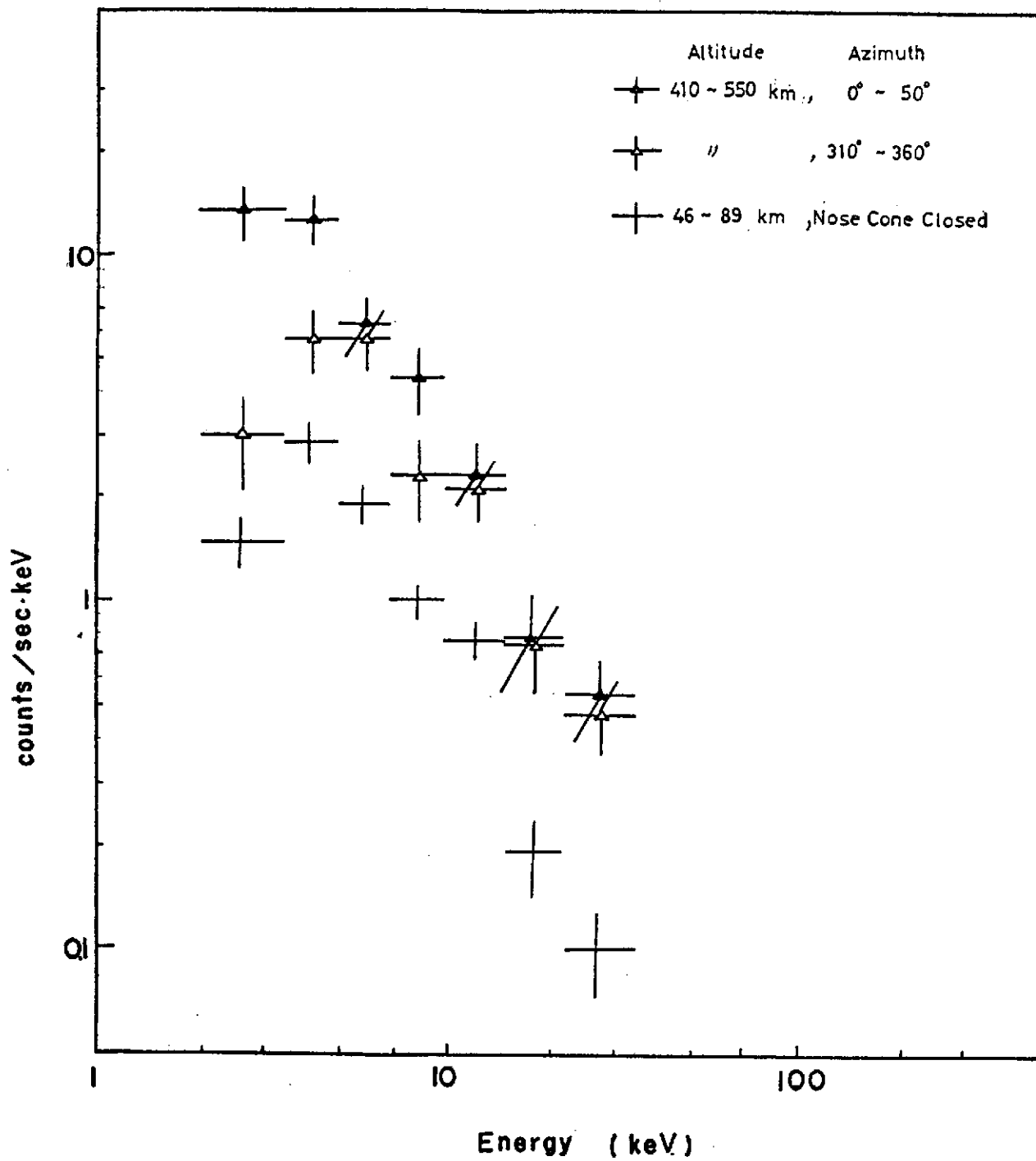


Fig. 3b



N24-28250

4. Low Energy (10eV to 10 keV) Equatorial Particle Fluxes....J. D. Winningham (including Soft Particle Fluxes Near the Equator....W. J. Heikkila)

## LOW ENERGY (10eV to 10keV) EQUATORIAL PARTICLE FLUXES

In this report three things will be done. The first will be corrections and additions to the paper entitled "Soft Particle Fluxes near the Equator" by W.J. Heikkila (attached as Appendix A) which was based on ISIS-1 satellite data. The second part will deal with preliminary data obtained from a sounding rocket launched at the magnetic equator (Lima, Peru). Finally, conclusions relative to x-ray contamination will be drawn.

### ISIS-1 Results

In the third paragraph of Heikkila's paper the pitch angle distribution of equatorial particle fluxes was discussed. Due to erroneous magnetometer data the pitch angles used in this discussion were wrong. Reexamination of the magnetometer data reveals that the two peaks in the angular distribution lie at the extrema of the angular scan ( $\sim 70^\circ$  and  $110^\circ$ ), not at  $90^\circ$ . Thus the anomalous angular behavior disappears. The complete angular distribution is thus unknown because of the incomplete angular scan relative to the magnetic field.

In Figure 1 several spectra are shown that represent one rotation of ISIS-1. Spectra 1, 2, 3 represent particles moving down the field line into northern ionosphere and spectra 4, 5, 6 represent particles moving up field lines towards the magnetic equator, i.e. the former are "direct" fluxes and the latter are "albedo" fluxes. The spectra observed are remarkably similar to those observed in the auroral zone. The "direct" fluxes exhibit a relative maximum in the few keV range and the "albedo" a power law spectrum with increased fluxes at low energies

(i.e. added secondaries). This behavior is remarkable since most auroral acceleration mechanisms are assumed inoperative at the equator. Even with the improved data from the sounding rocket the source and acceleration of these particles is a mystery.

Examination of concurrent topside sounder data on ISIS-1 revealed a positive correlation between a region of turbulent (i.e. non equilibrium) ionosphere and particle fluxes. This ionospheric condition is referred to as equatorial spread F and has been studied extensively with bottomside ionospheric sounders and backscatter radars.

The perigee of ISIS crossed the magnetic equator at four local times (0400, 1000, 1600, 2100) during the lifetime of the particle spectrometer. No fluxes were observed at 0400 and 1000 local time. At 1600 a few instances of particles were observed. At 2100 essentially all passes included detectable equatorial fluxes. This is in agreement with the frequency of occurrence of equatorial spread F.

It should be kept in mind that the total number of ISIS-1 equatorial passes available was less than 100, thus the statistical accuracy is poor. Because of this poor sampling no statement can be made on seasonal dependence.

Longitudinally the strongest fluxes were observed from Africa to western South America with the weakest observed in the Indian sector. Again the statistical accuracy of these statements are poor due to the limited data set.

#### Sounding Rocket Results

On March 28, 1974 at 2100 local time a Black Brant IV B was launched from the magnetic equator (the Chilca Rocket Range, south of Lima, Peru) into an equatorial spread F event. Spread F was observed from ~270 to 450 km with the

Jicamarca incoherent backscatter radar. Spatially coincident with the spread F fluxes of 10eV to 12keV electrons were observed. Figure 2 shows typical spectra observed. They are quite similar in shape and magnitude to those observed with ISIS-1 (see Figure 1). Preliminary magnetometer data indicates that the spectra labeled Spin Max correspond to particles moving away from the magnetic equator ("direct") and Spin Min to those moving towards the magnetic equator. The angular scan of the rocket was essentially complete and indicates that the "direct" fluxes are nearly isotropic. This is indeed surprising because of the low altitude of the measurement, i.e. essentially in the absorbing layer.

A VLF/ELF receiver on the rocket indicated broad band emissions to be present in the region of particles and spread F. Equatorial VLF emissions have been observed previously by Gurnett with the INJUN 3 satellite..

#### Conclusions Pertinent to X-ray Contamination

It was pointed out at the symposium that methods for rejecting particles of less than 100keV in x-ray detectors have been developed. Thus the data (10eV to 12keV) I present simply gives a measure of what has to be rejected to what level. Extrapolation of the spectra I present to higher energies would be meaningless. A more concrete approach would be to survey all data available in the 100keV and above range from satellites with perigees less than 1000 km. Presumably some best "safe haven" launch site could be chosen based on this survey.

Some effort at failure cross-fertilization would seem to be in order between particle and x-ray measurements. Each has something that could be constructive to the other.

ISIS I  
20 FEBRUARY 1969

ORBIT 242

TIME

$\theta_p$

1	—	20:50:47	74°
2	- - -	20:50:49	77°
3	.....	20:50:51	84°
4	- · - · -	20:50:53	93°
5	- - -	20:50:55	101°
6	- · - · -	20:50:57	103°

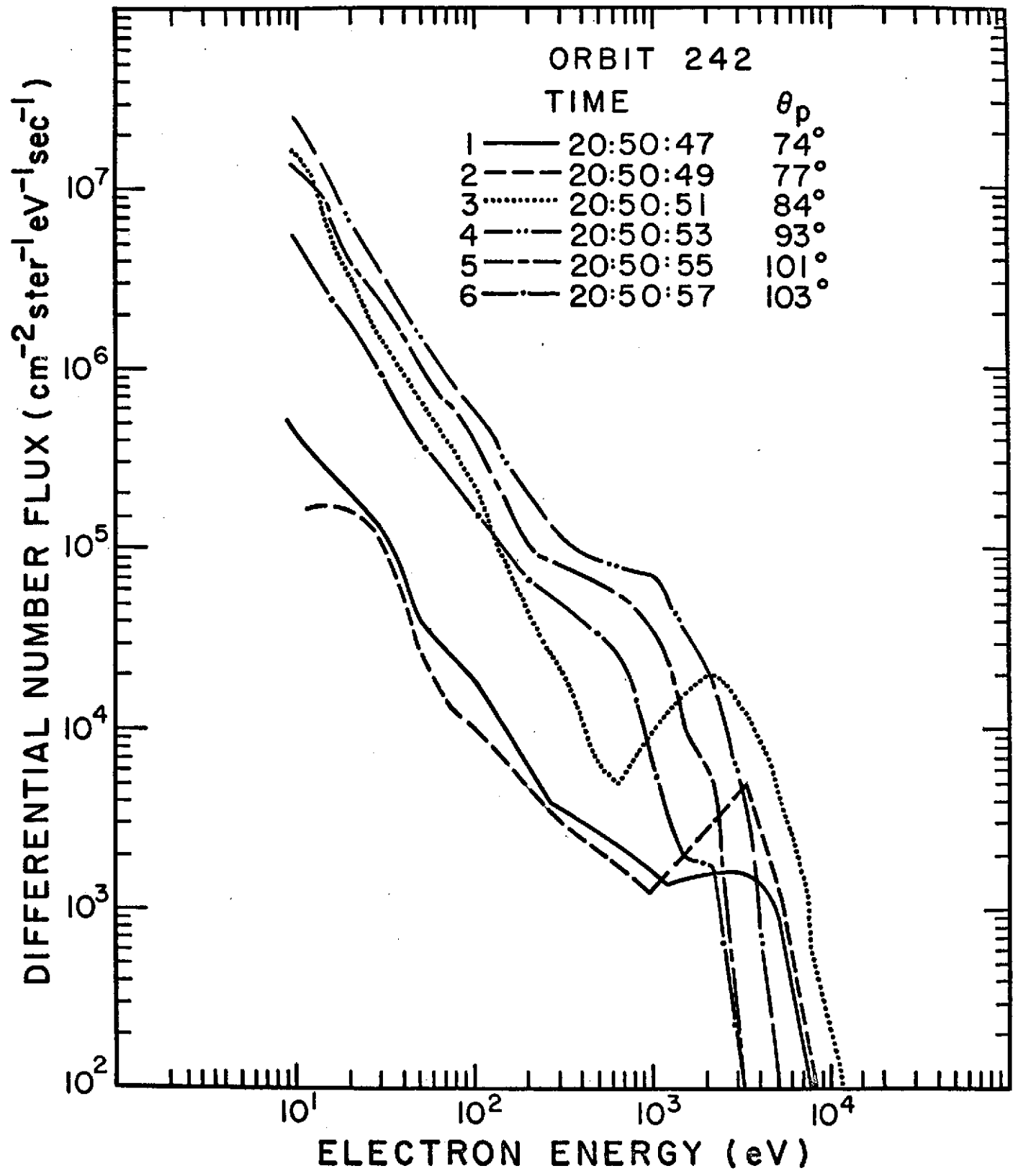


Figure 1

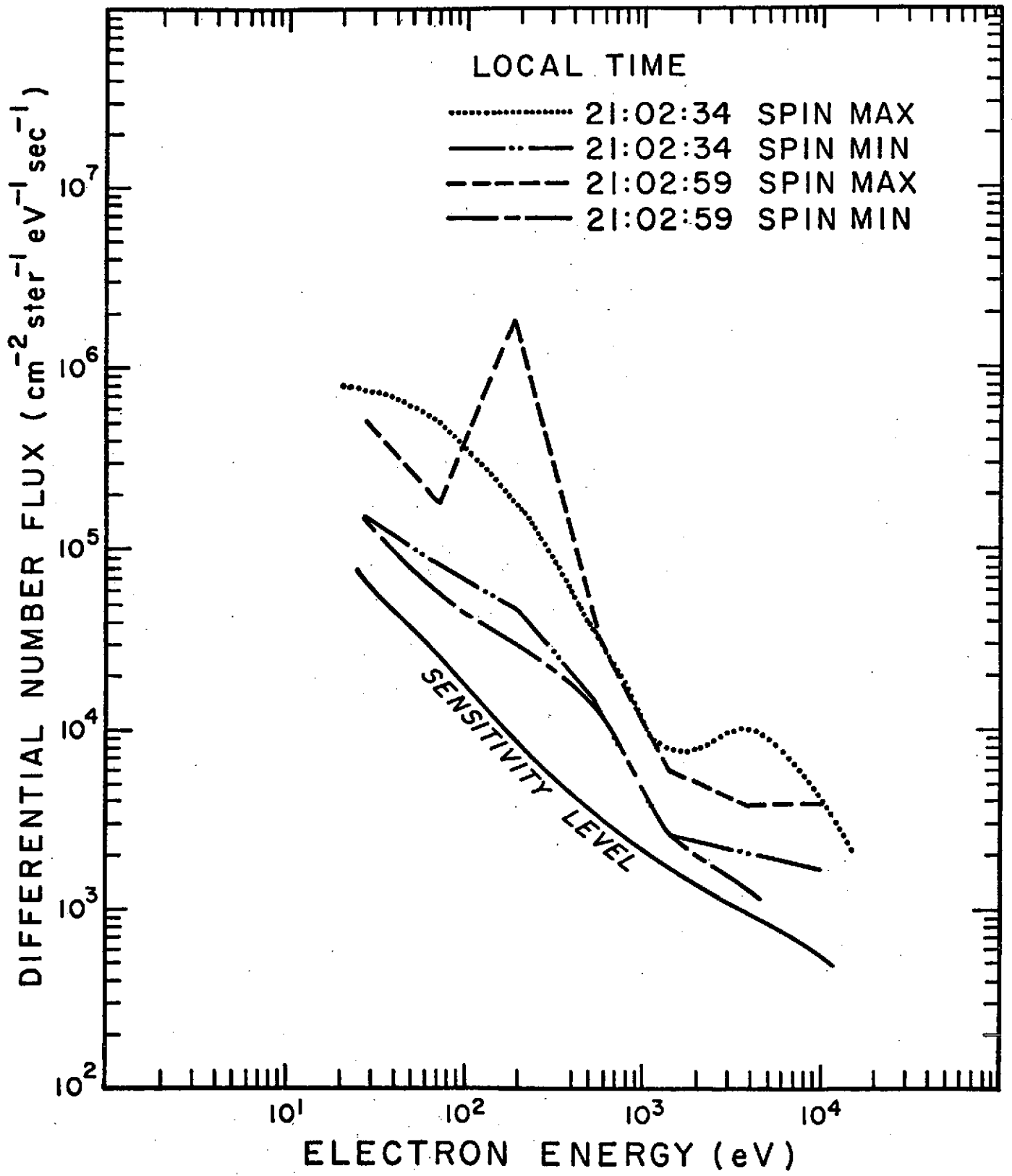


Figure 2

## Soft Particle Fluxes near the Equator

W. J. HEIKKILA

*University of Texas at Dallas 75230*

A few observations have been reported of ionospheric low-energy electrons and protons at low latitudes [Freeman, 1962; Galperin and Krassovsky, 1964; Galperin *et al.*, 1970a, b; Hilton *et al.*, 1964; Krassovsky *et al.*, 1964; Knudsen, 1968], but because of their inconclusive nature they have not attracted much attention. More detailed measurements have now been obtained by means of the soft particle spectrometer on the Isis 1 satellite.

The instrument has been described in detail by Heikkila *et al.* [1970]. Briefly, it uses an electrostatic deflection system followed by electron multipliers to provide the differential spectra for negative and positive particles (hereafter called electrons and protons) in the energy range 10 to 10,000 eV per unit charge. The results are conveniently presented for preliminary analysis in the form of spectrograms, as in Figure 1, where the counting rate is used to intensity modulate a presentation of particle energy versus time. The dark portions show high counting rates, in the form of spin-dependent maxima with two maxima per satellite spin period of 20.4 sec. The collimator axis is normal to the satellite spin axis, which at this time pointed near the south celestial pole. The range of pitch angles scanned was  $70^\circ \leq \alpha \leq 110^\circ$ , with a resolution of  $\pm 8^\circ$  [Heikkila *et al.*, 1970]. Plots are also shown of the integrated particle and energy fluxes calculated from the data shown in the spectrograms.

The existence of intense fluxes of both electrons and protons near the equator, in the late evening period, is shown by the data for this and other passes. The energy spectrum is broad, extending up to several keV. The pitch angle distribution is highly anisotropic; according to the measured magnetic aspect the distribution is essentially that of a trapped population with pitch angle  $\alpha = 90^\circ$ . The flux of electrons with

$\alpha = 90^\circ$  on this occasion reached  $5 \times 10^8 \text{ cm}^{-2} \text{ ster}^{-1} \text{ sec}^{-1}$  carrying  $10 \text{ ergs cm}^{-2} \text{ ster}^{-1} \text{ sec}^{-1}$ , comparable with intense auroral zone values; because of the trapped distribution, of course, this is not the precipitated flux. Corresponding numbers for protons were about an order of magnitude lower.

The pitch angle distributions are surprising in that alternate maxima are unequal. The particle drift speeds must be very small ( $< 100 \text{ m/sec}$ ) compared with their total speed ( $\sim 10^7 \text{ m/sec}$  for 1-keV electrons), and hence the distribution should be axially symmetric. Since the  $\alpha = 90^\circ$  condition is sampled twice per satellite spin, there should be two equal maxima per spin. The flux in fact shows strong directional asymmetries; for example, the eastward flux (the series of maxima spaced 20.4 sec apart, including one at exactly 0349 UT in Figure 1) was at times nearly 10 times as great as the westward (the alternate set of maxima). The weaker maximum in fact virtually disappeared at times. The proton angular distribution was also peaked at  $90^\circ$ . It is significant that for the more energetic protons above 1 keV the two maxima per spin were of more nearly equal amplitude during the period near 0349 (as shown by the total energy flux) when the two electron peaks differed by about a factor of 10. On the other hand, the lower energy protons below 100 eV showed one stronger maximum per spin,  $180^\circ$  out of phase with the stronger electron maximum. Thus far no completely satisfactory explanation of these asymmetries has been found, although strong spatial gradients may be involved. Another unexplained asymmetry is that of the flux intensities on either side of the magnetic equator; perhaps this is related to the different altitudes and magnetic field strengths.

Since these results are of a rather surprising nature, a few words on their reliability may be appropriate. There is no hint of any instrumental malfunction, either on the basis of the house-

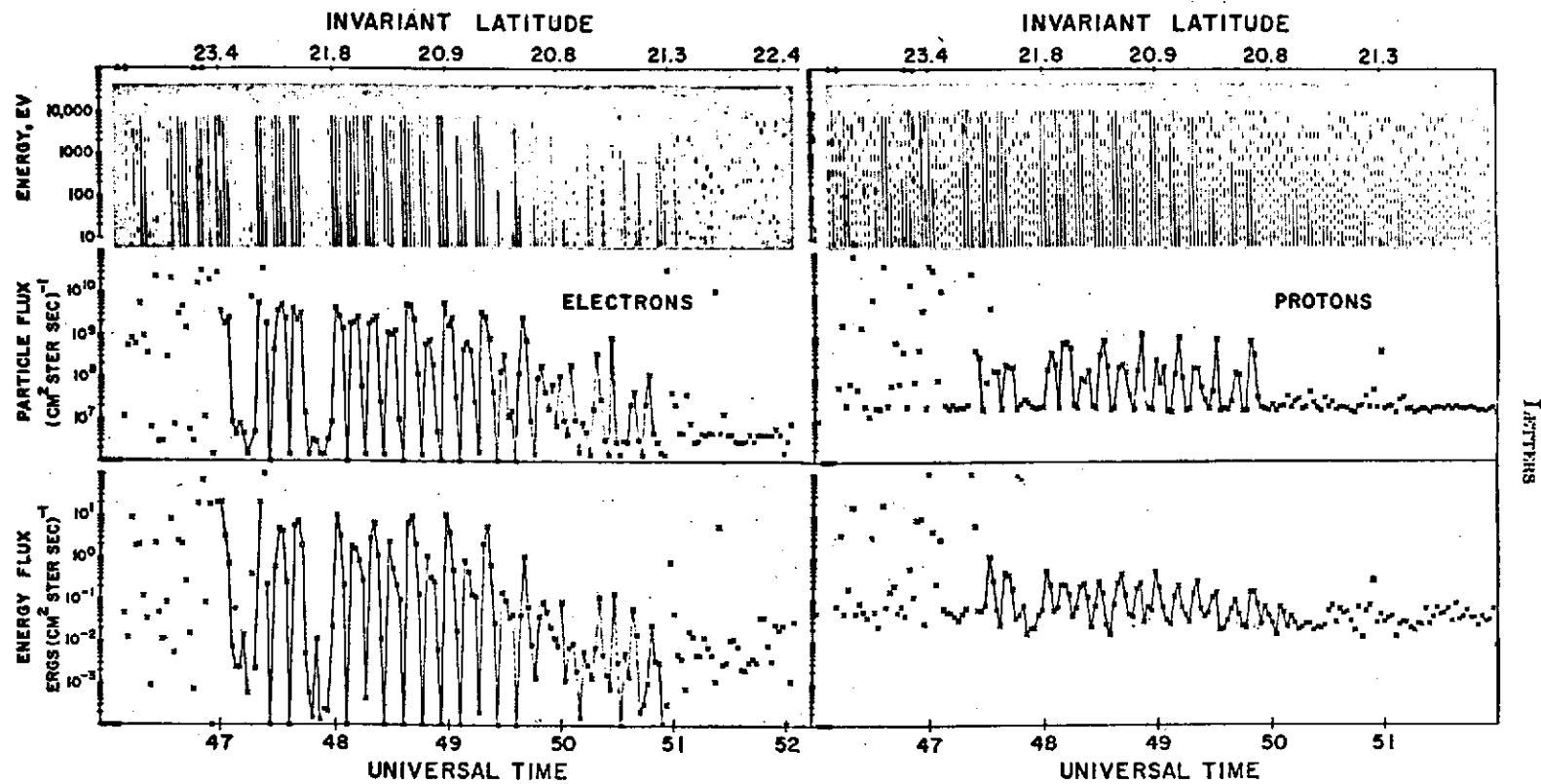


Fig. 1. Electron and proton data for a transequatorial pass of Isis 1 on orbit 77, February 6, 1969, at 0300 hours UT plus the minutes shown. The geographic latitude, longitude, and altitude are 6°N, 82°W, and 627 km for the beginning of the pass and 17°S, 83°W, and 840 km for the end, respectively; the local time was about 2203. A few data points near the beginning of the pass are spurious.

keeping telemetry or the nature of the data at this and other times. The few obviously bad data points at the beginning of the pass are due to poor telemetry. Interception by the satellite of the particles gyrating about the geomagnetic field lines is a minor effect. In short, there seems to be no need whatever to question the data, except for numerical uncertainties of the order of  $\pm 40\%$  [Heikkila et al., 1970].

An obvious problem posed by these observations is the source of these particles. No local acceleration mechanism adequate to produce kilovolt energies is known, although weak processes may operate through plasma compression associated with convection, or through plasma instabilities. The inner Van Allen belt may perhaps be a source, since very little is known about the low-energy component there. In this regard it should be noted that particles below some 10 keV will have small east-west drifts owing to the outward gradient of the geomagnetic field, and thus they will participate in  $\mathbf{E} \times \mathbf{B}$  drifts due to electric fields of dynamo or magnetospheric origin. After sunset the plasma drifts downward at some 10 to 50 m/sec [Farley et al., 1970], whereas during the day the drift is upward. This may explain the negative finding of Frank and Swisher [1968] regarding equatorial soft particles during the morning hours. Further observations, particularly concerning local time and altitude variations, should help to answer these questions. The possible association of these particles with other equatorial phenomena, such as ionospheric ducts and spread *F* region structure, VLF radio noise, and various optical emissions, is an interesting possibility. Preliminary comparisons with other ionospheric measurements made on the same satellite suggest such correlations; these will be discussed in future publications.

*Acknowledgments.* This work was supported under NASA grant NAS5-0112.

## REFERENCES

- Farley, D. T., B. B. Balsley, R. F. Woodman, and J. P. McClure, Equatorial spread *F*; Implications of VHF radar observations, *J. Geophys. Res.*, **75**(31), 1970.
- Frank, L. A., and R. L. Swisher, Energy fluxes of low-energy protons and positive ions in the earth's inner radiation zone, *J. Geophys. Res.*, **73**, 442, 1968.
- Freeman John W., Detection of an intense flux of low-energy protons or ions trapped in the inner radiation zone, *J. Geophys. Res.*, **67**, 921, 1962.
- Galperin, Yu. I., and V. I. Krassovsky, Investigations of the upper atmosphere using the artificial earth satellites Cosmos 3 and Cosmos 5, *Space Res.* **4**, North-Holland, Amsterdam, 1964.
- Galperin, Yu. I., N. V. Jorjio, I. D. Ivanov, I. P. Karpinsky, E. L. Lein, T. M. Mulyarchik, B. V. Polenov, V. V. Temny, N. I. Fedorova, B. I. Khazanov, A. V. Shifrin, and F. K. Shuiskaya, Satellite 'Cosmos-261' study of geoactive corpuscles and photoelectrons, 2, Measurements of low energy electrons, *Kosm. Issled.*, **8**(1), 103, 1970a.
- Galperin, Yu. I., V. A. Gladyshev, I. D. Ivanov, I. P. Karpinsky, B. I. Khazanov, T. M. Mulyarchik, B. V. Polenov, A. V. Shifrin, F. K. Shuiskaya and V. V. Temny, Satellite 'Cosmos-261' study of geoactive corpuscles and photoelectrons, 3, Measurement of low-energy ions, *Kosm. Issled.*, **8**(1), 120, 1970b.
- Heikkila, W. J., J. B. Smith, J. Tarstrup, and J. D. Winningham, The soft particle spectrometer in the Isis-1 satellite, *Rev. Sci. Instrum.*, **41**, 1393, 1970.
- Hilton, H. H., J. R. Stevens, and A. L. Vampola, Observations of large fluxes of low-energy electrons, *Trans. AGU*, **45**(4), 602, 1964.
- Krassovsky, V. I., Yu. I. Galperin, N. V. Jorjio, T. M. Mulyarchik, and A. D. Bolyunova, Investigations of the upper atmosphere using the artificial earth satellites Cosmos 3 and Cosmos 5 *Space Res.* **4**, North-Holland, Amsterdam, 1964.
- Knudsen, William C., Geographic distribution of *F*-region electrons with about 10-eV energy, *J. Geophys. Res.*, **73**, 841, 1968.

(Received October 8, 1970.)

5. AE-LEE Measurements at Low and Mid  
Latitude....R. A. Hoffman, J. L. Burch  
and R. J. Janetzke

N74-28251

AE-LEE MEASUREMENTS AT  
LOW AND MID LATITUDE

By

R. A. Hoffman  
J. L. Burch  
R. J. Janetzke

NASA-Goddard Space Flight Center  
Greenbelt, Maryland 20771

June 1974

## INTRODUCTION

Shortly after the Low Energy Electron Experiment (LEE) on the Atmosphere Explorer-C was turned on following launch, an unexpected phenomenon was encountered at mid-latitudes: a counting rate was acquired with one maximum per roll. It was immediately surmised that the experiment was observing the low latitude fluxes of Freeman (1962) and Heikkila (1971). However, further analysis of the initially acquired data cast some doubt on the validity of that assumption, and, in fact, even on the validity of the counts registered by the detectors. Most recent analysis shows that these counting rates occur when the detectors are looking in the ram direction of the spacecraft and the spacecraft is near perigee, and are indeed not due to properly analyzed charged particles.

Thus, after showing the probable cause of these counting rates, this paper will present some upper limits to true fluxes at low altitudes in the energy range 200 ev to 25 kev from the LEE experiment, and will also present a small amount of OGO-4 data taken at mid-latitudes.

## EXPERIMENT

The LEE-C experiment contains three identical detectors, each comprised of an electrostatic analyzer for species and energy selection, and a Bendix Spiraltron as the particle sensor. A schematic of the detector is shown in Figure 1, with dimensions shown which are pertinent to this discussion. A detailed description of the experiment is given in Hoffman et al., (1974).

The detector system is well baffled with a sunshade containing six window frame knife edge baffles. A defining aperture slit 2 mm x 6 mm is in front of the concentric cylindrical analyzer plates, which are manufacturer from beryllium. These plates have an arc length of  $60^\circ$ , a mean radius of curvature of 4 cm, and a plate gap of 2 mm. The application of bipolar pair of voltages on the plates provides the species and energy selection, the  $\pm$  pair for electrons and  $\mp$  pair for

protons. Two detectors have this voltage stepped between  $\pm 10$  volts (for 200 eV particles) and  $\pm 1250$  volts (for 25 keV particles), and one detector has fixed voltages of  $\pm 250$  to measure 5 keV electrons. The 16 logarithmically spaced steps are synchronized to the telemetry main frame, thus providing an energy spectrum every second. Behind the analyzer plate is the Spiraltron, with the front end essentially grounded. It is operated in the gain saturated mode (Evans, 1965). There is no acceleration grid between the analyzer plates and sensor.

The detector apertures look out  $45^\circ$  between the X and Y axes of the spacecraft. The spin axis of the spacecraft, Z, was placed perpendicular to the orbital plane so that the spacecraft either rolls or skids along the orbit. The roll period during the acquisition of data which will be discussed was about 15 seconds, so that energy spectra were acquired 15 times per roll.

#### RAM INDUCED COUNTING RATES

An example of apparent low-latitude, low altitude fluxes appears in Figure 2 as two energy-time spectrograms, the top for electrons, bottom for protons. Below is plotted the pitch angles of the measurements from nearly  $0^\circ$  to nearly  $180^\circ$ . Note that in these data taken shortly before midnight local time, there is one sharp maximum in the fluxes per roll, at 1627:57 U.T., 1628:13 U.T., etc. These maxima occurred when the detectors were pointed in the direction of the velocity vector of the satellite, the ram direction, and in this case at an angle of about  $60^\circ$  to the magnetic field direction. No azimuthally symmetric fluxes were detected.

In Figure 3 we plot the total number of counts from the 5 keV electron detector in the pitch angle region containing these counts as a function of altitude of the measurement. Data from the fixed energy detector were used because the stepped energy detector data are an unknown convolution between energy step and angle from the ram direction. Since the data in Figure 3 indicate a definite relationship between the counting rates and altitude we next considered the relationship

between the counting rates and the neutral density. This is plotted in Figure 4, using the U. S. Standard Atmosphere, 1962. This excellent linear functional dependence between the counting rates and neutral density indicates that either the counts are due to neutral particles being rammed into the detector and being counted at an extremely low efficiency ( $\sim 10^{-20}$ ), or they are due to some other particle with a similar scale height. Apparently the detection process involves the voltage on the analyzer plates because the highest counting rates in both stepped energy detectors occur when the maximum voltages are applied to the plates. Note in Figure 1 that at such times there are voltages of  $\pm 1250$  volts from the analyzer plates to the grounded entrance apertures of the Spiraltrons.

#### UPPER LIMITS TO NATURALLY OCCURRING FLUXES

While no systematic approach to investigating the existence of low latitude, low altitude fluxes has been undertaken with the AE-C data, a number of passes of data have been inspected for large fluxes of electrons. Since such particles are thought to be at least pseudo-trapped, we plot in Figure 5 the satellite trajectories during these passes in magnetic coordinates: magnetic local time (MLT) (local time reckoned from the earth's dipole axis) and invariant latitude (which is a function of  $L$  value). Several of the passes crossed the equator at altitudes in the range 200 to 300 km, and in no cases were large fluxes of either protons or electrons encountered. In fact only upper limits to fluxes in the range 200 eV to 25 keV can be given.

If one count would occur at each energy step in the electron detector, the integrated flux from 300 eV to 25 keV would be about  $1 \times 10^6$  electrons/cm<sup>2</sup>-sec-ster. Without a detailed analysis of the data, including long time averages, it appears reasonable to claim that usually the counting rates were less than one count in each energy step when the satellite was in the latitude and altitude range of interest.

This is three to four orders of magnitude less than the values reported by Heikkila (1971) and Winningham (1974).

A set of seven somewhat similar electrostatic analyzers were flown in an auroral particles experiment on OGO-4 in 1967, each making a measurement at a fixed energy. Four of the detectors were always pointed radially away from the earth. Early in the life of the satellite the experiment had a fairly low noise level, during which time a few passes of data at mid latitudes were acquired. Energy spectra at four  $L$  values obtained from the four radially directed detectors are shown in Figure 6. These data should be considered upper limits, since all noise counts may not have been successfully removed. The integrated flux from 700 eV to 25 keV at  $L = 2$  was about  $6 \times 10^6$  electrons/cm<sup>2</sup>-sec-ster.

#### CONCLUSIONS

Although large fluxes of electrons at low or mid latitudes have not been observed by either the Atmosphere Explorer-C or OGO-4 experiments, there has been no systematic approach to searching the data for the existence of such particles. If these particles do exist, they are either restricted in local time or governed by some transient geophysical parameters.

ACKNOWLEDGEMENTS

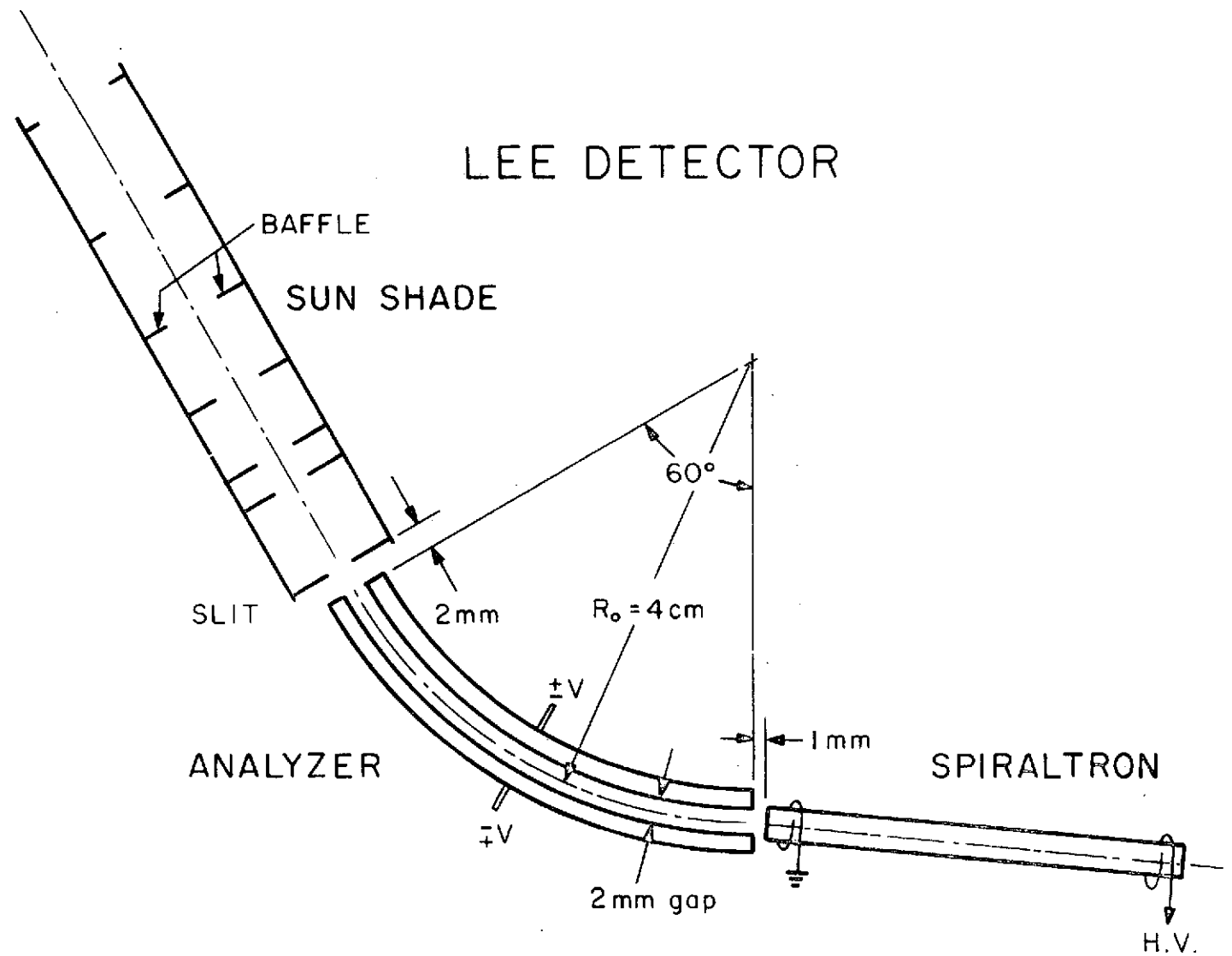
The OGO-4 data from the Auroral Particles Experiment were analyzed by D. G. Torr and M. M. Torr.

FIGURE CAPTIONS

- Figure 1. Schematic diagram of the detectors flown in the LEE experiment on AE-C with pertinent dimensions indicated.
- Figure 2. An electron spectrogram, an energy-time method of plotting the flux measurements, showing the single maximum in the counting rate each roll of the satellite. A darkening grey shading designates a higher flux.
- Figure 3. Total counts accumulated by the 5 keV electron detector per roll of the satellite, in the angular region of the single maximum in the counting rate, as a function of altitude.
- Figure 4. Same data as displayed in Figure 3 plotted as a function of number density of the neutral atmosphere. The line is an estimated linear relation between the counts and density.
- Figure 5. Locations of mid and low latitude measurements in a magnetic local time (MLT), invariant latitude coordinate system. "P" is the location of perigee, about 150 km. The numbers along the tracks are altitude in kilometers. All satellite passes began at high altitudes in the northern hemisphere and proceed towards the equator. In several cases, the data acquisition continued across the equator into the southern hemisphere. The location the satellite crossed the equator is indicated by "E".
- Figure 6. Electron energy spectra at mid latitudes obtained from the Auroral Particles Experiment on the OGO-4 satellite. Fluxes are in electrons/cm<sup>2</sup>-sec-ster-keV.

## REFERENCES

- Evans, D. S., Low-energy charged-particle detection using the continuous-channel electron multiplier, R.S.I., 36, 375, 1965.
- Freeman, John W., Detection of an intense flux of low-energy protons or ions trapped in the inner radiation zone, J. Geophys. Res., 67, 921-928, 1962.
- Heikkila, W. J., Soft particle fluxes near the equator, J. Geophys. Res., 76, 1076-1078, 1971.
- Hoffman, R. A., J. L. Burch, R. W. Janetzke, J. F. McChesney, S. H. Way, and D. S. Evans, Low-energy electron experiment for Atmosphere Explorer-C and -D, Radio Science, 8, 393-400, 1973.
- Winningham, J. D. (this publication).



# LEE DETECTOR

Fig. 1

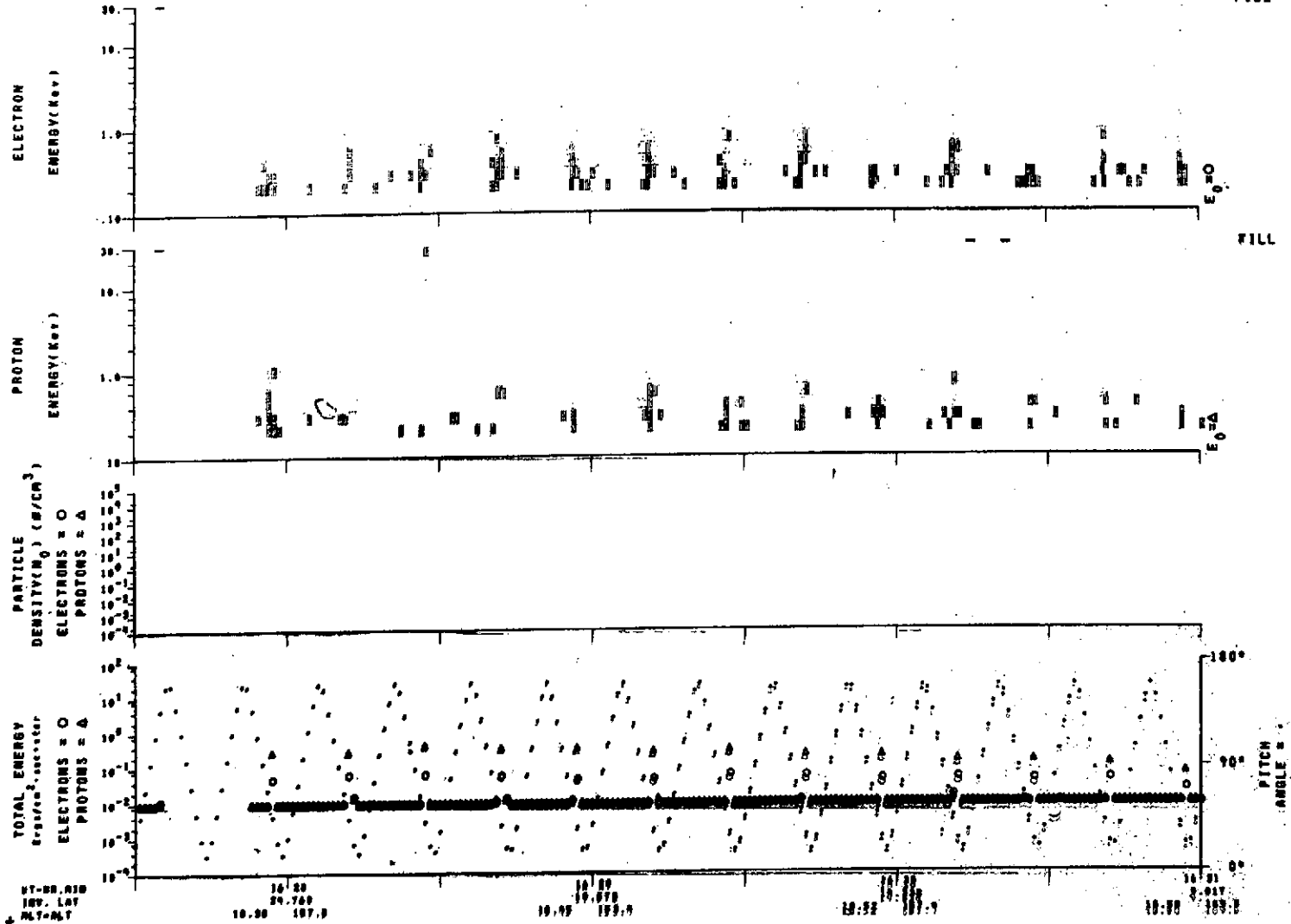
DAY 11 1-11-74

### AE-C LEE ANALYSIS PLOTS

ORBIT 289 Page 7

START TIME 16:27:30 INTENSITY LEVELS

0.21E+05	0.99E+05	0.96E+06	0.21E+07	1.00E+07	0.96E+08	0.21E+09	1.00E+09	0.96E+10	0.22E+11	1.00E+11
0.96E+04	0.21E+05	0.99E+05	0.96E+06	0.21E+07	1.00E+07	0.96E+08	0.21E+09	1.00E+09	0.96E+10	0.22E+11



HT-00-R10  
INV. LAT  
MT-MT

10:00 24.700  
10:00 107.0

10:00 19.070  
10:00 199.0

10:00 107.7

10:00 2.047  
10:00 109.0

Fig. 2

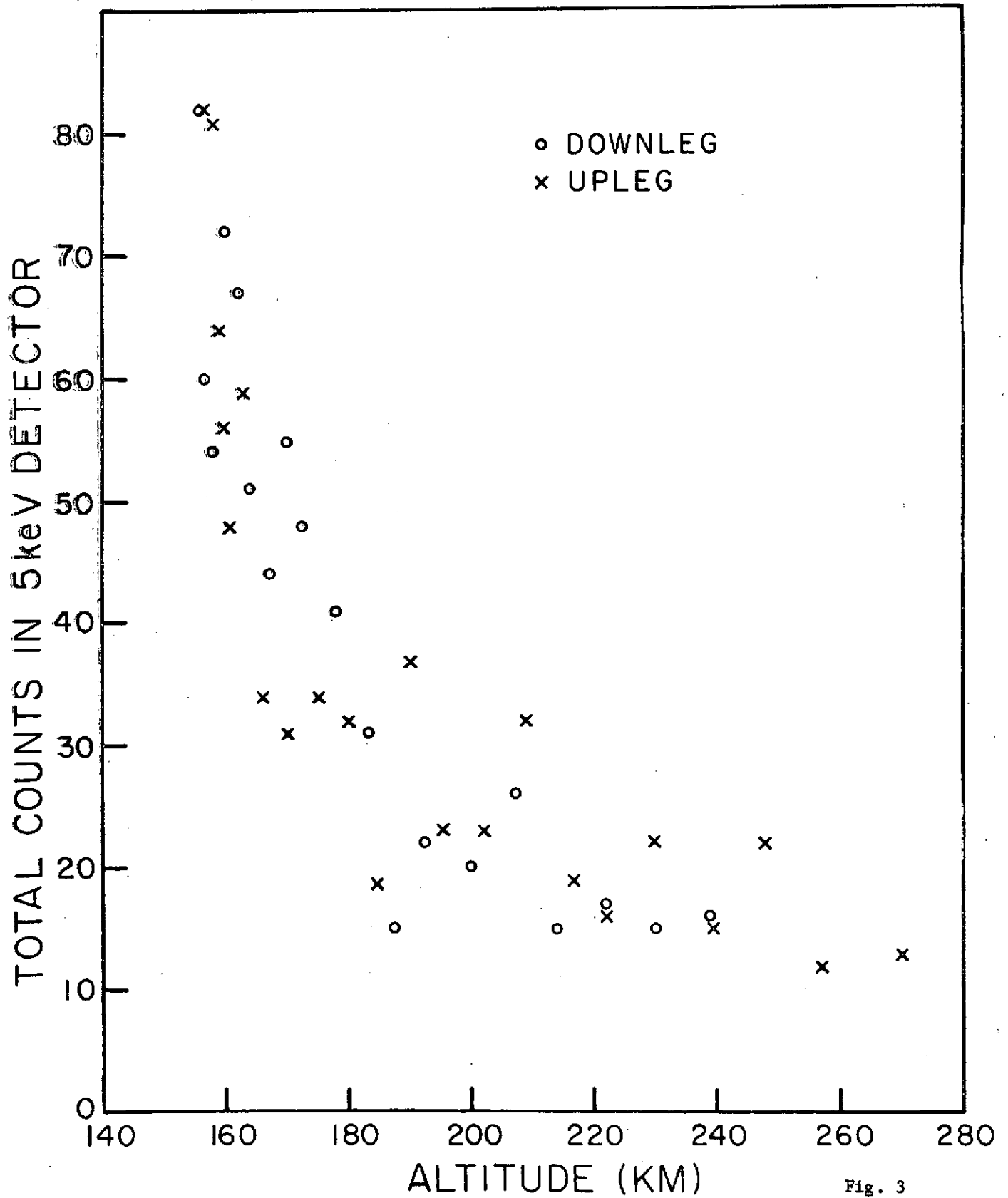


Fig. 3

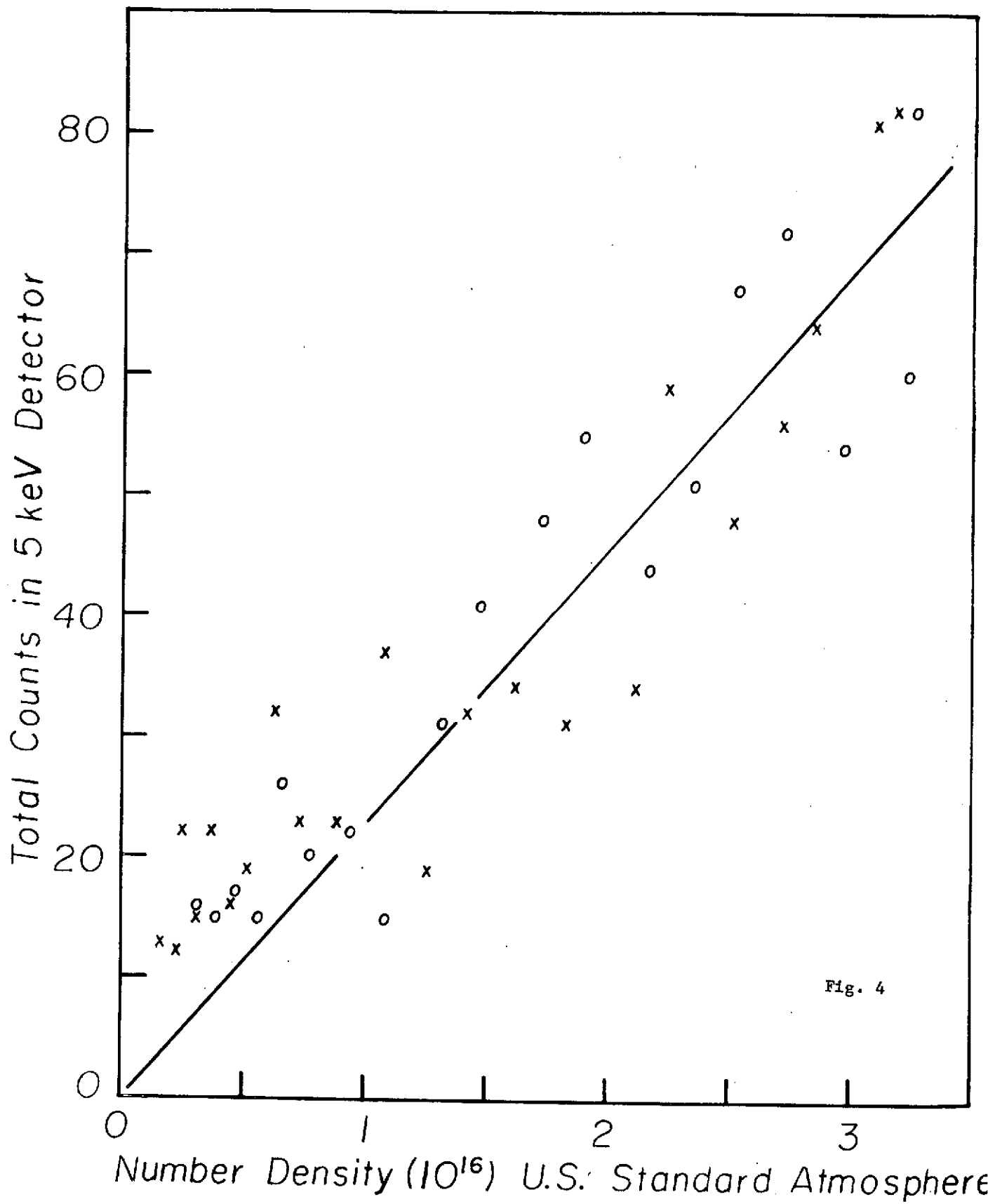


Fig. 4

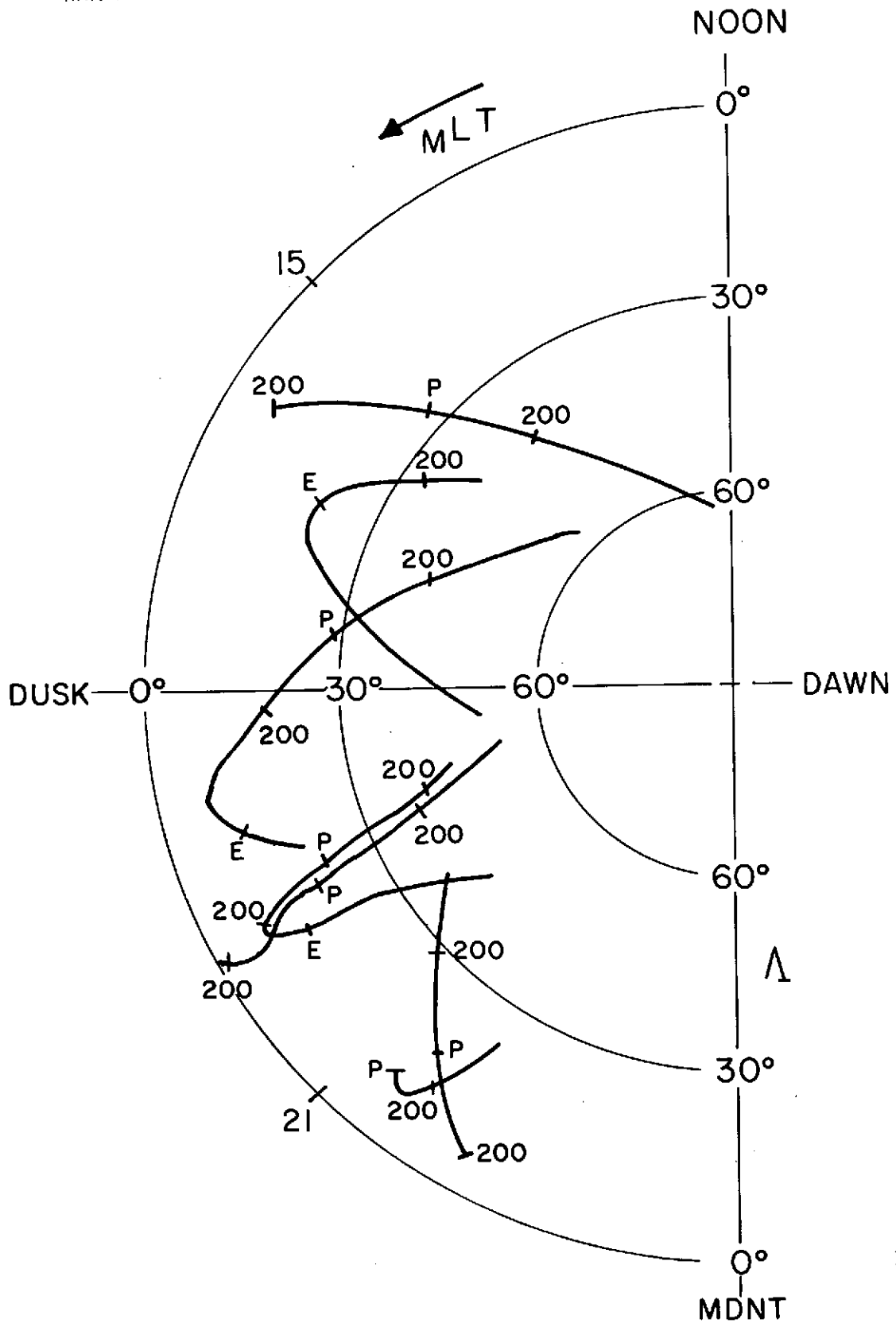


Fig. 5

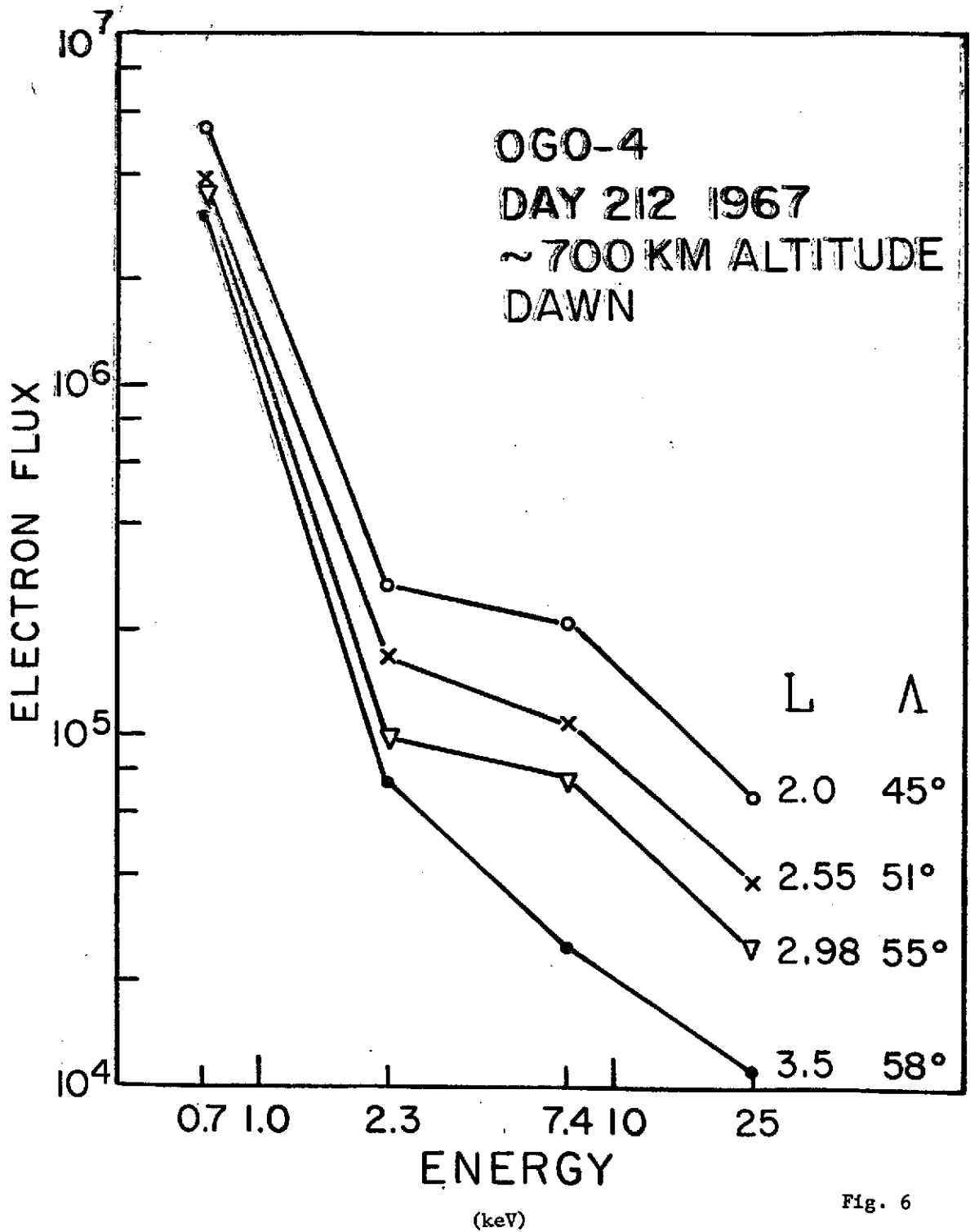


Fig. 6

6. Midlatitude Electron Precipitation:  
A Possible Source of Contamination  
of Galactic X- and  $\gamma$ -Ray Measurements  
....T. J. Rosenberg

N74-58252

Midlatitude Electron Precipitation: A Possible Source  
of Contamination of Galactic X- and  $\gamma$ -Ray Measurements

T.J. Rosenberg

Institute for Fluid Dynamics and Applied Mathematics

University of Maryland

College Park, Maryland 20742

INTRODUCTION

The measurement of galactic X- and  $\gamma$ -rays by balloon, rocket, and satellite instrumentation is conducted in the presence of background radiations of local origin. Either by direct penetration, or by secondary radiations produced in payload materials, photon detectors may at times give spurious responses, particularly if the "background" radiations are non-steady. For example, satellites in the interplanetary medium encounter variations of low energy particle flux (solar wind plasma) as well as energetic particle and x-ray fluxes during solar eruptions.

Within Earth's magnetosphere, satellites and rockets encounter trapped and precipitated particles whose fluxes are controlled in large measure by the level of geomagnetic activity. Balloon instruments, while normally too low in the atmosphere to be affected by direct particle penetration (apart from cosmic rays), are subject to contamination by bremsstrahlung x-rays produced by precipitated electrons stopped at higher altitudes. To minimize contamination caused by electron precipitation, most galactic X- and  $\gamma$ -ray measurements made from within the magnetosphere are conducted at equatorial or relatively low-to-middle latitudes where the influence of auroral effects is expected to be small. However, there

is mounting evidence that even at these latitudes electron precipitation should be considered an important factor.

Few direct measurements exist of the precipitation of electrons at latitudes much below the auroral zones. Potemra and Zmuda (1970) summarized some rocket and satellite measurements and concluded that precipitating energetic electrons ( $E > 40$  keV) are important to the formation of the nighttime midlatitude D region. Recently, Imhof et al (1973, 1974) measured precipitating and quasi-trapped electrons ( $E > 130$  keV) with a low altitude polar-orbiting satellite from the outer edge of the inner radiation belt ( $L \sim 1.4 - 1.8$ ) through the slot region (to  $L \sim 3.5$ ). Previously, Heikkila (1971) reported the presence of intense fluxes of low energy electrons and protons ( $E < 10$  keV) trapped at low altitudes near the equator.

Certain, less direct, ionospheric effects have long suggested that electron precipitation is important at middle and low latitudes. Knudsen and Sharp (1968) discussed anomalous  $F_2$ -region electron concentration enhancements in the South Pacific and extending from the South Atlantic magnetic anomaly eastward to the edge of Africa which they attribute to the precipitation of electrons with energies from a few eV to a few keV. Sauter and Knuth (1967) and Balrose and Thomas (1968) proposed that precipitating particles (probably electrons with energy  $\sim 50$  keV) cause the pronounced after effects on phase and absorption measurements of radio waves from VLF to HF following some magnetic storms. Electron precipitation ( $E > 40$  keV) has also been proposed as the cause of the shorter duration substorm-related phase and amplitude perturbations frequently observed on nighttime midlatitude VLF and LF propagation paths (Balrose, 1968; Reder and Westerlund, 1970; Doherty, 1971; and Potemra and Rosenberg, 1973).

In this paper only the substorm-related VLF phase perturbations are considered. If such perturbations are indicative of electron precipitation at middle-to-low latitudes, then their relatively high frequency of occurrence perhaps 100 or more per year (E.H. Radler, personal communication), is evidence that electron precipitation at these latitudes may pose a problem to some galactic X- and  $\gamma$ -ray measurements.

### OBSERVATIONS

An example of the VLF phase effect is shown in Figure 1. Other examples are illustrated in Saus and Rosenberg (1974). In this figure, sixteen phase recordings are placed in descending order with respect to the highest L shell along each path. The relationship of the great circle paths to projections of magnetic L shells on the ionosphere at 100-km altitude is shown in Figure 2. Information pertaining to the transmitter and receiver sites is provided in Table I.

A majority of the paths in Figure 1 show the nearly simultaneous onset of a phase advance at ~ 0820 UT. As shown previously for this event by Potemra and Rosenberg (1973), who used a more limited data set, this time corresponds closely with the onset of a magnetic substorm. On most perturbed paths the event lasted until 1000-1100 UT. Several paths exhibited secondary maxima between 0850 and 0920 UT.

With the larger data set available here, it is possible to examine the spatial extent of the perturbed region, although not in great detail because of the long lengths of paths and the fact that only a fraction of the total length of a path may be affected. None of the paths shown in Figure 1 exceeds  $L = 3.6$ . Of the paths that reached  $L \gtrsim 2.5$  only the paths NAA-NELC, NLK-NOBHA, and OM/T-DEAL failed to respond significantly

at 0820 UT. The paths below  $L = 2.5$  were only weakly perturbed. These data suggest that the longitudinal extent at middle latitudes was confined to the region within the extremes of the grid defined by the undisturbed essentially cross-L paths NLK-NOBHA and OM/T-DEAL located at the western and eastern ends, respectively. The latitudinal extent in the equatorward direction reached at least to  $L \sim 1.7$  with major perturbations limited to  $L \gtrsim 2.5$ . Note that the perturbed region reaches sites such as Wallops Island, Virginia and Palestine, Texas where rocket and balloon observations of galactic X- and  $\gamma$ -rays are conducted. Rosenberg and Saus (1974) have found that in general the lowest latitude paths are least often perturbed, but the equatorward extent increases with increasing geomagnetic activity.

#### DISCUSSION

Since all perturbed paths exhibit phase advances either initially or throughout the event, the predominant ionospheric effect corresponds to a reduction of the VLF reflection height. As discussed by Potemra and Rosenberg (1973) this reduction could be caused by the precipitation of energetic electrons ( $E > 40$  kev) which will enhance ionization below the normal undisturbed nighttime level of  $\sim 85$  km. In particular, they showed that nighttime VLF phase is very sensitive to small enhancements of incident electron flux,  $J(E > 40 \text{ kev}) \lesssim 10^3 \text{ cm}^{-2}\text{-sec}^{-1}\text{-ster}^{-1}$ , that would be only marginally detectable, if at all, by other indicators of electron precipitation such as bremsstrahlung x-rays and riometer absorption.

Figures 3 and 4 (Figures 6 and 7 from Potemra and Rosenberg, 1973) illustrate these points. In Figure 3 computed ionization rates are shown for model incident electron energy spectra of the form  $J(> E) \sim e^{-E/E_0}$  for  $E_0 = 10, 30, 50,$  and  $100$  kev and unit flux  $J(E > 40 \text{ kev}) = 1 \text{ cm}^{-2}\text{-sec}^{-1}\text{-ster}^{-1}$

in each case. The ionization rates due to other sources which are expected to be important in the nighttime D region are also shown in this figure. To produce ionization at 85 km comparable with that produced by the ionization of NO by scattered H Ly  $\alpha$ , which is expected to be the dominant source of ionization at this altitude, electron fluxes of  $10-100 \text{ cm}^{-2}\text{-sec}^{-1}\text{-ster}^{-1}$ , depending on the value of the spectral parameter, are required. For comparison, Figure 4 gives a rough measure of the incident electron flux required to account for a VLF phase perturbation. This figure shows the phase advance computed for the NLK-APL path (not shown in Figure 1 but essentially the same as the NLK-NOBDC path) for the model electron spectra used in Figure 3. An electron flux between 100 and  $1500 \text{ cm}^{-2}\text{-sec}^{-1}\text{-ster}^{-1}$  (for a range of electron energies between 100 and 30 keV, respectively) would produce the 8  $\mu\text{sec}$  phase advance (dashed line) observed on this path. The  $E_0 = 10 \text{ keV}$  curve illustrates that VLF propagation is not very sensitive to low energy electron influx. However, it should be borne in mind that the spectrum of precipitating electrons in these events might well extend to lower energies than those ( $E > 40 \text{ keV}$ ) to which nighttime VLF propagation is sensitive.

Few substorm-related VLF phase perturbations are observed in the daytime. During daytime, electron energies in excess of several hundred keV are required to perturb VLF propagation because the ionospheric reflection height is then near 70 km.

SUMMARY

From the few direct measurements available, and from inferences drawn from ionospheric observations, it would appear that the precipitation of electrons at middle and even low latitudes may occur more frequently than is generally supposed. VLF radio wave propagation measurements at night support this contention for electrons with energies  $\gtrsim 40$  kev. The flux levels, except in unusual circumstances, are much lower than those typical of auroral latitudes, but nevertheless may pose a problem to some measurements of galactic X and  $\gamma$ -rays. Less is known about the precipitation of lower energy electrons on either the night or day sides.

ACKNOWLEDGMENTS

The assistance of Mr. F.A. Saus in organizing the data presented is appreciated. I thank Dr. T.A. Potemra, Applied Physics Laboratory, Silver Spring, Md., Dr. F.H. Reder, U.S. Army Electronics Command, Ft. Monmouth, N.J., Dr. G.M.R. Winkler, U.S. Naval Observatory, Washington, D.C., Mr. D. Monger, U.S. Naval Observatory, Perrine, Fla., Dr. E.R. Swanson, U.S. Naval Electronics Laboratory, San Diego, Calif., and Mr. B.E. Blair, NBS, Boulder, Colo. for supplying copies of the propagation recordings. This work was supported in part by the National Science Foundation under grant GV-28841X.

## REFERENCES

- Belrose, J.S., Radio wave propagation, AGARD Lecture Ser., no. 29, 1968.
- Belrose, J.S. and L. Thomas, J. Atmos. Terr. Phys., 30, 1397, 1968.
- Doherty, R.H., Radio Sci., 6, 639, 1971.
- Heikkila, W.J., J. Geophys. Res., 76, 1076, 1971.
- Imhof, W.L., E.E. Gaines and J.B. Reagan, J. Geophys. Res., 78, 4568, 1973.
- Imhof, W.L., E.E. Gaines and J.B. Reagan, Evidence for the resonance precipitation of energetic electrons from the slot region of the radiation belts, J. Geophys. Res., 79, in press, 1974.
- Knudsen, W.C. and G.W. Sharp, J. Geophys. Res., 73, 6275, 1968.
- Lauter, E.A. and R. Knuth, J. Atmos. Terr. Phys., 29, 411, 1967.
- Potemra, T.A. and T.J. Rosenberg, J. Geophys. Res., 78, 1572, 1973.
- Potemra, T.A. and A.J. Zmuda, J. Geophys. Res., 75, 7161, 1970.
- Reder, F.H. and S. Westerlund, AGARD Conf. Proc., no. 33, 103, 1970.
- Rosenberg, T.J. and F.A. Saus, Conf. Proc. NATO ASI on ELF-VLF Radio Wave Propagation, D. Reidel Publ. Co., Dordrecht, Holland, in press, 1974.
- Saus, F.A. and T.J. Rosenberg, Univ. of Maryland Tech. Note BN-771 (revised) 1974.

TABLE I. VLF TRANSMITTER AND RECORDING SITES

TRANSMITTER	FREQUENCY (kHz)	LOCATION	GEOGRAPHIC COORDINATES		RADIATED POWER (KW)
NBA	24.0	BALBOA, PAN.	9.1 N	79.7 W	1000
GBR	16.0	RUGBY, ENG.	52.4 N	1.2 W	350
NLK	18.6	JIM CREEK, WA.	48.2 N	121.9 W	1000
OM/T	13.6	TRINIDAD	10.7 N	61.6 W	20
NAA	17.8	CUTLER, ME.	44.7 N	67.3 W	1000
OM/HA	12.2	HAIKU, HA.	21.4 N	157.8 W	20
WWVL	20.0	BOULDER, CO.	40 N	105.5 W	40

RECEIVER	ORGANIZATION	LOCATION	GEOGRAPHIC COORDINATES	
DEAL	U.S. ARMY ELECT. CMD.	FT. MONMOUTH (DEAL), N.J.	40.3 N	74 W
APL	JOHNS HOPKINS U.	SILVER SPRING, MD.	39.2 N	76.9 W
NOBDC	U.S. NAVAL OBS.	WASHINGTON, D.C.	38.9 N	77.1 W
NOTSS	U.S. NAVAL OBS.	PERRINE, FLA.	25.6 N	80.5 W
NOBHA	U.S. NAVAL OBS.	HAWAII	21.5 N	158 W
NELC	U.S. NAVAL ELECT. LAB.	SAN DIEGO, CAL.	32.8 N	117.1 W
NBSBD	NAT. BUR. OF STANDARDS	BOULDER, CO.	40 N	105.4 W

## FIGURE CAPTIONS

- Figure 1. Phase recordings from sixteen sub-ionospheric VLF propagation paths arranged in descending order with respect to the highest L shell along each path. See Table I for transmitter-receiver designations.
- Figure 2. Map of great circle propagation paths used for the January 2, 1971 event. Dashed curves indicate the projections of magnetic L shells onto the ionosphere at 100-km altitude.
- Figure 3. Ionization rates in the nighttime ionosphere due to several sources. For precipitated electrons, the unit flux  $J (E > 40 \text{ kev}) = 1 \text{ cm}^{-2}\text{-sec}^{-1}\text{-ster}^{-1}$  was used with spectra of the form  $J (> E) \sim e^{-E/E_0}$  for the values of  $E_0$  indicated. See Potemra and Rosenberg (1973) for references to the other sources shown.
- Figure 4. Computed phase variation for the NLK-APL path versus electron flux  $J (> 40 \text{ kev})$  for different e-folding energies. The dashed line at 8  $\mu\text{sec}$  is the maximum NLK-APL disturbance observed during the January 2, 1971 event at 0920 UT.

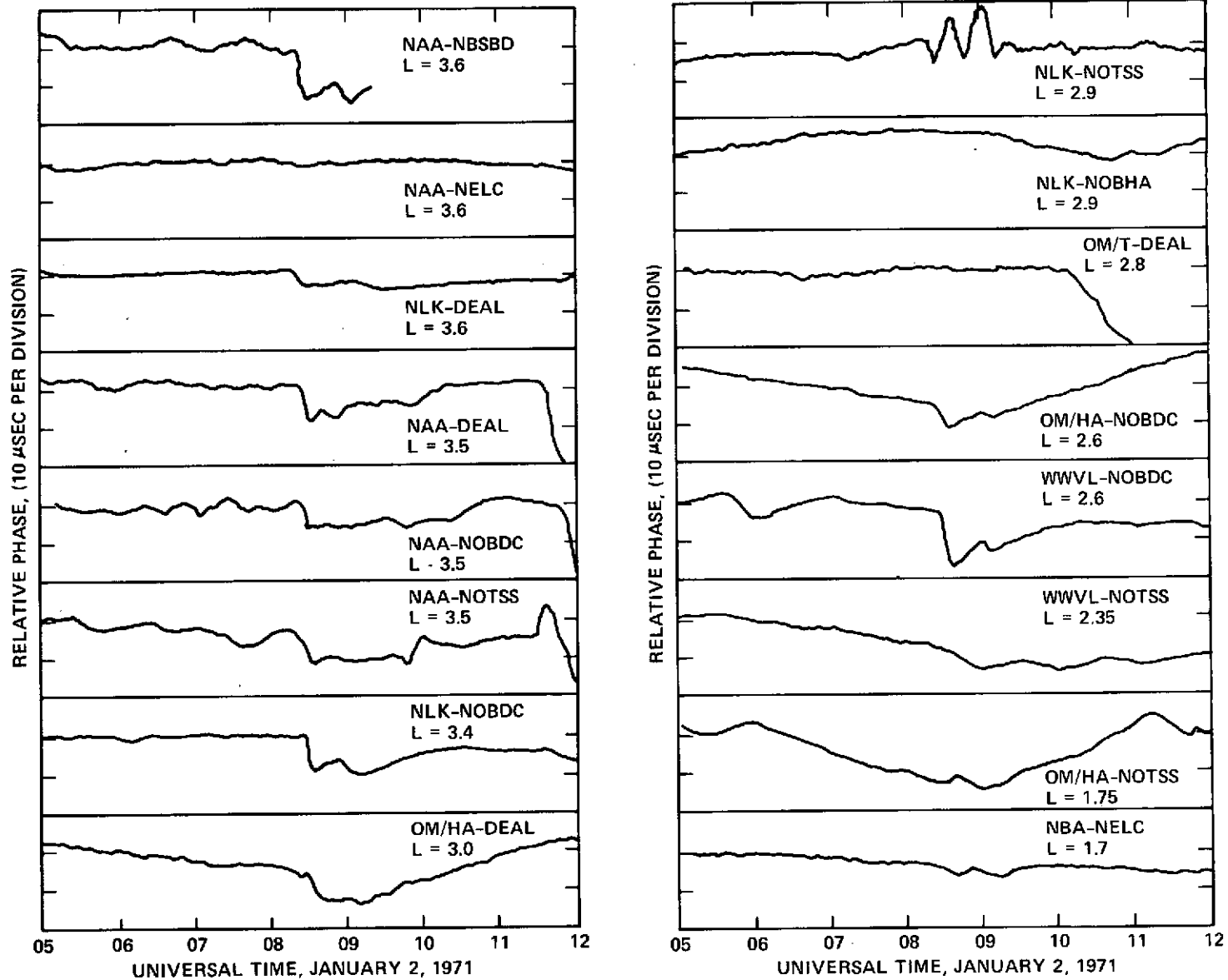


Figure 1.

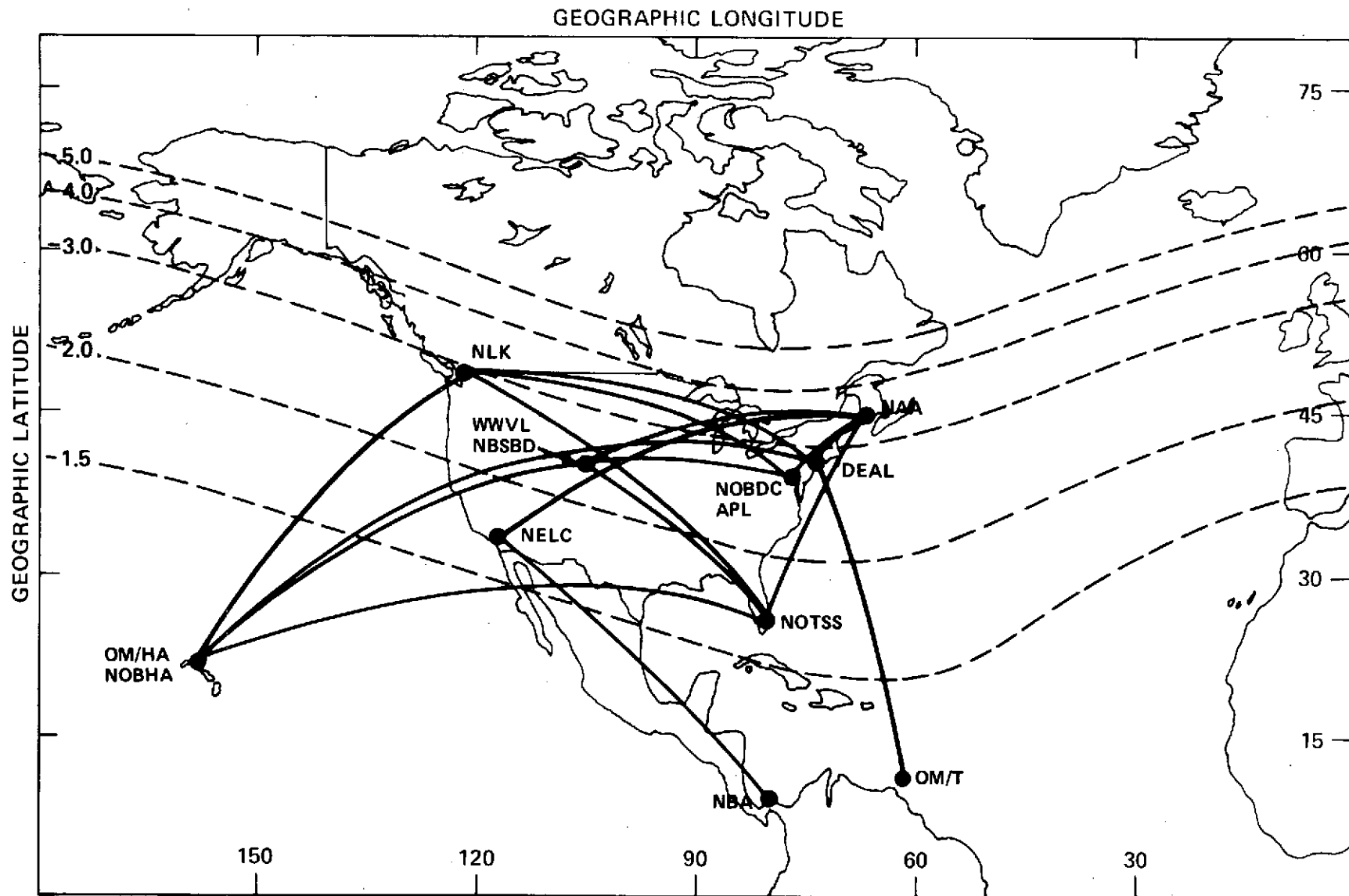


Figure 2.

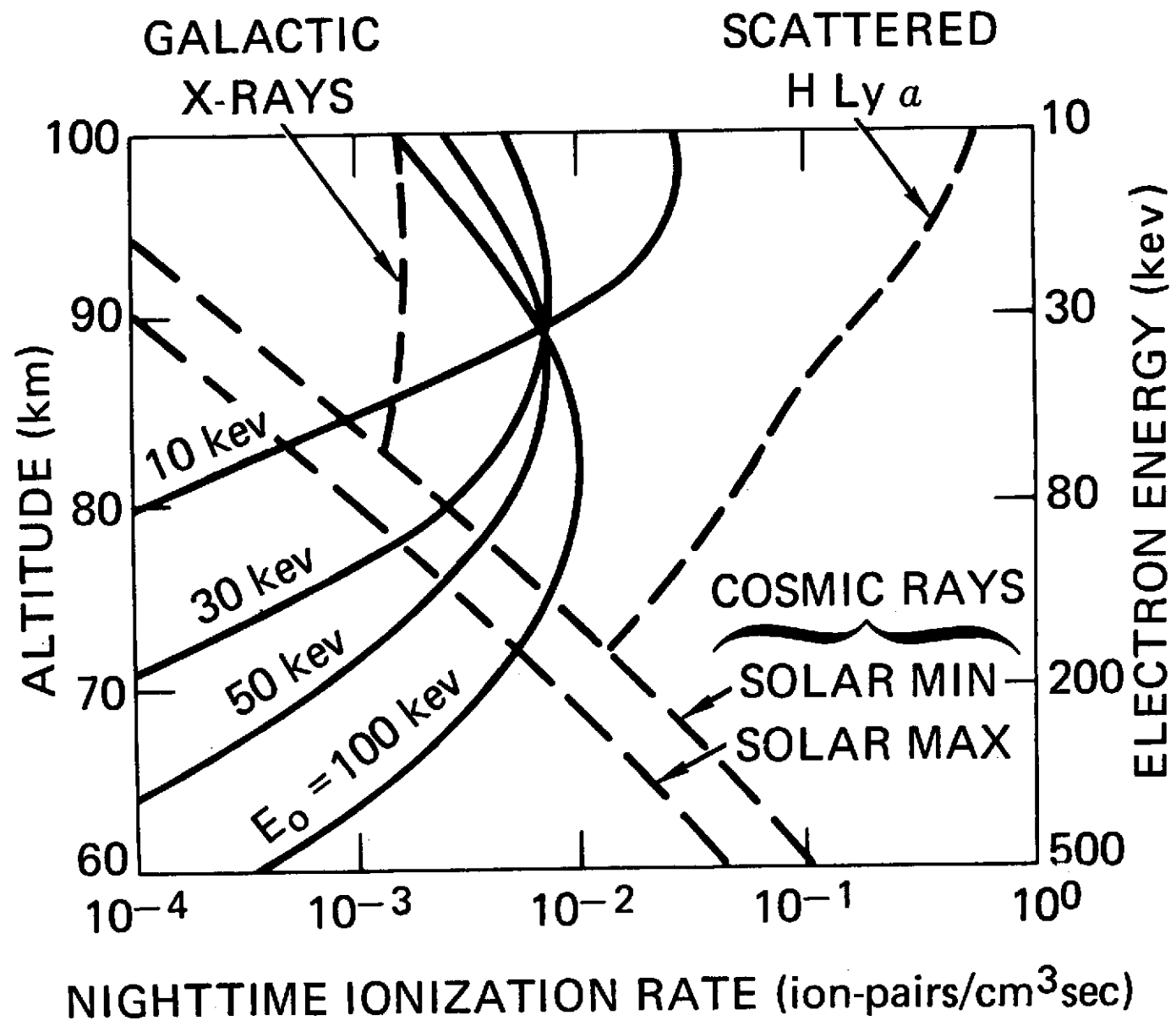


Figure 3.

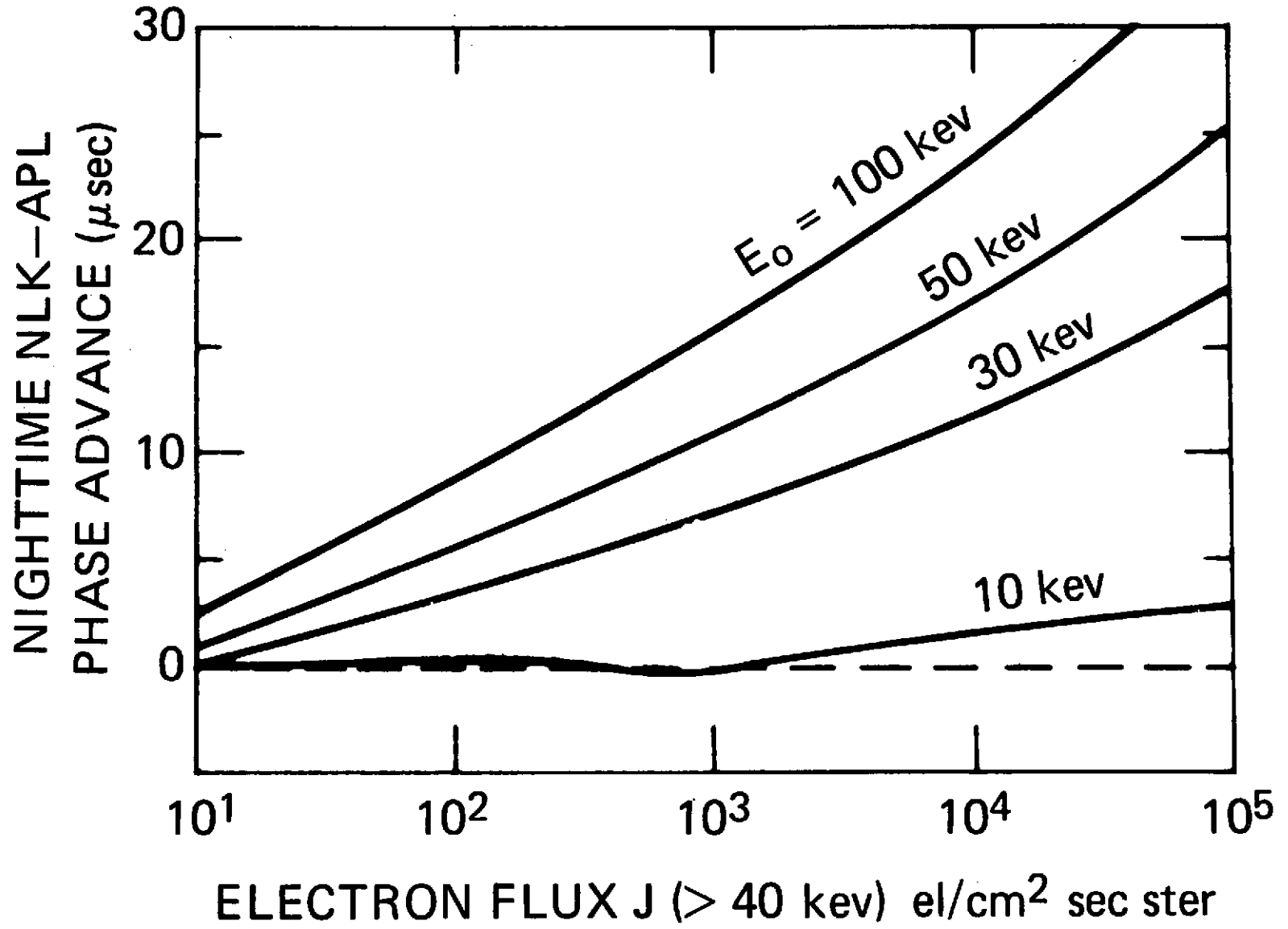


Figure 4.

7. Electron Contamination in a Mid-Latitude Soft X-Ray Astronomy Experiment During an Intense Magnetic Storm....S. Naranan, H. Friedman, G. Fritz, R. C. Henry and S. Shulman

ELECTRON CONTAMINATION IN A MID-LATITUDE  
SOFT X-RAY ASTRONOMY EXPERIMENT DURING  
AN INTENSE MAGNETIC STORM

NW-28253

S. Naranan\*, H. Friedman, G. Fritz,  
R. C. Henry<sup>+</sup>, and S. Shulman

E. O. HULBURT CENTER FOR SPACE RESEARCH  
Naval Research Laboratory  
Washington, D. C. 20375

June 1974

\*On leave from Tata Institute of Fundamental Research,  
Bombay, India.

+Also at The Johns Hopkins University, Department of Physics,  
Baltimore, Maryland.

Submitted to Proceedings of Conference on Particle  
Contamination in Low Energy X-Ray Astronomy Experiments  
held at NASA Headquarters, Washington, D. C. on 26 April 1974.

## INTRODUCTION

A large area X-ray sky survey payload was launched from White Sands Missile Range (106°W, 32°N) on 1 Nov 1972 at 0530 hours U.T. The launch time coincided with intense geomagnetic activity (3 hour Kp index = 8) following a solar flare. The data have been analysed to determine possible contamination of X-ray data by large fluxes of low energy electrons that can precipitate down to low altitudes during magnetic storms. There is clear evidence in the data for low energy electrons of 10 - 50 keV contributing appreciably at ~ 200 km altitude in the 1 - 10 keV X-ray energy channels of the proportional counters used for the X-ray observations. The McIlwain parameters L and B for this altitude at White Sands are 1.25 and 0.46G, respectively. Most of the contribution occurs at large pitch angles with respect to the local magnetic field direction. The extent of electron contamination depends on the counter window thickness. In the present experiment, electrons did not affect appreciably X-ray data in X-ray energy channels below 1 keV.

## EXPERIMENTAL DETAILS

The rocket payload consisted of two decks of proportional counters each with a pair of counters back-to-back looking 180° apart. Two counters each had an effective area of 1200 cm<sup>2</sup> with 2.0 micron thick kimfol

window and with  $\sim 47\%$  transmission efficiency at the carbon K-edge of 0.25 keV. The other two counters had similar areas but had 3.2 micron thick teflon windows with  $\sim 22\%$  transmission at the fluorine K-edge of 0.66 keV. Kimfol counters had honeycomb collimators with circular field of  $7^\circ$  FWHM and the teflon counters had a field of view  $10^\circ$  FWHM. All the counters had wire-wall anti-coincidence counters on five sides to minimize non-X-ray background. Pulse heights were telemetered in 512 channels. In-flight calibration was provided by exposing the detectors to  $\text{Fe}^{55}$  (5.9 keV X-rays) sources at the beginning and in the middle of the flight. These calibrations indicated that two kimfol detectors and one teflon detector performed nominally. One teflon detector malfunctioned.

The rocket had a spin rate of  $68^\circ$  per sec, and the spin axis precessed on a cone of half angle  $44.5^\circ$  at  $0.54^\circ$  per sec. The X-ray view directions perpendicular to the spin axis scanned nearly 25% of the sky during the flight, mostly in the southern galactic latitudes between galactic longitudes  $40^\circ$  and  $220^\circ$ . The rocket reached a peak altitude of 205 km, and most of the data analysis is confined to altitudes above 150 km.

### EXPERIMENTAL RESULTS

The pulse height distributions of the proportional counter data, clearly show peaks corresponding to the

0.25 keV (Carbon K-edge) in the kimfol counter and to the 0.66 keV (Fluorine K-edge) in the teflon counter. These peaks indicate that X-rays are being observed below 1 keV. However, in the higher energy channels (above 1 keV) the distribution of counting rates over the sky is uneven, contrary to the well known isotropic distribution of cosmic diffuse X-rays above 1 keV. It is therefore likely that there is appreciable contamination by particles - low energy electrons - which are known to precipitate into the lower atmosphere during intense magnetic storms.

To correlate counting rates with the local geomagnetic field direction, the rates were mapped in  $10^\circ \times 10^\circ$  bins in a coordinate system with the local magnetic north (at WSMR) along the positive z-axis. Fig. 1 shows such a map for events which deposited 1 - 6 keV of energy in the detector. Also shown is the "sea-level" horizon (rocket horizon at 200 km altitude is  $\sim 15^\circ$  lower than the "sea-level" horizon). The most striking feature is the presence of two enhanced regions of intensity at  $\sim 90^\circ$  pitch angle (angle between particle direction and magnetic field direction) on the horizon,  $180^\circ$  apart in the West and East directions. Part of the excess on the W horizon is due to the strong X-ray source Ser XR-1. On eliminating the times when the detectors crossed Ser XR-1, it is found that the fluxes are approximately equal in the W and E directions. The intensities begin to fall off at pitch angles below  $90^\circ$ . The counting rates in the regions at

small pitch angles (170-225 counts/sec) are typical of diffuse cosmic X-ray flux measured in other experiments. It is therefore probable that the excess counting rates (above 225 counts/sec) in the map are due to electrons, and they are dominant on the horizon and at  $90^\circ$  pitch angle.

The payload instrumentation included a measurement of particles crossing the detector and the anti-coincidence shield surrounding it. Fig. 2 shows these "coincidence" rates on a map similar to Fig. 1. The map shows clearly up-down symmetry, i.e. similar intensities in regions  $180^\circ$  apart. This symmetry could be due to high energy particles capable of crossing the detector and the anti-counter in either direction. If they are electrons or protons their energies would exceed 10 or 70 Mev, respectively. The lowest intensity regions (800-1150 counts/sec) correspond to normal cosmic ray proton background of  $\sim 1$  particle/cm<sup>2</sup> sec. The enhanced fluxes are again observed at the same two regions, near W and E horizon at  $90^\circ$  pitch angle, as in Fig. 1.

A map of the counting rates in the last channel - the "overflow" channel corresponding to  $\geq 12$  keV energy deposition in the proportional counter and in anti-coincidence with the shield is shown in Fig. 3. The counting rates are much higher than those predicted from the cosmic X-ray background. The electrons contributing to these

rates have energies between 20 and 60 keV. Again, we notice quasi up-down symmetry and enhanced emission in the same regions as in Figs. 1 and 2.

Figs. 1, 2, 3 provide evidence for preferential occurrence of particles in X-ray energy channels above 1 keV in directions correlated with geomagnetic field. But in the lower energy energy channels there is no evidence for appreciable particle contaminations. Fig. 4 is a map of counting rates in  $0.25 \pm 0.1$  keV energy band of the kimfoil counters. First, we do not see any enhanced emission at  $90^\circ$  pitch angle on the W and E horizons; on the contrary we see low intensity, typical of X-rays suffering atmospheric absorption near the horizon. In general, there is no correspondence between the 0.25 keV map and the other three maps where particle contributions are evident. An exception is the region of higher than average intensity above E horizon at low pitch angles (counting rates 265-350 counts/sec); this region correlates in position with enhanced emission regions in Figs. 1, 2 and 3 suggesting possible contamination by electrons in 0.25 keV channel as well. In that case, it is unclear why similar correlation is not seen in other regions, where the electron contamination is even higher. Further evidence for the absence of any appreciable electron contamination below 1 keV - both in the kimfol and teflon counters - is provided by spectral data and calculations of electron

efficiencies in various energy channels discussed later.

If the counting rates in the low energy channels are indeed predominantly due to X-rays, it is appropriate to replot the maps in the galactic coordinate system. Fig. 5 shows two such maps in energy bands  $0.25 \pm 0.1$  keV and  $0.3 - 0.9$  keV of the kimfoil counters. The map shows an unexpected gradient in galactic longitude, and also enhanced emission at all latitudes in the longitude interval  $180$  to  $230^\circ$ . The enhanced intensity at the south galactic pole (SGP) is approximately equal to that at the north galactic pole (NGP) observed in an earlier NRL survey experiment of March, 1970<sup>(1)</sup>. The higher fluxes at low galactic latitudes ( $160^\circ < l^{\text{II}} < 200^\circ$ ) may partly be accounted by soft X-rays from some discrete X-ray sources shown in the figure. The bright feature at  $l^{\text{II}} \approx 205^\circ$ ,  $b^{\text{II}} \approx -45^\circ$ , about  $30^\circ$  across ("Hot Spot") near 3U0431-10, a weak 3U Uhuru catalog source, could be a cosmic X-ray source. We cannot exclude atmospheric X-rays contributing to the regions of higher than normal X-ray intensity. However, it is unlikely that they are bremsstrahlung X-rays produced locally in the collimator walls by low energy electrons, since the local electron fluxes inferred from Figs. 1, 2 and 3 are too small to account for the observed enhancement of X-rays.

The most convincing evidence to rule out particles as being responsible for high intensity regions in

Figs. 4 and 5 is provided by the energy spectra measured in the two regions: (1) South Galactic Pole region (Fig. 6a, b) defined by  $60^\circ < \ell^{II} < 240^\circ$ ,  $-60^\circ < b^{II} < -90^\circ$ , and (2) "Hot Spot" defined by  $195 < \ell^{II} < 210$  and  $-30^\circ < b^{II} < -48^\circ$ . In the kimfol counters there is a prominent peak at 0.25 keV and in teflon counters a peak at 0.66 keV, as expected for X-rays. Similar spectra are obtained for the "Hot Spot" also. Any appreciable electron contamination would tend to wash out the peaks. Further, these spectra have shapes almost identical to the spectral shapes derived for regions of normal X-ray intensity (regions with counting rates 210-315 counts/sec).

#### ELECTRON ENERGY SPECTRUM

We can make a rough estimate of the electron flux and its energy spectrum in the two enhanced emission regions in Fig. 1 (1 to 6 keV map). There are many complex problems in such an analysis. The electron fluxes critically depend on altitude, direction and pitch angle, and they may be affected by the orientation of the rocket with respect to the local geomagnetic field direction. The latter effect is important because the gyromagnetic radius of low energy electrons is small (a few meters at 10 keV) and the rocket velocity is negligible compared to the electron velocities. The low energy electrons can be absorbed in the rocket body and the amount absorbed

can depend on the orientation of the long axis of the rocket with respect to the magnetic field direction. The effective collimator width will also depend on the electron energy because of scattering in collimator walls. Also, at higher energies electrons can penetrate collimator walls at large angles to the collimator axis. Finally, effects of range straggling and proportional counter resolution will also have to be considered.

We have employed the following procedure to obtain an estimate of the electron flux and the electron spectrum. First, we deduced a set of curves for the probability that electrons of different energies would deposit an amount of energy corresponding to any given energy band-width in the kimfol and teflon counters (Fig. 7). These are obtained as follows: We used a range energy relation for electrons from the summary of experimental measurements and theoretical calculations given by Gledhill<sup>(2)</sup>. The relation is a simple power law of the form

$$R_p = 2.8 \times 10^{-4} (E/10)^{1.70} \quad 3 < E < 100 \text{ keV}$$

where  $R_p$  is the range in air in  $\text{g cm}^{-2}$ . Ranges in kimfol, teflon and argon-methane gas mixture are determined by assuming  $R_p \propto \langle Z \rangle^{-1/3}$ , where  $\langle Z \rangle$  is the mean atomic number of the material. Straggling is taken to account by the semi-empirical expression for electron transmission as a function of material thickness given by Subba Rao<sup>(3)</sup>. This relation is based on experimental data for electron

energies down to 10 keV. We have adopted a method similar to the one used by Touhy and Harries<sup>(4)</sup> to find the effective contribution of electrons of different energies in various energy channels. The electron energy (without straggling) corresponding to a 2 micron range in kimfol is  $\sim 9$  keV and that corresponding to a 3.2 micron range in teflon is  $\sim 18$  keV. Each pulse height level is converted to an equivalent thickness of window material corresponding to 50% transmission at that energy. This thickness is added to the actual window thickness to give an effective window thickness for each energy level. The probability of an incident electron penetrating the counter window and having an energy exceeding the energy level is assumed to be the same as the probability of an electron penetrating the effective window. The probability of an electron registering in any given energy level is then given by the difference in the transmission probabilities for the lower and upper bounds of the energy level.

The electron contributions to counting rates in different energy levels at the regions of high intensity near the W and E horizons were determined by subtracting as a background the counting rates observed in regions corresponding to the normal diffuse X-ray intensity (regions with counting rates 200 - 300 counts/sec in Fig. 5). To obviate consideration of counter resolution,

counts were grouped in broad energy channels: 0.9-3.4 keV, 3.4 - 7.6 keV and 7.6 - 10.7 keV for the kimfol counters, and 2.1-5.0 keV, and 5.9 - 12.0 keV for the teflon counters. It was assumed that the effective collimator FWHM is the geometrical value - i.e.  $7^\circ$  for the kimfol counters, and  $10^\circ$  for the teflon counters.

Two types of differential electron energy spectra,  $N(E)$  were considered: (a) a power law spectrum  $A E^{-\gamma}$  and (b) an exponential spectrum  $C e^{-E/E_0}$ , where  $E$  is the electron energy and  $A$ ,  $\gamma$ ,  $C$  and  $E_0$  are constants. The assumed spectra are folded with the efficiency curves of Fig. 7. The best fit to the measured counting rates in the five energy channels (3 in kimfol and 2 in teflon) is obtained with an exponential spectrum  $N(E) = 12e^{-E/7.5}$  electrons/ (cm<sup>2</sup>sec ster keV)  $E > 7.5$  keV. The measured counting rates in different energy bands were within 30% of the values predicted by the above spectrum. The calculations show that most of contribution comes from 10 - 20 keV electrons in the kimfol counter, and 15 - 30 keV electrons in the teflon counter. The above spectrum gives a total flux of  $\sim 33$  electrons/ (cm<sup>2</sup>sec ster) for electrons above 7.5 keV. This total flux is insensitive to the actual spectral shape of the electrons.

The efficiency curves of Fig. 7 further reinforce the earlier conclusion that electrons do not contribute appreciably to the low energy channels below 1 keV.

For instance, at all electron energies the ratio of counts in the 0.25 keV channel (channel A) and 0.35 - 0.9 keV channel (channel B) of the kimfol counters is  $\sim 0.3$ , whereas the observed ratios at the south galactic pole (Fig. 6a, 6b) and "Hot Spot" are  $\sim 1.7$ . Similarly at all electron energies, the ratio for electrons in the 0.66 keV band in kimfol and teflon counters is  $> 5$ , whereas the observed ratio is close to 1.0.

### SUMMARY AND CONCLUSION

Low energy electrons of energy  $> 10$  keV were found deep in the atmosphere (as low as 200 km altitude) in sufficiently large numbers to affect X-ray measurements in proportional counters above 1 keV in a soft X-ray astronomy rocket experiment launched at White Sands Missile Range. This is presumably due to the intense geomagnetic storm (3 hour  $K_p$  index = 8) that coincided with the launch time. The particles appear preferentially at two regions at large pitch angle directions with respect to the local magnetic field near the West and East horizon. Large pitch angles suggest that even electrons of energy as low as 10 keV can be quasi-trapped at low L values ( $L = 1.25$ ), during an intense magnetic storm. The increase in flux is not in all azimuthal directions in the plane perpendicular to the magnetic field, but is confined to two regions near the W and E horizons. The significance of this is not clear. The differential

electron energy spectrum at these two regions can be approximately given by an exponential spectrum of the form  $e^{-E/7.5}$ , and the electron flux above 7.5 keV is  $\sim 33$  electrons/( $\text{cm}^2 \text{ sec ster}$ ). There is some evidence in the data that the electron spectrum depends on the pitch angle.

While the electrons do affect the X-ray measurements above 1 keV, they do not contaminate seriously X-ray measurements in the lower energy channels confined to narrow energy bands at the carbon and fluorine K-edges of 0.25 keV and 0.66 keV respectively. We cannot rule out atmospheric X-rays being partly responsible for enhanced X-ray intensities below 1 keV in certain regions of the sky. The observed electron fluxes are however too small to account for these as bremsstrahlung X-rays produced either in the atmosphere or the collimator walls.

## REFERENCES

- (1) A. Davidsen, S. Shulman, G. Fritz, J. F. Meekins,  
R. C. Henry, and H. Friedman, *The Ap. J.*, 177, 629, (1972).
- (2) J. A. Gledhill, *J. Phys. A.*, 6, 1420, (1973).
- (3) B. N. Subba Rao, *Nucl. Inst. and Methods*, 44, 155, (1966).
- (4) I. R. Touhy and J. R. Harries, *J. Geophys. Res.*, 78,  
8381, (1973)

## FIGURE CAPTIONS

- Fig. 1. Distribution of counting rates in the 1 - 6 keV energy range of the kimfol counters. The local magnetic field direction (North) at WSMR is the positive z-axis. Parallels of latitude correspond to different pitch angle directions. The "sea level" horizon, local zenith and the direction of the North and South Galactic Poles (NGP, SGP) are also shown. The region where X-rays from the Crab nebula dominate, is shown.
- Fig. 2. Distribution of counting rates of particles crossing the kimfol detector and the surrounding anticoincidence shield. The coordinate system is the same as in Fig. 1.
- Fig. 3. Similar to Fig. 1, except that the counting rates are for the "overflow" channel corresponding to energy deposition above 12 keV in the kimfol detectors.
- Fig. 4. Similar to Fig. 1, except that counting rates are for the 0.25 keV band corresponding to the carbon K-edge of the kimfol windows.
- Fig. 5. The top figure is the same as Fig. 4 remapped in the galactic coordinate system. Some discrete X-ray sources are also shown. The bottom figure is for the 0.3-0.9 keV energy range of the kimfol counters.
- Fig. 6. Fig. 6(a) is the spectrum of events observed in one of the kimfol counters in the region near the South Galactic Pole. 6(b) is the spectrum from the teflon

counter. In both, pulse heights are converted to energies using in-flight calibration.

Fig. 7. Calculated curves of counter efficiencies as a function of incident electron energy in various energy channels. Left is for the kimfol counters and right is for the teflon counter. Channels H in the left, and G in the right are the overflow channels. (See text)



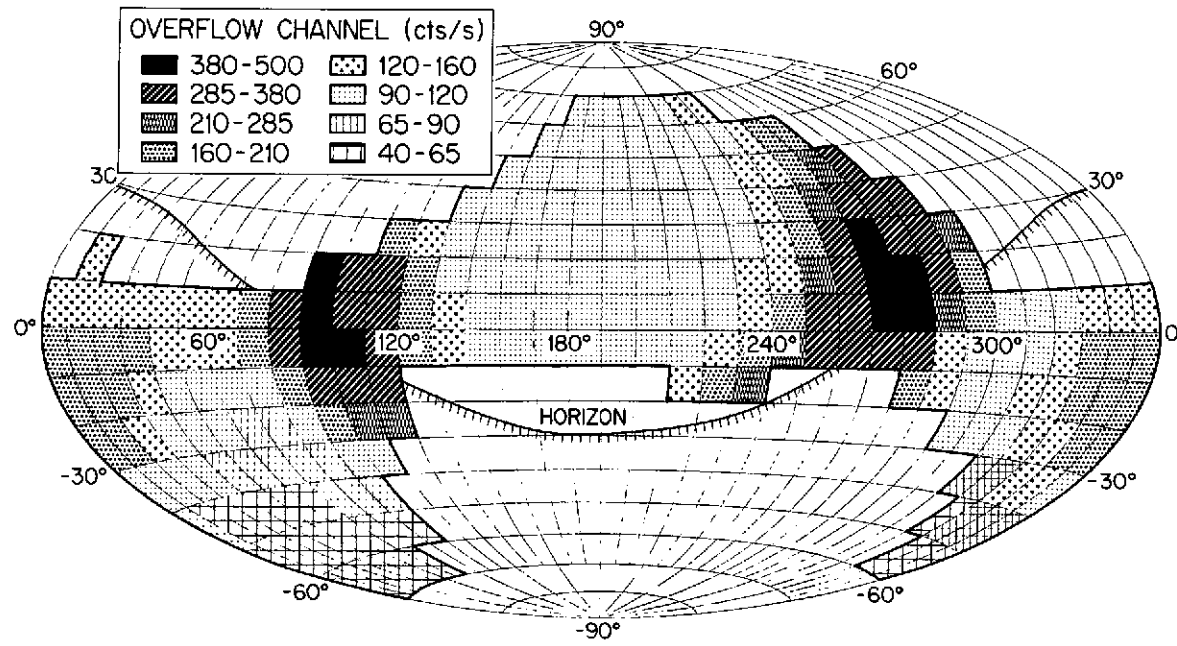


Fig. 3

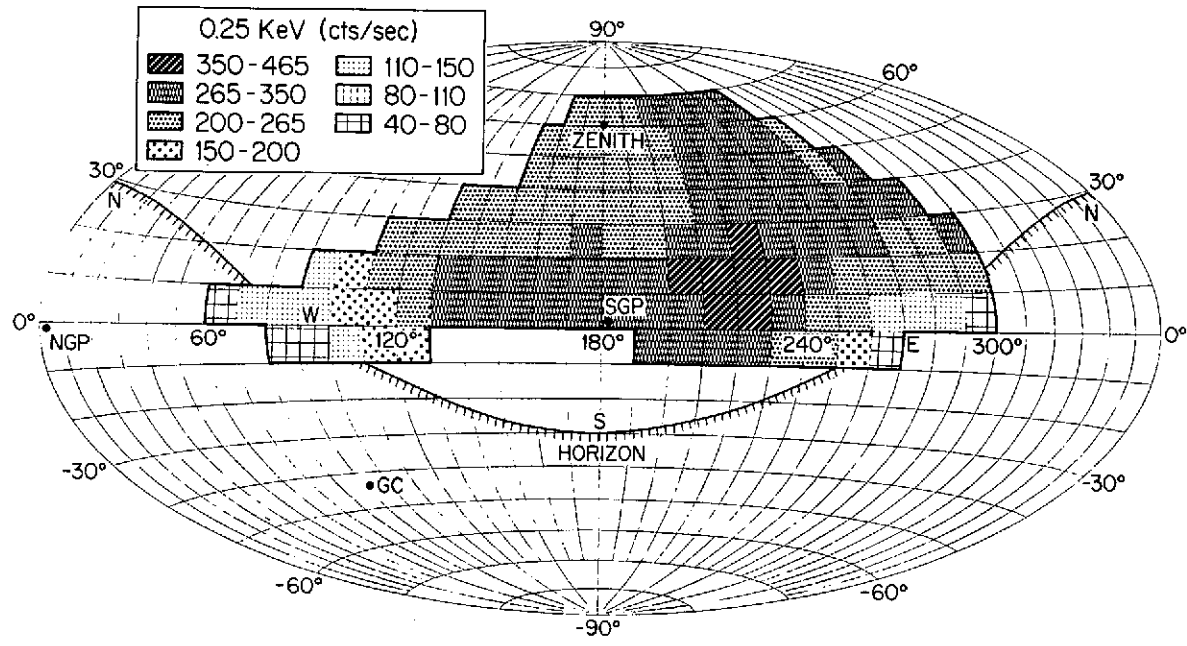
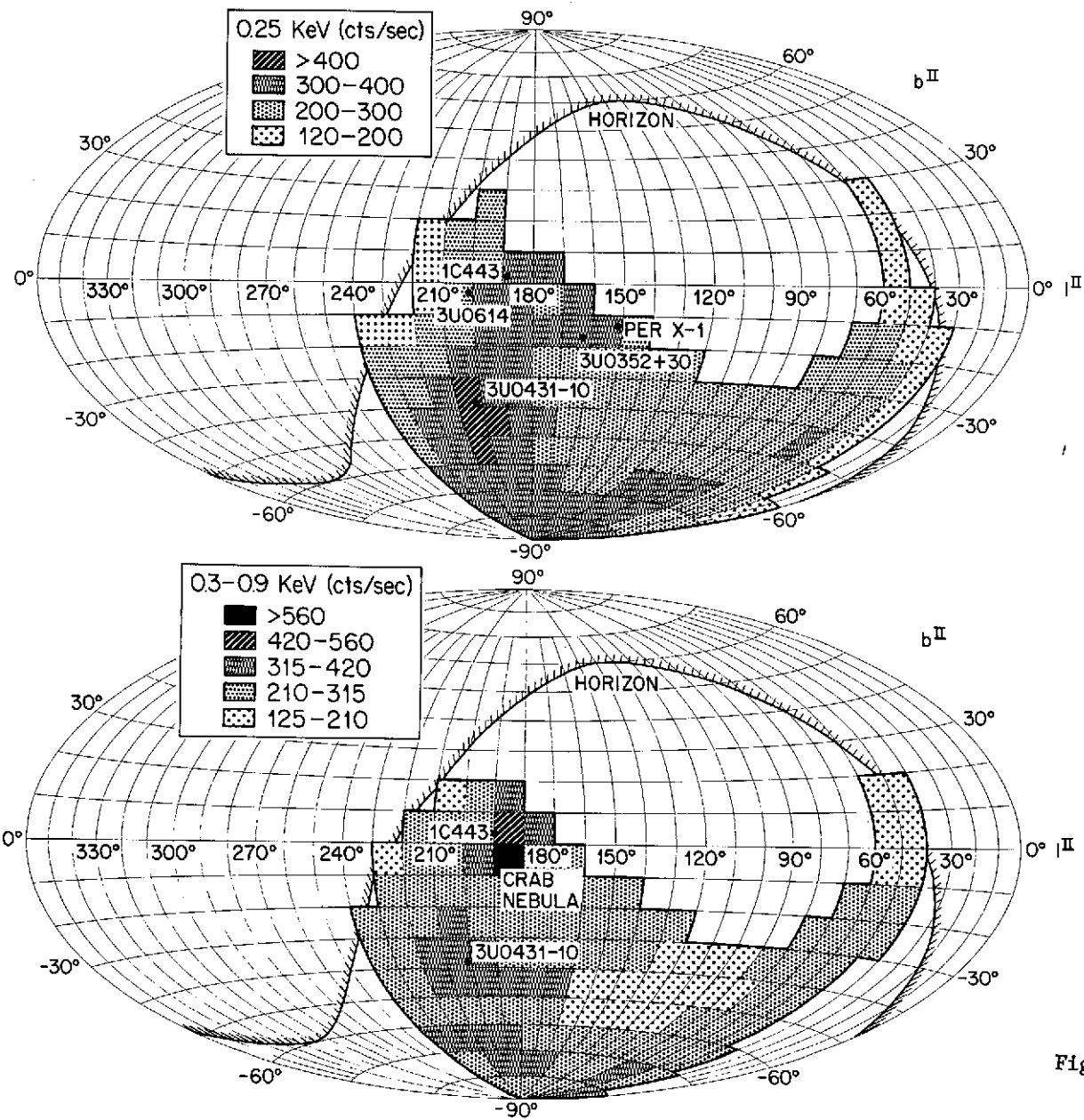


Fig. 4



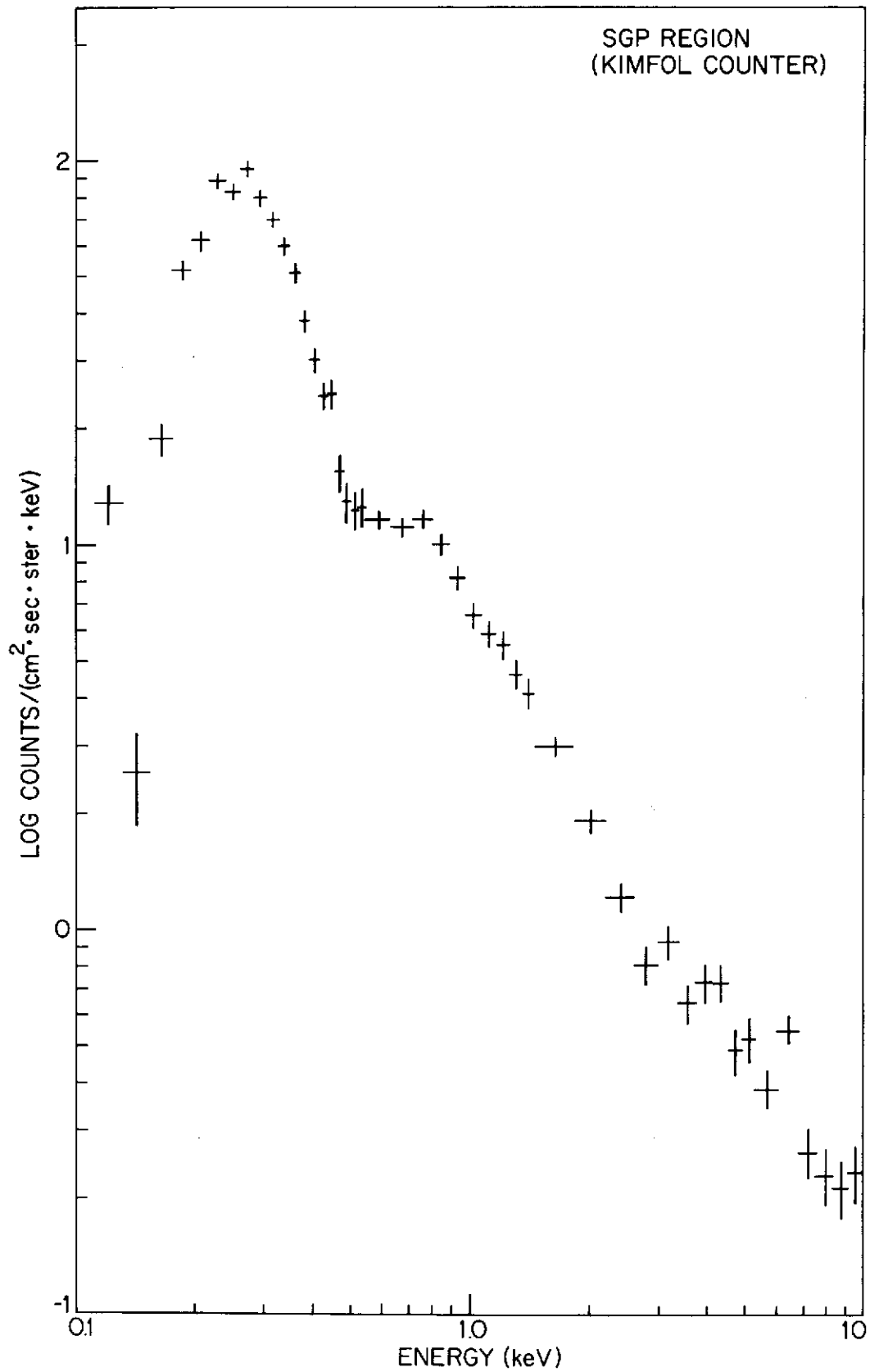


Fig. 6a

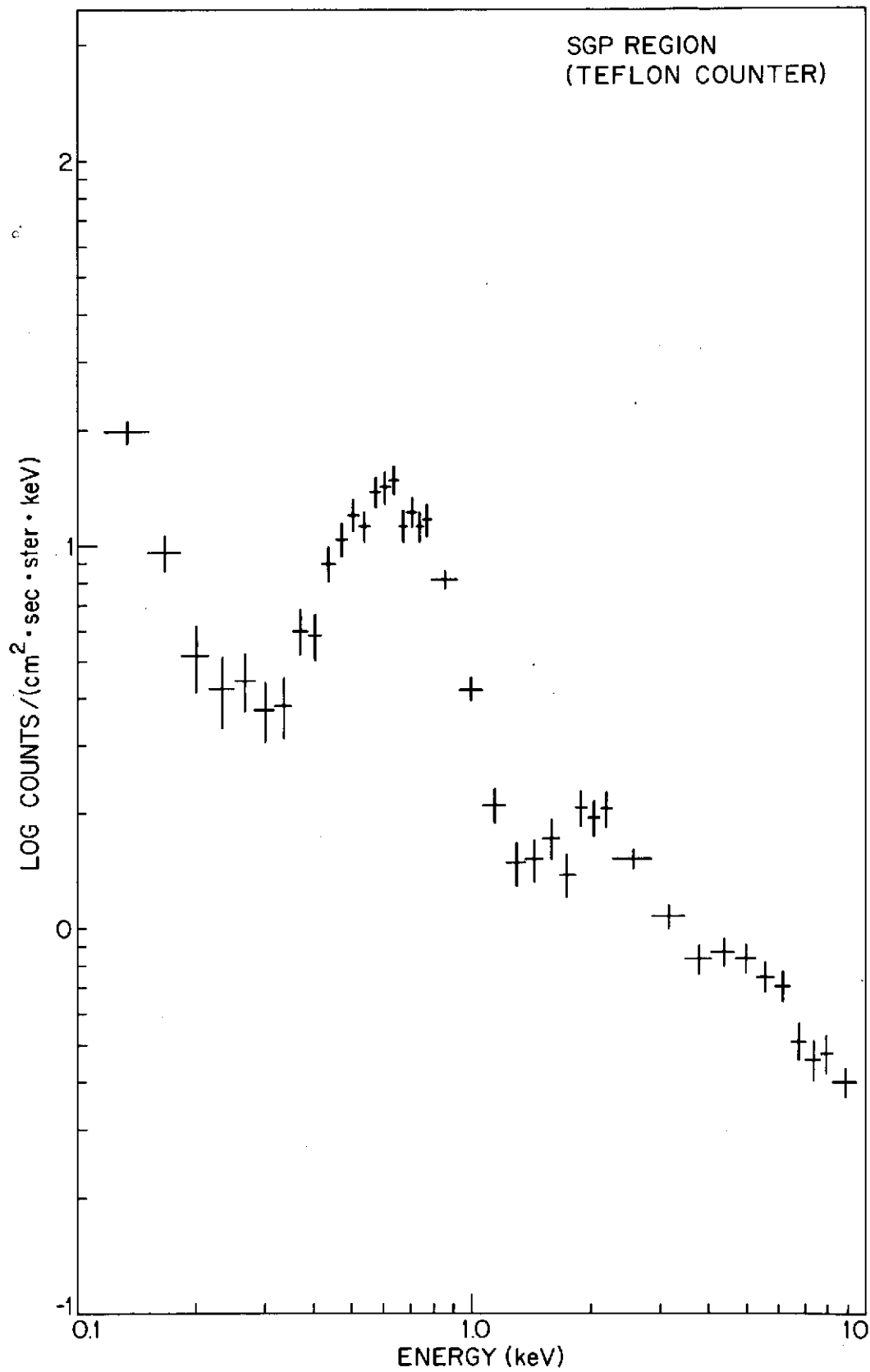


Fig. 6b

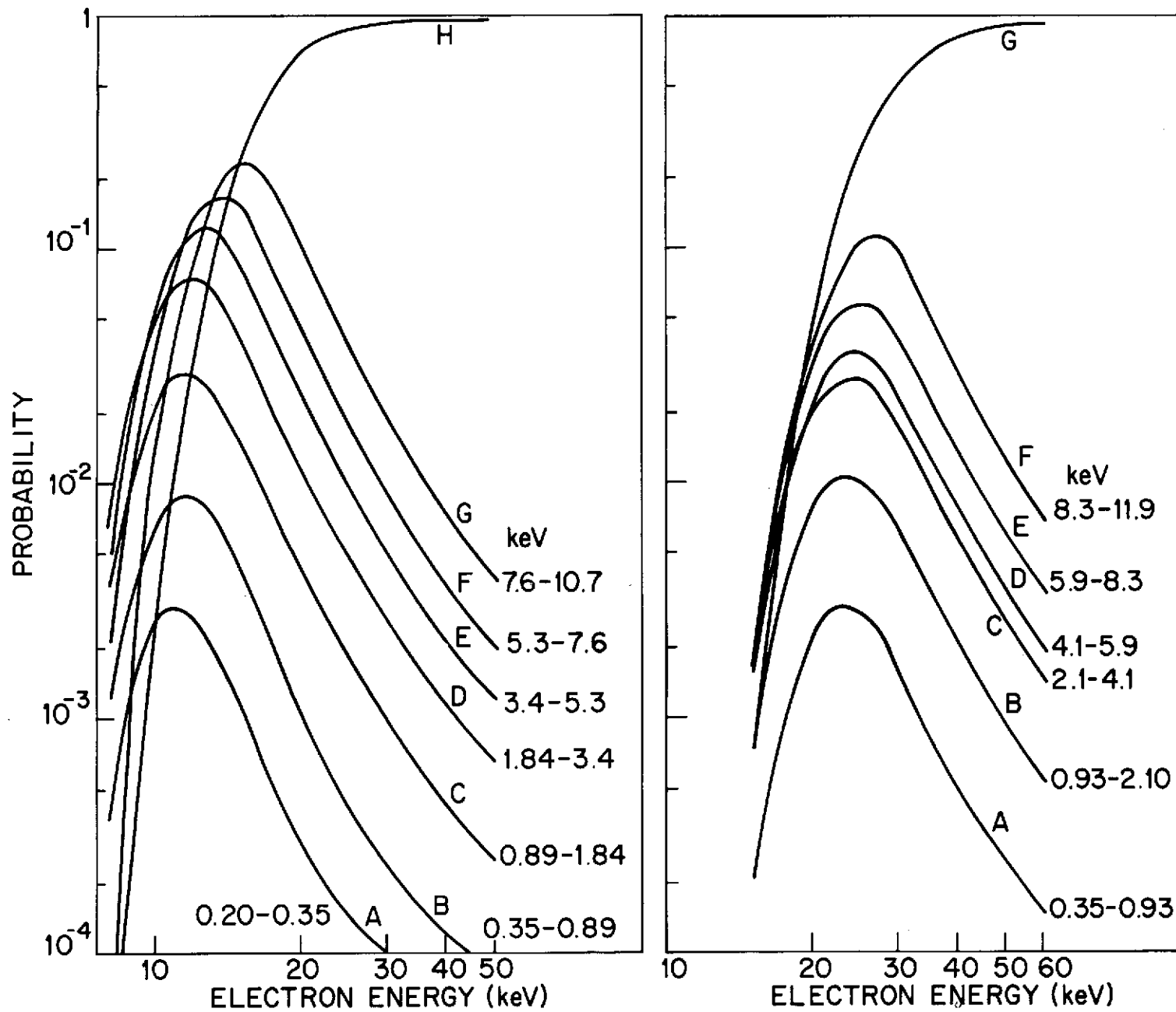


Fig. 7

8. Soft X-Ray Bremsstrahlung and  
Flourescent Line Production in  
the Atmosphere by Low Energy  
Electrons....W. Kraushaar

N74-28254

SOFT X-RAY BREMSSTRAHLUNG AND FLUORESCENT LINE  
PRODUCTION IN THE ATMOSPHERE BY LOW ENERGY ELECTRONS

W. Kraushaar

Physics Department

University of Wisconsin

Madison, Wisconsin 53706

Low energy quasi-trapped or precipitating electrons that are capable of by-passing magnetic rejection schemes and penetrating the counter windows of soft X-ray detectors are a serious annoyance, have been observed by most soft X-ray rocket groups and will undoubtedly be more serious at satellite altitudes. Fortunately there are several clues that reveal the presence of electrons (pulse height distribution, angular distribution) so that at least one can usually avoid accepting or reporting faulty X-ray data in their account.

X-rays produced in the residual atmosphere above particularly a rocket-borne detector are potentially a more serious hazard because they may easily be mistaken for X-rays of cosmic origin. The danger is great in the "discovery" of previously undetected broad features in the soft X-ray sky and, of course, small in the study of small diameter known objects, such as a supernova remnant, where the detector can be moved from on to off the source or background subtraction.

Intense fluxes of low energy electrons in and near the auroral zones are well known, and atmospherically-produced bremsstrahlung is probably responsible for the enormous soft X-ray intensities reported by Baxter et al. (1969) and Hukla and Wilson (1971). At low to moderate geomagnetic latitudes (the site of most soft X-ray rocket launches) there has until recently been very little low energy electron data taken at altitudes where bremsstrahlung could be an important effect.

The low energy ( $E > 100$  eV) electron data from ISIS (Heikkila, 1971 and Inningham, private communication) suggested that atmospherically-produced bremsstrahlung could be serious. But since the satellite perigee was 570 km nothing was revealed about the electron fluxes at lower altitudes where, because of the larger air densities, bremsstrahlung could result in very

large X-ray intensities. Some of these matters were discussed by Prilutskii, Rozental and Shukalov (1971) and by Mack and Kondo (1973).

Data from the recently launched Atmospheric Explorer C has permitted better or at least other estimates of the bremsstrahlung. R. A. Hoffman of the Goddard Space Flight Center kindly provided me with some preliminary low energy electron data taken at altitudes as low as 150 km and emphasizes that not all features of the data are well understood as yet. An approximate representation of what Hoffman describes as a typical high flux spectrum is shown in Figure 1. If one assumes that this number of electrons exists everywhere above 150 km, adopts a high density atmospheric and computes the bremsstrahlung using the Bethe-Heitler cross-section, the predicted zenith flux is  $\sim 2 \text{ (cm}^2\text{-s-st)}^{-1}$  in the X-ray energy region 100-280 eV or about 10% of the corresponding measured quantity from directions near the galactic plane. I have chosen to use the highest electron fluxes reported by Hoffman and a high density model atmosphere in these estimates. (A "medium" density atmosphere reduced the 10% mentioned above to about 2%). It is nonetheless clear that bremsstrahlung by low energy electrons should be of some concern in interpreting the soft X-ray diffuse background, especially since the effect could be enhanced by factors of order 10 near the 90° horizon.

Bleeker, Deerenberg, De Korte and I discussed these matters in Leiden during the fall of 1973 and considered the K-fluorescent lines of oxygen and nitrogen as a possible tracer or tag from electron-induced atmospheric X-ray production.

At Wisconsin we have computed, using the electron cross-sections for K-shell fluorescent emission measured by Tawara, Harrison and de Heer (1973), the N and O fluorescent line fluxes for a variety of assumed electron spectra. We also computed the bremsstrahlung for the same electron spectra and Figure 2 shows the ratio (N+O) line flux/bremsstrahlung flux for electron spectra of

the form  $E^{-\gamma}$  for various values of  $\gamma$ . The detailed response of a detector to the complex incident spectra depends critically, of course, on the counter window composition and thickness.

One of the windows used by our group is  $48 \mu\text{g cm}^{-2}$  Kimfol +  $44 \mu\text{g cm}^{-2}$  Formvar +  $4 \mu\text{g cm}^{-2}$  colloidal carbon. A typical counter response (pulse height distribution) to cosmic X-rays is shown in Figure 3, and is well represented by  $160 W^{-1} \exp(-W/0.32) + 11 W^{-1.3}$  with  $W$  the X-ray energy in KeV. The calculated response of this same counter to the X-ray spectrum generated by an electron spectrum  $E^{-\gamma}$  incident upon an optically thin gas in which the ratio of oxygen to nitrogen atoms is 0.4 is shown in Figure 4. For values of  $\gamma$  near one, it appears that the N and O lines do indeed provide a characteristic tag on atmospherically-produced X-rays. Steeper spectra (large values of  $\gamma$ ) provide little or no tag since there are too few electrons energetically capable of exciting the O and N lines. The preliminary electron spectra available from ISIS and Atmospheric Explorer C seem to show values of  $\gamma$  near one.

On two occasions we have observed an enhanced soft X-ray intensity at the horizon. These are evidently earth-associated since they are not present when the same celestial directions were viewed at other times at small zenith angles. Circumstances of sun position make scattered solar X-rays an unlikely explanation. There is no striking evidence for the O and N lines discussed here and we can only speculate that perhaps a steep electron spectrum was present.

At satellite altitudes there is very little nitrogen and the usual plastic counter windows have much higher transparencies at oxygen K than at nitrogen K. Hence the line to bremsstrahlung ratios should be larger than at rocket altitudes. Satellite-borne soft X-ray detectors will of course easily view the same celestial directions under a variety of geophysical

geomagnetic circumstances so will have an important advantage over rocket observations. In the meantime it is probably well to view with suspicion rocket-detected features in the soft X-ray sky that have not been observed on more than one occasion, particularly if the zenith angle of the observation was large.

The help of Wilt Sanders with the computations is appreciated. Rocket X-ray work at the University of Wisconsin is supported under NASA Grant NGL 50-002-044.

## References

- Baxter, A. J., Wilson, B. G., and Green, D. W. 1969, Canadian J. Phys. 47, 2651.
- Shukla, P. G. and Wilson, B. G. 1971, Ap. J. 164, 265.
- Heikkila, W. J. 1971, J. Geo. Res. 76, 1076.
- Prilutskii, O. F., Rozental', and Shukalov, I. B. 1971, Sov. Ast. A. J. 14, 669.
- Mack J. E. and Kondo, Y. Preprint 1973.
- Tawara, H., Harrison, K. G., and de Heer, F. J. 1973, Physica 63, 351.
- Winningham, private communication 1973.

## Figure Captions

1. Crude representation of preliminary low energy electron data from Atmospheric Explorer C.
2. X-ray flux in electron-excited nitrogen and oxygen K- $\alpha$  lines/low energy bremsstrahlung flux versus  $\gamma$  of the assumed electron spectrum  $E^{-\gamma}$ .
3. Typical proportional counter response to low energy cosmic X-rays. The window and incident spectra are described in the text.
4. Proportional counter response to X-radiation produced by  $E^{-\gamma}$  spectra electrons incident upon a gas of oxygen to nitrogen number ratio = 0.4.

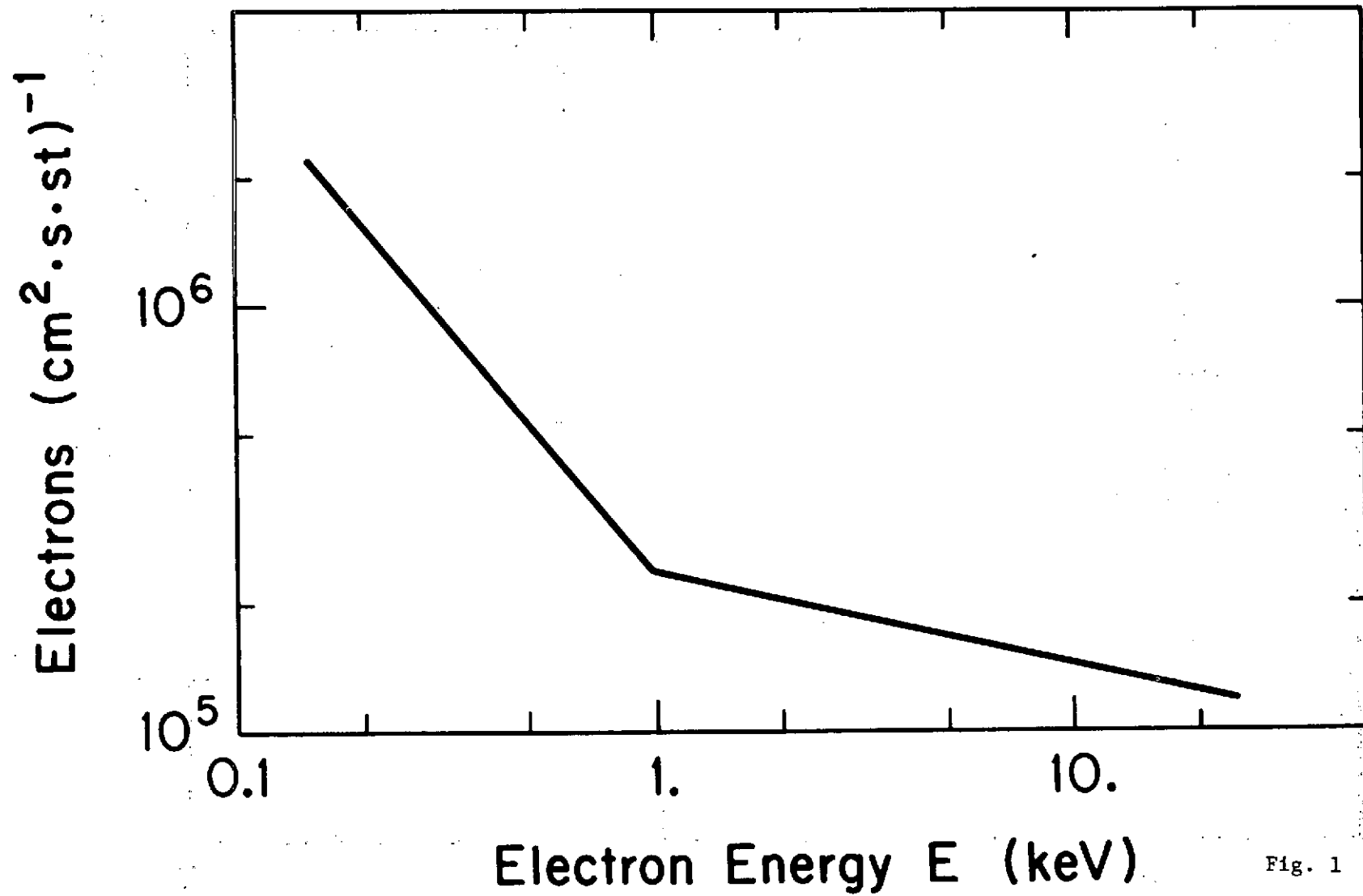


Fig. 1

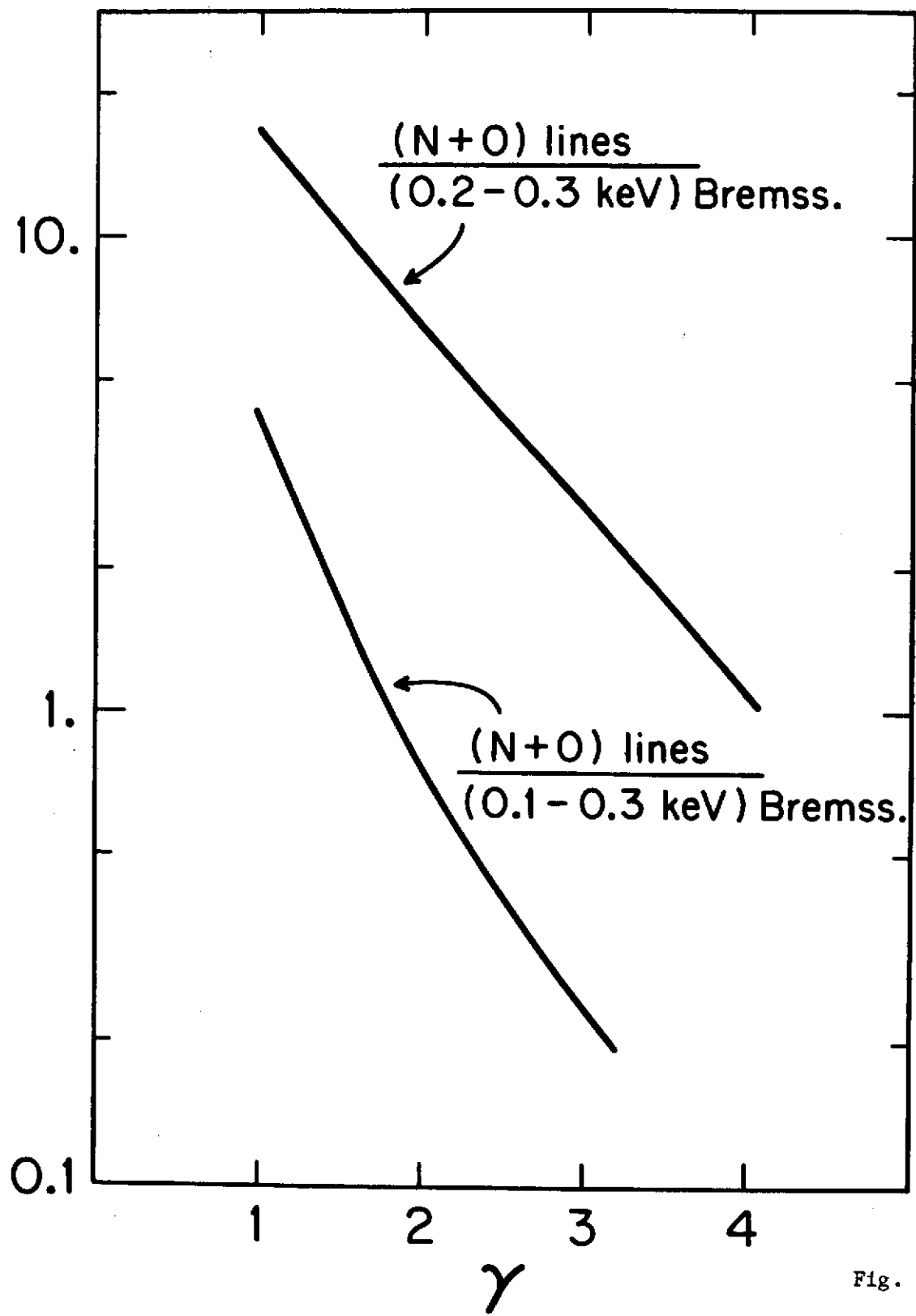


Fig. 2

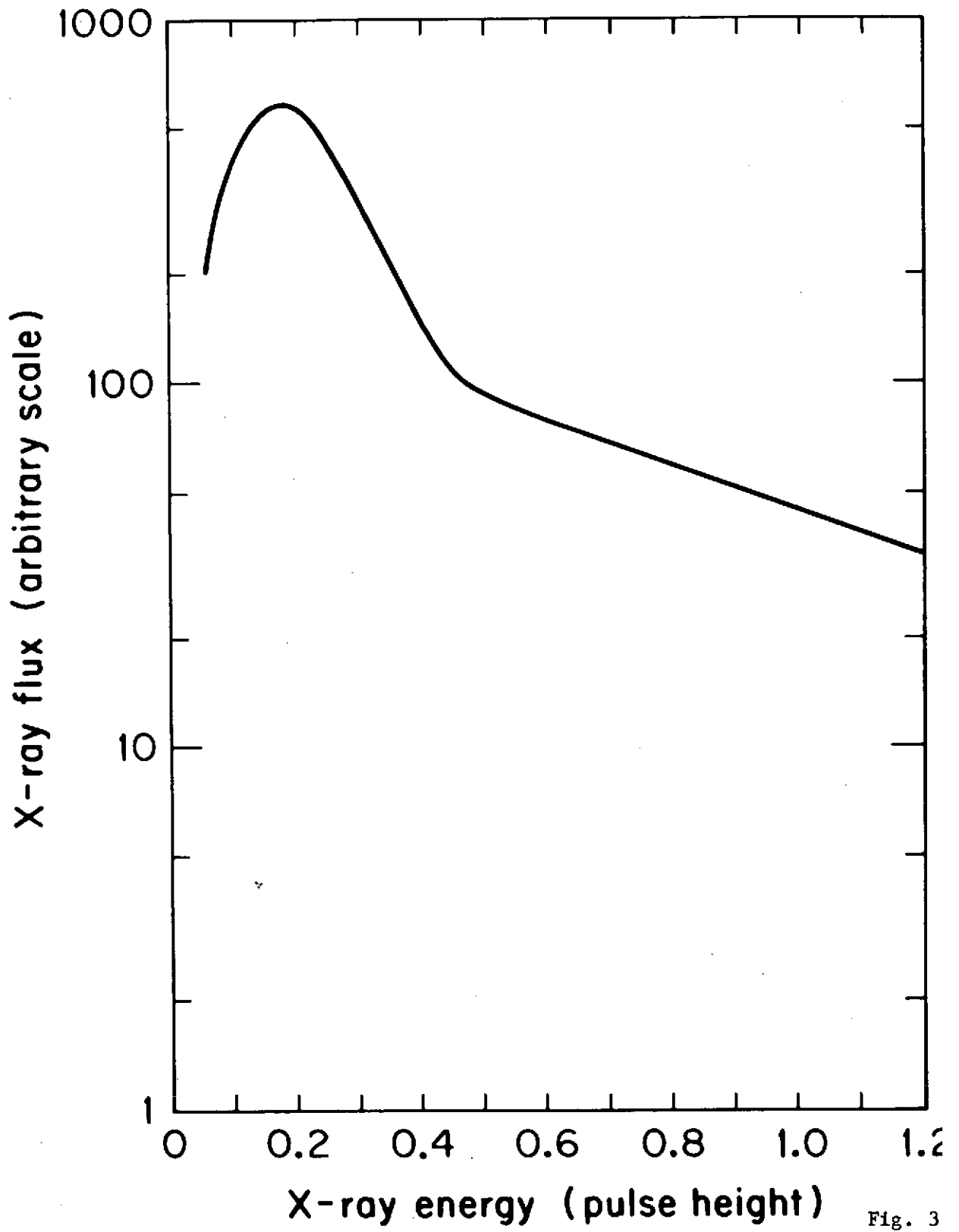


Fig. 3

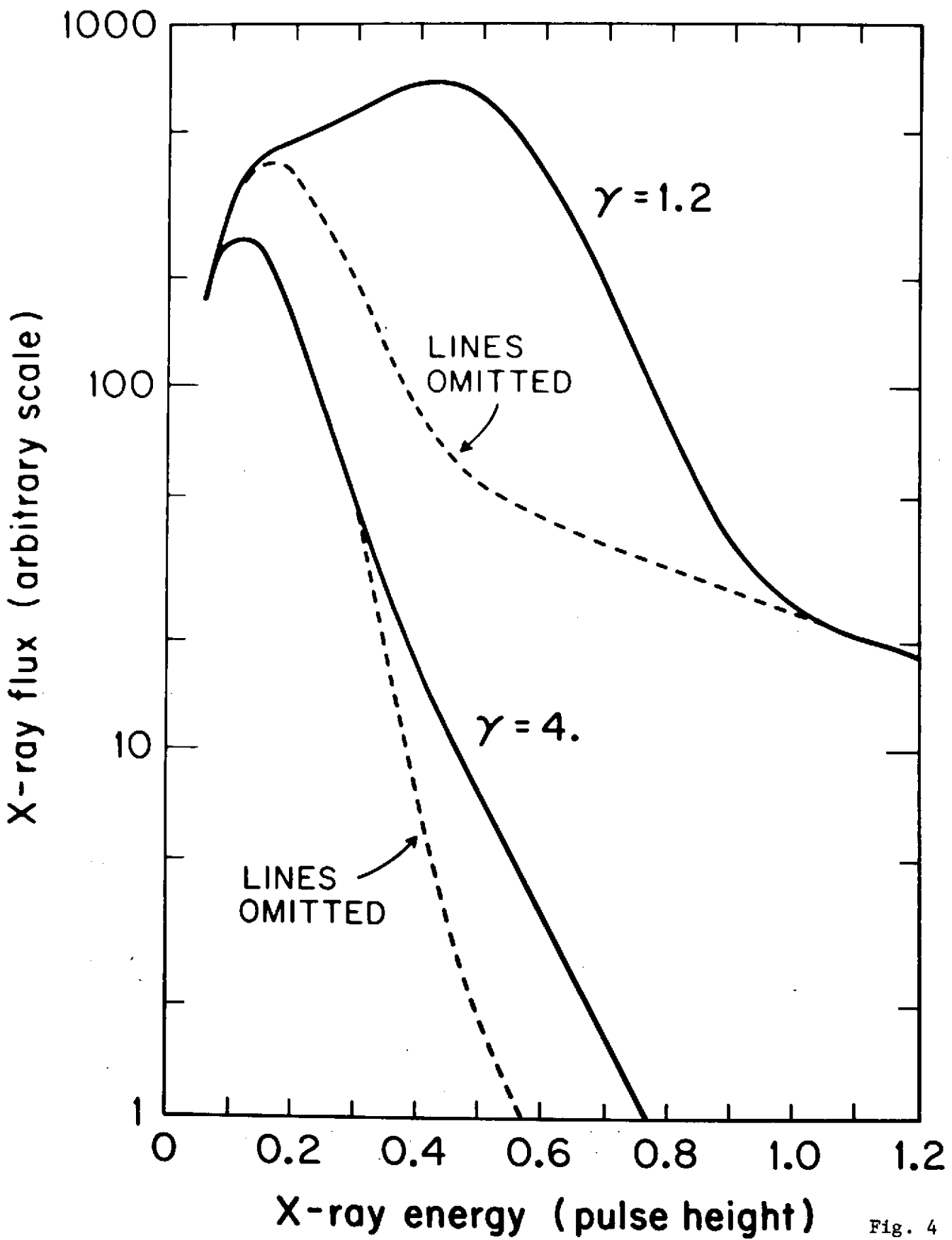


Fig. 4

9. Geomagnetic Background Events  
Observed by UHURU....D. Schwartz

N74-58255

GEOMAGNETIC BACKGROUND EVENTS OBSERVED BY UHURU\*

Daniel A. Schwartz

Center for Astrophysics  
Smithsonian Astrophysical Observatory/Harvard College Observatory  
Cambridge, Massachusetts 02138

26 April 1974

\* Invited contribution to the conference on Particle Contamination of Low Energy X-ray Astronomy Experiments, NASA Headquarters, 26 April 1974.

## ABSTRACT

Problems due to sporadic background events observed by Uhuru (Small Astronomy Satellite - A) have not been examined systematically since they do not compromise the study of discrete X-ray sources. Nevertheless, direct particle effects and auroral type X-ray events in the atmosphere may occasionally occur. Therefore, even on the geomagnetic equator, an experiment must be prepared to recognize and eliminate such events when the ultimate level of sensitivity is desired.

## INTRODUCTION

I wish first to acknowledge the work of the Uhuru group (R. Giacconi et al. 1971; Tananbaum et al. 1971) in reducing and analyzing the data. Since I have not been a member of that group, it is a significant fact that I am giving this talk; namely, that non-X-ray background problems in general have been so slight that they did not interfere with the pursuit of the scientific objectives of studying X-ray sources.

It is well known that direct counting of electrons can contaminate X-ray astronomy experiments in the range below a few keV in typical rocket-flight environments (Hill et al. 1970; Seward 1974). The OSO-III satellite, at a  $33^\circ$  inclination and 550 km altitude, encountered serious problems with geomagnetic electrons which led to the rejection of about 80 percent of the data from the UCSD 7-200 keV X-ray experiment (Schwartz 1969, 1970). The main purpose of this paper is to ask qualitatively whether the same types of events seen on the OSO mission can occur in the region near the geomagnetic equator covered by Uhuru.

In accordance with the informal nature of this conference, I stress that the present work is not an unbiased and systematic investigation for sporadic events. I have looked only at superposed data from the first seven weeks in orbit, 12 December 1970 to 25 January 1971. In looking for sporadic events the data is biased by occurring only during orbit night, only when the given collimator views the sky (eliminating simultaneous coverage by both collimators for much of the data), and by applying certain selection criteria to the raw data in order to eliminate contamination from the superposed data.

## INSTRUMENTATION

Uhuru carries two banks of proportional counters, each with about  $840 \text{ cm}^2$  open area. Side 1 has  $0.52^\circ \times 5.2^\circ$  FWHM collimation and seven pulse height channels between 2.1 and 19.8 keV. Side 2 has  $5.2^\circ \times 5.2^\circ$  FWHM collimation, and seven pulse height channels between 1.8 and 10 keV. Each bank has an integral channel which gives counting rates between about 2 and 6 keV, and which is designated "X1" or "X2", respectively. The proportional counters have 2.5 mil thick ( $4.5 \text{ milligram/cm}^2$ ) beryllium windows. This thickness corresponds to the most probable range of about a 55 keV electron (f. Roy and Reed, 1968). Because straggling is a dominant effect near the end of the range, electrons with energies up to perhaps 100 keV may penetrate the Be window with a residual energy in the bandwidth of interest. Pulse shape discrimination (PSD) rejects relativistic particles which may deposit a small amount of energy over a long path length. This rejection has greater than 99 percent efficiency for primary cosmic rays. Further details of the instrument are given by Giacconi et al. (1971) and Jagoda et al. (1972).

Uhuru is in a nearly circular orbit with about 550 km semi-major axis and at a  $3.02^\circ$  inclination. The orbital period is thus about 96 minutes, with two-thirds of this time occurring in the sun-lit portion. For the eclipse portion of the orbit, the aspect solution is solved to an accuracy of about one arcminute, based on star sensor data.

## STABLE BACKGROUND

It was recognized early that Uhuru was sensitive to trapped particles in the lower edge of the South Atlantic anomaly region (Tananbaum, private communication). The geographic region in which the X2 rates were observed to double from

20 sec<sup>-1</sup> to 40 sec<sup>-1</sup> was approximated as a trapezoid extending from -9° to -32° longitude (minus longitude is west of Greenwich) at zero latitude, and from 0° to -82° longitude at -3° latitude. In figure 1, this region falls below and to the right of the short solid line marked "U". For comparison, the dashed line indicates the South Atlantic Anomaly region empirically derived by the OSO-III X-ray experiment. The small displacement of the OSO border probably reflects the fact that the 92 mg/cm<sup>2</sup> Be window on that experiment was sensitive only to higher energy electrons. The dotted line represents the region of B-L space swept out by the Uhuru orbits over one sidereal day.

If the minimum excess of 20 counts/sec is interpreted as the direct counting of ~ 60 keV electrons, the equivalent intensity of these is about 0.1 electron/(cm<sup>2</sup>sec keV ster) at 60 keV. This is a reasonable extrapolation of the maps of trapped radiation (cf. Vette 1966).

The next logical step is to ask what contamination might result from a stable, quasi-trapped distribution of electrons outside of the region defined as the South Atlantic Anomaly. The signature of such electrons is a peak at pitch angles perpendicular to the magnetic field. In figure 2 a pitch angle distribution is plotted for a single day of data. The total counts, exposure time, and average angle to the magnetic field were recorded for 89 samples (nominally 20 seconds each) when the earth filled the 5° x 5° aperture. These were binned in 10° increments to generate figure 2. The loss cone angle was 40-50° for this region of B-L space. There is not a statistically significant perpendicular pitch angle distribution. For these data an upper limit can be set at about 0.5 sec<sup>-1</sup>, or about 3 x 10<sup>-3</sup> electrons/(cm<sup>2</sup>sec keV ster) at 60 keV.

## SPORADIC EVENTS

The superposed X2 data from a total of 11 days coverage between 18 December 1970 and 8 January 1971 were scanned for an event with the signature of being at least twice the collimator full width of  $10^{\circ}$ , in apparent angular extent, and of being greater than 3 sigma above the local background for at least part of the event duration. Events which satisfied the second part of this criterion were assumed to be possible X-ray sources by the Uhuru superposition algorithm, and for these a printout is automatically generated containing the spectrum during each satellite spin through the given azimuth on that given day. I then required further that only one of the individual spins would show the enhanced counting rate. This procedure discovered no events about 5 counts/sec in the superposed data. From the strength of the events described below, I estimate that this limit corresponds to 50 counts/sec excess X2 rate during an event of 1 minute duration.

Two events occurring later than 8 January 1971 had been noticed and pointed out to me by members of the Uhuru analysis group. Figure 3 shows the appearance of one of these in the superposed X2 data for 16 January 1971. The event extends from about  $256^{\circ}$  to  $310^{\circ}$  azimuth. This corresponds to about two minutes in time since the spin rate is about  $0.5^{\circ}/\text{sec}$ . The apparently abrupt onset reflects the fact that the event was in progress when the satellite underwent a day to night transition (only night data is superposed).

Azimuths between  $190^{\circ}$  and  $220^{\circ}$  and  $310^{\circ}$  and  $360^{\circ}$  reflect the isotropy of the diffuse X-ray background (about 16-17 counts/sec) plus the stability

of the non-X-ray background (3-4 counts/sec). The latter arises primarily from secondary effects of the cosmic rays. At azimuth  $222^{\circ}$  the very weak source 3U 1439-39 appears, and at  $240^{\circ}$  the strong, variable source 3U 1516-56 (CIR X-1) appears. The triangles at azimuths  $270^{\circ}$  and  $290^{\circ}$  represent 3 sigma fluctuations within the sporadic event.

The spectrum of the excess at azimuth  $290^{\circ}$  during 13 seconds after U. T. 1418:41 is shown in figure 4. (SMC X-1 may be partially within the field of view at azimuth  $290^{\circ}$ , but contributes less than 5 percent of the X2 rate at the event time.) The counting rates per second per channel are plotted against the mid-point energy of the channel. No corrections are applied to account for the detector response. The crosses represent an average counting rate when the  $5^{\circ} \times 5^{\circ}$  collimator views the sky away from discrete sources. Those rates are subtracted from the total rates to give the net spectrum due to the event, shown as the solid dots.

The very steep spectrum is suggestive of X-rays, arising as bremsstrahlung from a steep spectrum of electrons. One cannot directly tell if the bremsstrahlung occurs in the collimator, or in the earth's atmosphere. At this time the collimator was scanning about  $30^{\circ}$  above the horizon; therefore, the interaction presumable occurs in the collimator. The counters are looking at  $140^{\circ}$  -  $150^{\circ}$  to the magnetic field lines, which is within the loss cone angle of  $50^{\circ}$  for this satellite position ( $75^{\circ}$  east longitude,  $-2.8^{\circ}$  latitude). The event thus arises from precipitating electrons, which are moving up the local magnetic field line.

The spectral signature of an event presumed to arise from direct particle contamination is shown in figure 5. Enhanced counting rates were observed at azimuths between  $300^{\circ}$  and  $360^{\circ}$  in the side 1 superposed data on 24 January 1971.

The superposition program picked out possible sources at azimuths  $320^\circ$ ,  $344^\circ$ , and  $347^\circ$ , each of which showed increased rates only at the universal times 1438:14, 1439:03, and 1439:08, respectively. The crosses show the average of the rates at the azimuths plus the background rates at adjacent azimuths for all times other than during the event. The circles give the net counting rates per channel at each of the three above times. Again, the rate at the three-sigma azimuth plus the adjacent background are combined, since all are part of the same event. It turns out that the rates monotonically decrease with time for these three azimuths; however, this presumably reflects the motion of the satellite through a geographic region rather than time structure intrinsic to the event itself.

The enhanced counting rates are centered at a look direction  $100^\circ$  from the local magnetic field. Thus the particles are quasi-trapped: at this location ( $50^\circ$  to  $55^\circ$  east longitude) they will undergo magnetic reflection above the earth's atmosphere. Occurrence at this longitude is somewhat unexpected, since electrons would be lost as they drift eastward around the earth through the South Atlantic Anomaly region.

The counting rate spectrum shown in figure 5 reflects the spectrum of residual electron energy after passing through the  $4.5 \text{ mg/cm}^2$  Be window. Since this spectrum depends crucially on an accurate calculation of electron straggling near the end of range, I cannot infer the spectral shape of the electrons incident on the window. However, if I roughly assume that an incident electron bandwidth of 50 keV can contribute to the peak X1 counting rate of  $120 \text{ sec}^{-1}$ , the equivalent intensity of  $\sim 60 \text{ keV}$  electrons is  $4 \text{ electrons}/(\text{cm}^2 \text{ sec keV ster})$ .

## SUMMARY

I have presented the qualitative fact that, occasionally, sporadic background events occur even in an equatorial orbit. The Uhuru group has noticed that daytime data (not considered in this work) has both a higher level of non-X-ray background, and apparently more sporadic events (Schreier, private communication). Simultaneous data from both collimators, (not used here) would confirm uniquely the signature of various event types: auroral type X-rays will be seen through one collimator with the other counter bank giving normal rates; particle events will scale as the solid angle, being ten times more intense in side two; and gamma ray bursts will give about the same enhancement in both banks of counters.

## ACKNOWLEDGMENTS

I thank H. Tananbaum and other members of the Uhuru group for discussions. I especially thank D. Koch and W. Forman for assistance in using the reduced Uhuru data and for pointing out the sporadic events discussed above.

## REFERENCES

- Giacconi, R., Kellogg, E., Gorenstein, P., Gursky, H., and Tananbaum, H. 1971, Ap. J. (Letters), 165, L27.
- Hill, R.W., Grader, R., and Seward, F.D. 1970, J. Geophys. Res., 75, 7267.
- Jagoda, N., Austin, G., Mickiewicz, S., and Goddard, R. 1972, IEEE Trans. on Nucl. Sci., NS-19, 579.
- Roy, R.R. and Reed, R.D. 1968, Interactions of Photons and Leptons With Matter, (New York: Academic Press), p. 126 ff.
- Seward, F. 1974 (this conference)
- Schwartz, D.A. 1969, unpublished Ph.D. thesis, University of California at San Diego.
- Schwartz, D.A. 1970, Ap. J. 162, 439.
- Tananbaum, H., Kellogg, E., Gursky, H., Murray, S., Schreier, E., and Giacconi, R. 1971, Ap. J. (Letters), 165, L37.
- Vette, J.I., Lucero, A.B., and Wright, J.A. 1966, NASA SP-3024.

## FIGURE CAPTIONS

- Figure 1: South Atlantic Anomaly Boundaries. The dotted line denotes the region of B-L space swept out by the Uhuru orbits. The short solid line marked "U" shows the region (extending to higher L and lower B) where background rates were observed to double on Uhuru. The dashed line shows the anomaly region empirically defined by the UCSD X-ray experiment on OSO-III (Schwartz, 1969). The long solid line denotes the nominal magnetic equator.
- Figure 2: Pitch angle distribution of count rates when the earth completely filled the  $5^{\circ} \times 5^{\circ}$  aperture. All available data from one day are averaged. An excess at angles perpendicular to the field lines, which would indicate a stable population of trapped particles, is not observed.
- Figure 3: Counting rates from the  $5^{\circ} \times 5^{\circ}$  collimator superposed for one day and plotted against relative azimuth of a great circle on the sky. The enhanced counting rates over a region much wider than the collimator response at azimuths  $255^{\circ}$  to  $310^{\circ}$  indicates a sporadic event. The superposition program attempts to fit a triangle of  $10^{\circ}$  base wherever the counting rate exceeds the local background by three sigma.
- Figure 4: Apparent counting rate spectrum due to the event shown in figure 3. Crosses represent rates from the sky measured at other times. Solid dots represent the net rate from this event. The steep

spectrum is indicative of bremsstrahlung from a steep spectrum of electrons. In this case, the interaction is probably in the collimator walls.

Figure 5: The apparent counting rate spectrum observed on side 1 during an event inferred to be generated by particles at an angle of  $\sim 100^\circ$  to the magnetic field. The crosses represent the counting rate at all other passes through the same azimuths. The circles are the rates during the event, decreasing in time at intervals of 49 sec and 5 sec. The statistical error bars are less than the symbol size for rates greater than  $2 \text{ sec}^{-1}$ .

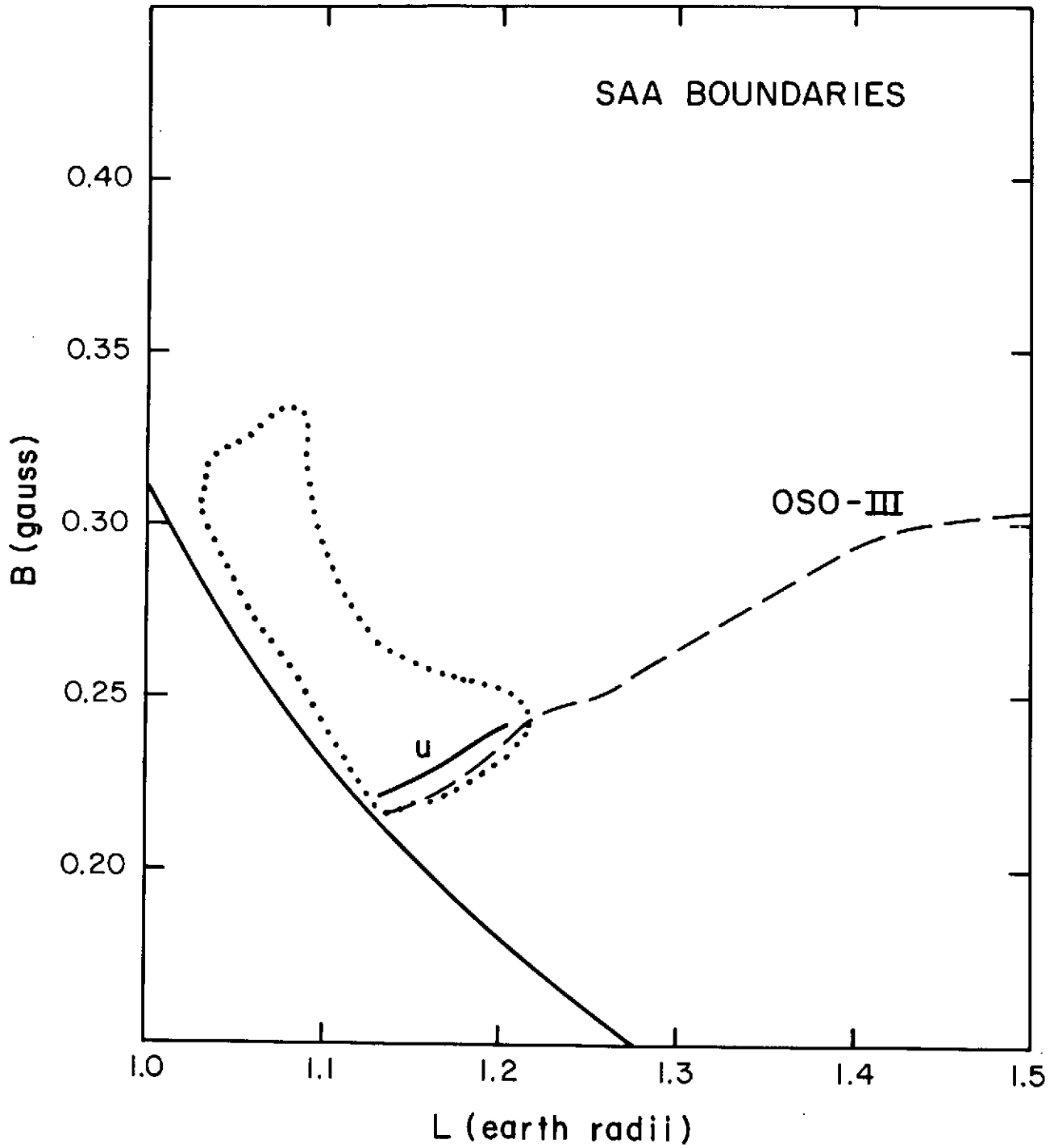


Figure 1

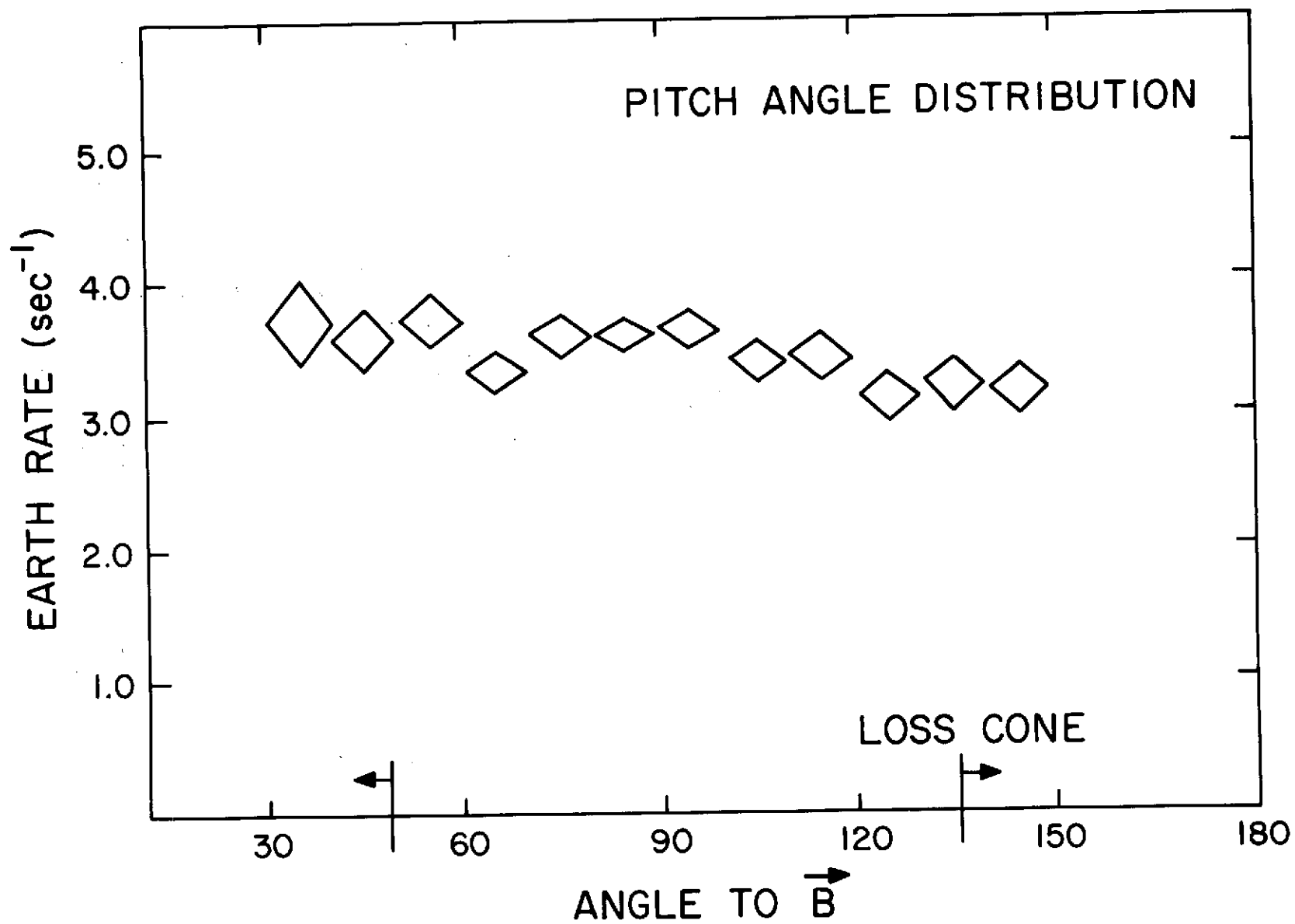


Figure 2

16 JAN 1971

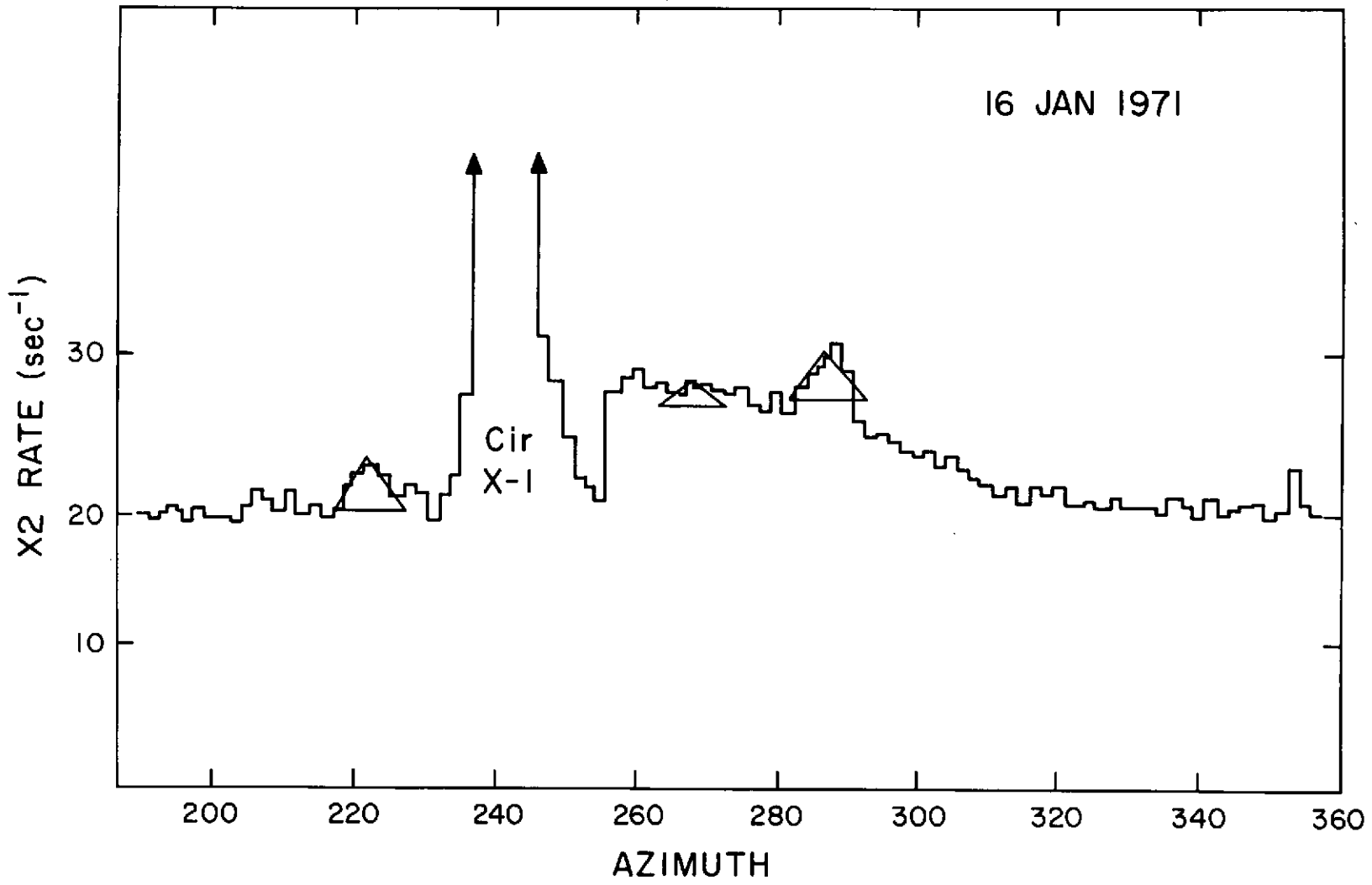


Figure 3

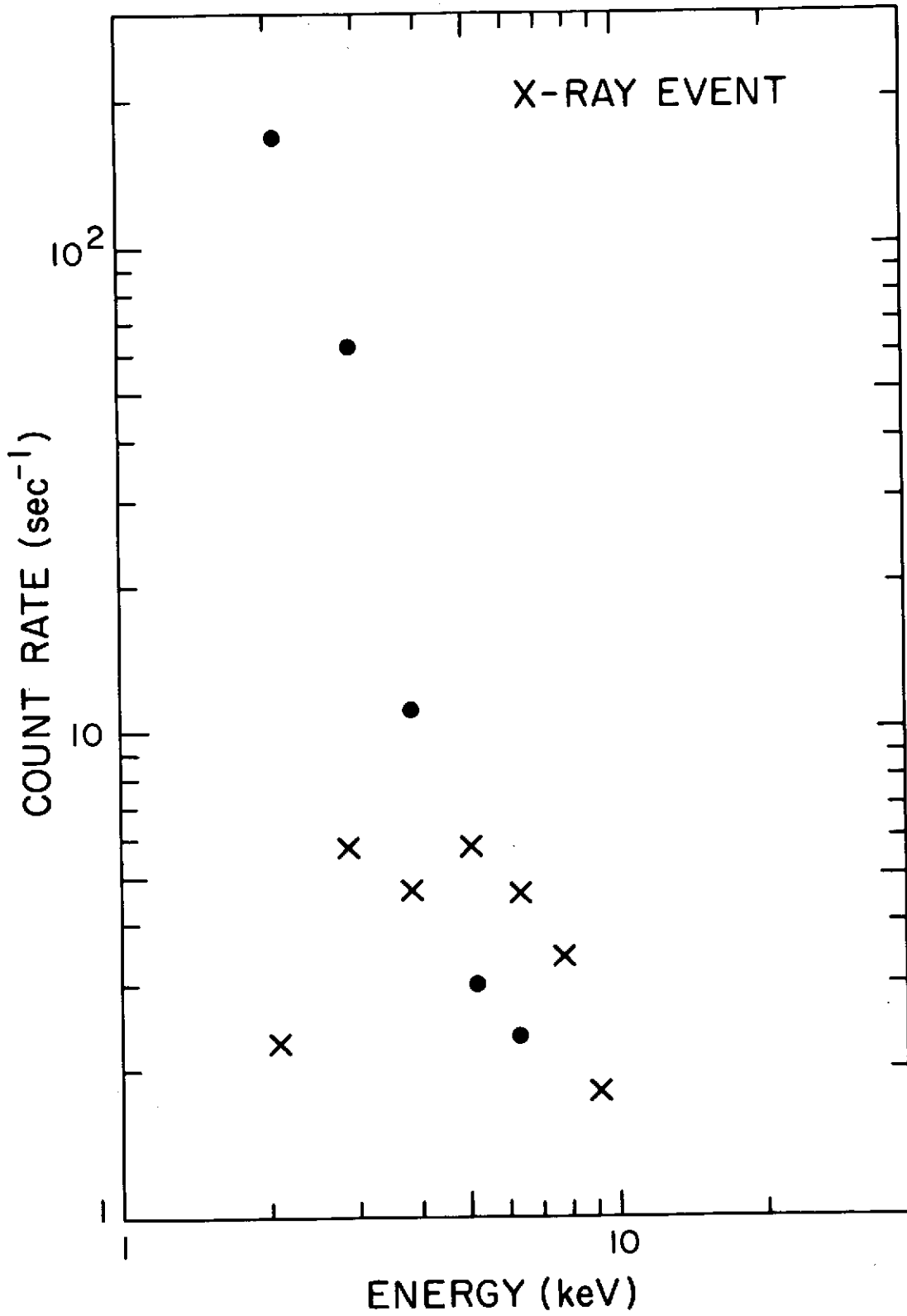


Figure 4

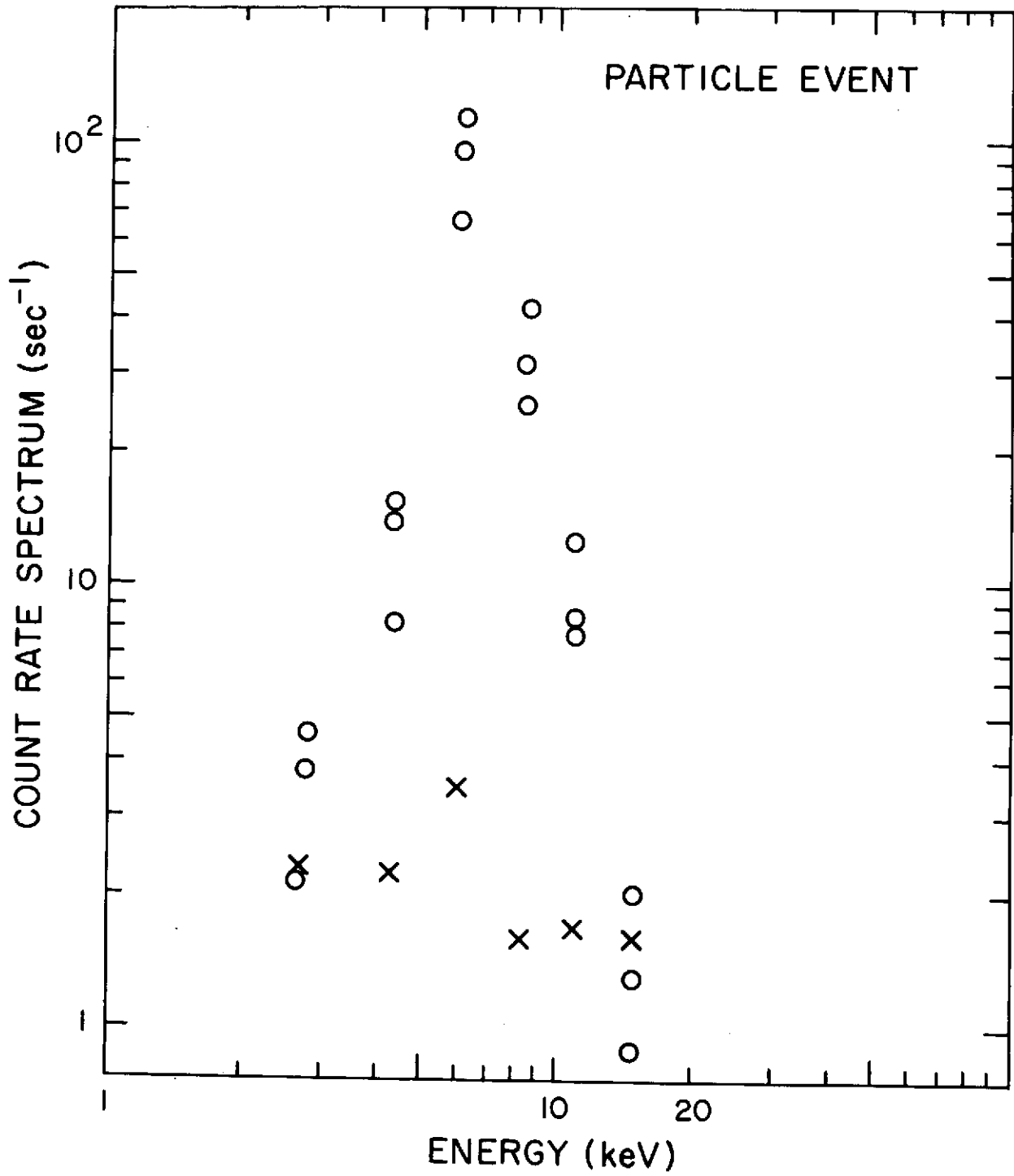


Figure 5

10. The Particle Background Observed by  
the X-Ray Detectors Onboard Copernicus  
....P. J. N. Davison

The Particle Background Observed by the  
X-ray Detectors Onboard Copernicus\*

P.J.N. Davison

Mullard Space Science Laboratory

\*Invited contribution to conference on Particle Contamination of  
Low Energy X-ray Astronomy Experiments, NASA Headquarters.

April, 26 1974.

N74-28206

The Particle Background Observed by the X-Ray Detectors Onboard "Copernicus"

P. J. N. Davison  
Mullard Space Science Laboratory

It should be made clear at the outset that the primary concern of this meeting, i.e. low energy electron contamination, is something about which the Copernicus detectors cannot make a direct statement. This is because our low energy telescopes are grazing incidence reflectors feeding small (1 cm<sup>3</sup>) detectors at their foci. Due to the baffles along the axis of the mirrors there is no direct path from the outside world to the detectors, so low energy electrons will only cause problems if they can scatter off the mirrors in such a way as to follow the photon path to the detectors.

So what I shall have to say will be primarily a description of the procedures we follow in subtracting background counts from the raw data, and how we recognize and treat anomalous behavior.

As is well known, the Copernicus satellite is capable of being pointed for many hours, to an angular precision which is a very small fraction of the detectors' field of view. Thus any variation in count rate is attributable to statistics or to source or background variation. This latter component does vary significantly round the orbit and also from orbit to orbit, depending on the orientation of the orbit relative to Earth. Figure 1 shows a typical plot of background rates and guard rates during several orbits.

Background determination for such a continuously pointed detector can be made by a variety of methods, including:

1. A shutter can be used to obscure the field of view at regular or irregular intervals.
2. The spacecraft (or possibly just the detecting system) can be slewed off-target at regular or irregular intervals.
3. A second, identical, detecting system pointing always off target.
4. Another counter can be used to monitor changes in background rate. The relation between the count in this detector and the background in the main counter must be known.

Method 4 is a variant of method 3.

There are, naturally, various precautions which must be taken with all these methods. 1 and 3 can give erroneous answers if the background varies significantly on a time scale comparable with the on-source/off-source repeat time. In 3 one must have truly identical counters or else the method

degenerates into 4. In addition the secondary system must not include any other X-ray source in its field of view. Method 4 requires that the relationship between the two (or more) counters be accurately known at all background levels encountered.

The two low energy (0.5-1.5/0.7-1.9 and 1.1-3.2/1.5-4.6 ke V) detectors on Copernicus were designed to use a regularly occulting shutter, and some work early in the life of the spacecraft was done using this method. However, an anomaly in the shutter operation was noted and it was decided not to operate the shutter mechanism. A wise decision, since some 10 months after launch the shutter operation was commanded on and the shutter promptly stuck - closed. With shutter operation vetoed (and indeed impossible on the 2.5-7.5 ke V detector which had no shutter anyway) we turned to the use of method 4. The 2.5-7.5 ke V detector comprises a pair of nominally identical proportional counters placed back to back, with a common gas, the active volumes being separated by an earthed grid. The back counter is used as an anticoincidence guard counter. PRD is also used in the front, or stellar counter, to reduce particle background. Estimates of the background count in the stellar counter are derived from the count in the guard counter (which accepts counts over a wider energy range than the stellar counter). The relationship has been derived from the data collected during times when the spacecraft is pointing at a Princeton target, and no known X-ray source is in the field of view of our detectors. This procedure is also used in deriving a background for use with the low energy telescopes. These telescopes have their own guard counters, but since these guards are inorganic scintillators, we still use the collimated proportional counter guard channel as a background monitor so as to avoid any problems due to the different response of inorganic scintillators to the background as compared with proportional counters. In addition, the low energy guard counters are scaled by a factor which is proportional to their count rate, whereas the 1-3 guard is unscaled. The low energy guards are therefore used (in data analysis) just to indicate if the 1-3 guard counter has overflowed its register.

As an indication of the reliability of the relation between guard count and stellar background count we have made some regression analyses, and find the correlation coefficient between the 1-3 background and the 1-3 guard rate to be 0.9. The correlation coefficient between the low energy telescopes and the 1-3 guard rate is 0.4; we attribute this fall in correlation coefficient to the low statistical precision of the low energy counters, for which background rates vary from 3 to 7 counts per frame. The comparable figure for the 1-3 stellar background count is 30 - 100 counts per frame, and for the 1-3 guard is 1000 - 3500 counts per frame. In practice we do not use the regression equation derived in the above analysis for computing backgrounds during observing sessions. Instead, we take all our background data and divide it up into 18 discrete levels corresponding to 18 contiguous bands of guard count rate. We then find the average stellar background count for each of these 18 guard count bins. The standard deviation of this average and also the uncertainty involved in a single frame of data are calculated from the observed background in the data set. The distribution of deviations is only slightly wider than normal - a background count of 36 counts in a single frame would have an uncertainty of 6.2 rather than 6.0.

How well does this procedure work in practice? Quite well, we believe, though we are still refining our procedures. We test the method by finding average counts for the various guard levels, averaged over several months. We then analyse the data from those Princeton targets which we have used in generating background numbers, by finding the background subtracted count averaged over 24 hours. Results are shown in figure 2. The background estimates were derived from data from day 100 to day 230 on that plot. It can be seen that there are in fact significant deviations (positive and negative) from zero, indicating that we hadn't got things quite right. But these deviations do appear to have some temporal structure, so now we generate averages for short periods spaced either side of the target of interest, and this tightens up the distribution quite significantly. In addition one can improve matters just by restricting one's analysis to a narrow range of guard counts. Figure 3 shows the daily background subtracted data for the guard range 1200 - 1300 counts per frame. The most significant positive deviations are caused by known weak X-ray sources in the field of view as indicated in figure 2. Restricting ourselves to a narrow range of guard levels is not necessarily serious, as 40% of our data is associated with guard counts in the range 1200 - 1500 counts per frame. Incidentally, note in figure 2 that the deviations are at the few counts per frame level, whereas the background count averaged over the day is in the region of 50 counts per frame.

In addition to the small systematic effects seen in figure 1, we do see occasional apparently random effects which we refer to as "spikes". In these cases, the count rate suddenly increases significantly above the rate predicted by the guard counter, and then decreases again after a few frames (say 5 minutes). These events are obviously easy to see during background runs. In 72,000 data frames, extending over 230 days, we saw about 250 frames when the background rate deviated from the predicted one by 4 or more. These deviations were all positive ones (excess counts). In addition they were not distributed uniformly in time but occurred in bunches. They also occurred when the satellite was north of 20°N or south of 20°S (possibly the latitude limits are farther from the equator than this, but poor statistics caused me to use coarse latitude and longitude bins when investigating this question). The observed longitude distribution indicated that in fact these spikes are occurring when the satellite approaches the auroral zones most closely. Figure 4 shows the geographical distribution of these spikes. Clearly for critical observations one could automatically exclude data gathered in these regions. In addition since we now have background shutters permanently in front of our low energy telescopes we can monitor the count rate in these telescopes for evidence of spikes. They do not show up in the 1-3 guard of course where the normal count rate is large enough to swamp the effect. The distribution in time and space of our spikes clearly indicates some auroral or solar related phenomenon; a check or correlation against geophysical data is next on our list. Incidentally, we do not believe our spikes to be related to gamma bursts.

Some final points. We find that for a given guard level, the background rate does show a small dependence ( 5-7 % ) on the longitude of the ascending

node of the satellite orbit. Clearly this effect could be worthy of consideration when looking at objects for a short time only, or when looking at temporal variations on a short time scale. This effect is currently under investigation. It should be noted that the systematic effects seen do not impact greatly on work already reported from this satellite due to their relatively small magnitude. We have not differentiated between data taken at different galactic latitudes. Since our 2.5-7.5 ke V counter gets only about 5% of its total count (at the lowest background level) from the diffuse background, this potential systematic error should normally be negligible.

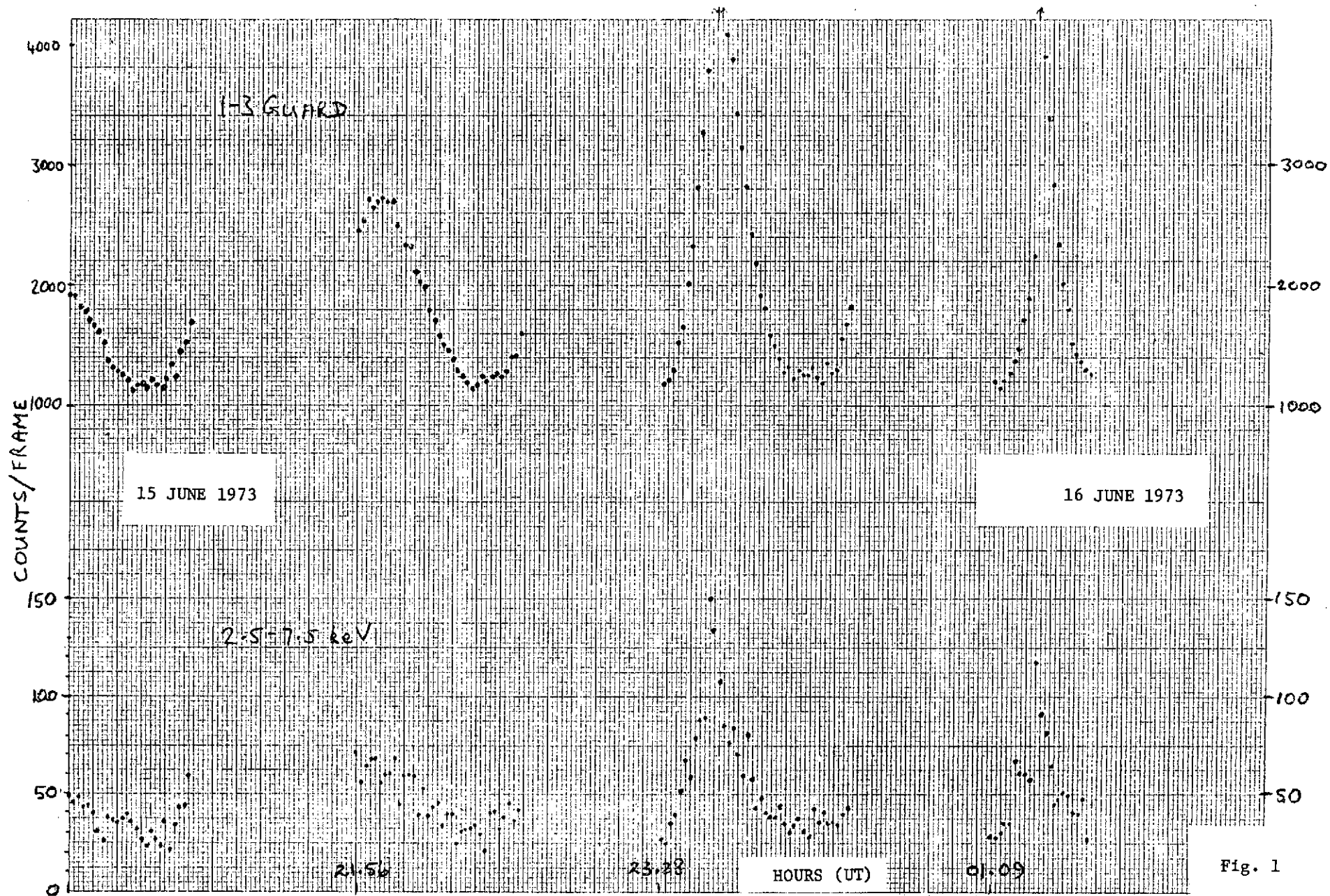


Fig. 1

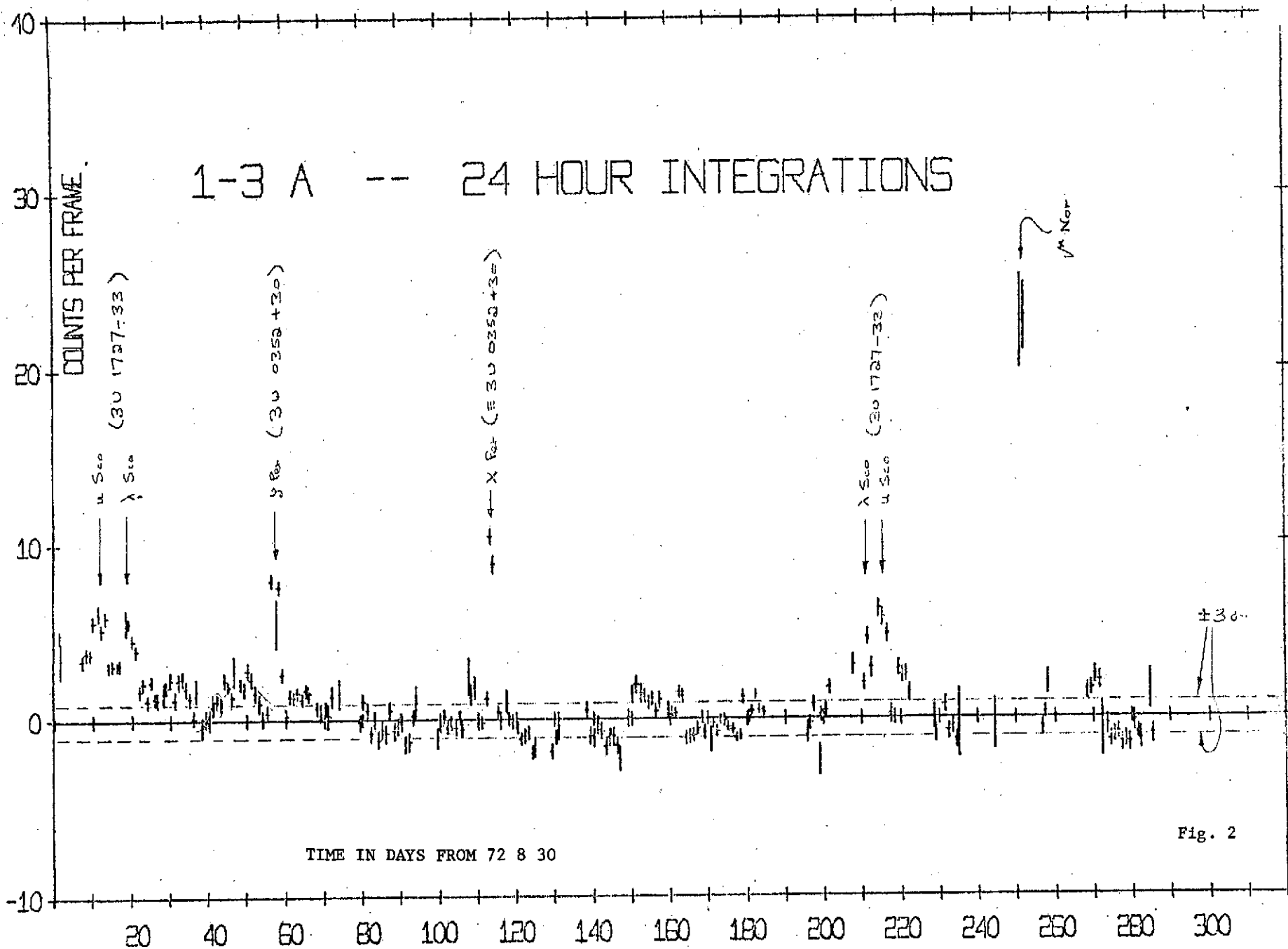


Fig. 2

1-3 A -- 1200-1300 GUARD BIN

COUNTS PER FRAME

30

20

10

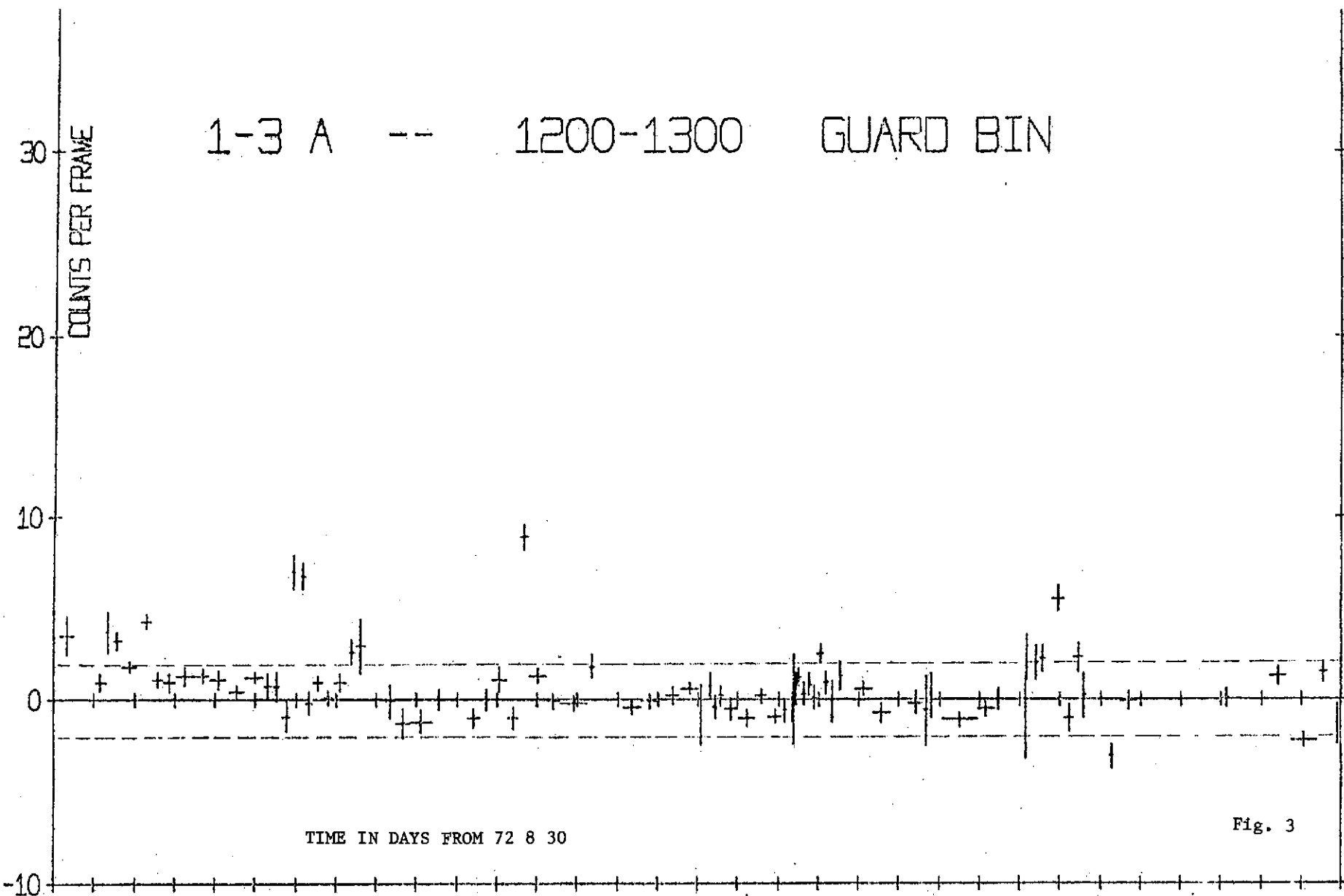
0

-10

20 40 60 80 100 120 140 160 180 200 220 240 260 280 300

TIME IN DAYS FROM 72 8 30

Fig. 3



GEOGRAPHICAL DISTRIBUTION OF 4 SIGMA DEVIATIONS  
30/8/72 → 4/4/73

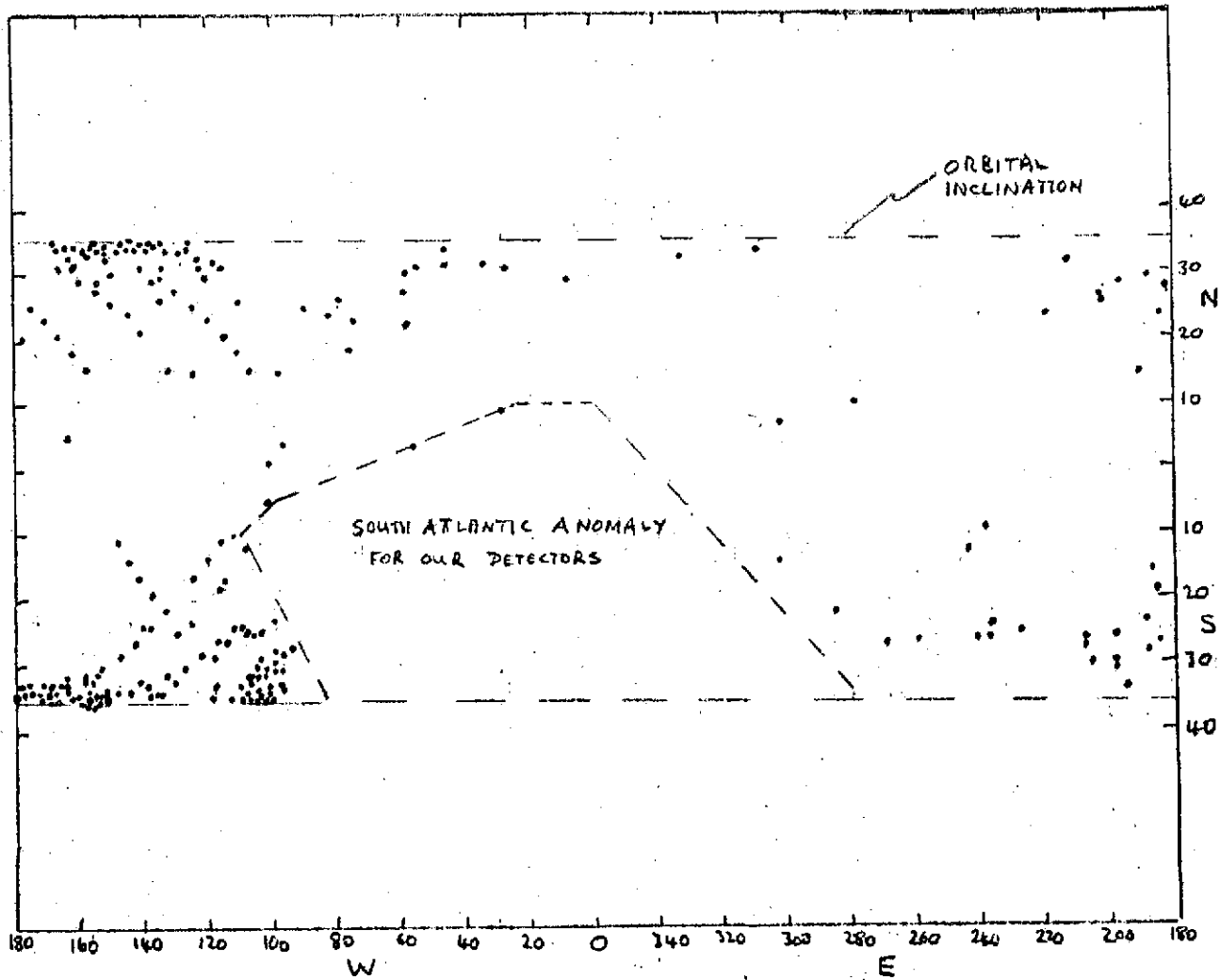


Fig. 4

11. A Survey of Trapped Low Energy  
Electrons Near the Inner Boundary  
of the Inner Radiation Zone from the  
OSO-7....J. E. Neighbors and G. W. Clark

N74-28257

A Survey of Trapped Low Energy Electrons  
Near the Inner Boundary of the Inner Radiation  
Zone from the OSO-7<sup>†</sup>

J.E. Neighbours and G.W. Clark

Department of Physics and Center for Space Research  
Massachusetts Institute of Technology  
Cambridge, Massachusetts

ABSTRACT

Data from the MIT X-ray experiment on the OSO-7 satellite were used to delineate the regions in B-L and geographic spaces where trapped radiation was encountered. The results pertain specifically to electrons with energies in a range of 10 keV centered on 55 keV which were encountered in an orbit between altitudes of 330 and 570 km and latitudes of  $\pm 33.3^\circ$ . A typical pitch angle distribution is fitted by a Gaussian with a FWHM of 28 degrees.

<sup>†</sup> Supported in part by Contract NAS 5-11082 from the National Aeronautics and Space Administration.

## INTRODUCTION

We report a survey of geomagnetically trapped electrons with energies in the range from 50 to 60 keV observed with the MIT X-ray detectors on the OSO-7 satellite. The region explored lies between altitudes of 330 and 570 km and latitudes  $\pm 33.3^\circ$ , corresponding to B-L rings with L values from 0.95 to 2.2 Re. Data are reported separately for magnetically quiet ( $A_p < 10$ ) and disturbed ( $10 < A_p < 45$ ) times. The results provide information on the low energy electron environment in a region of B-L space for which little data has been previously published. Strassinopoulos (1971) has summarized the data available as of 1964. References to more recent literature are given by Rosen and Sanders (1971) and by Pfitzer and Winkler (1968).

## INSTRUMENTATION

The measurements were made with a proportional gas counter in the MIT X-ray detector located in the wheel section of the Seventh Orbiting Solar Observatory. The satellite was launched on 1971 September 29 into a nearly circular orbit with an inclination of  $33.3^\circ$ . The instrument and its performance in X-ray observations have been described elsewhere (Clark et al. 1973). The data used in this study were obtained from the counter designated NE which is the first in a bank of four. The NE counter is sensitive to electrons with energies in a 10 keV

range centered at approximately 55 keV, and to protons with energies in a 10 keV range centered at approximately 1.2 MeV. The lower energy limits are set by the energy losses suffered in traversing the front window material and by the threshold energy of the NE counter. The upper limits are set by the upper level discriminator of the NE counter and the anticoincidence veto by the AR counter in back. The angular response of the detector is defined by a tubular collimator with an acceptance angle of  $3^\circ$  FWHM and a direction inclined  $15^\circ$  with respect to the wheel plane. A small Geiger counter shuts off the high-voltage supply to the entire counter system whenever it encounters a high flux of particles. No distinction can be made in our data between counts produced by electrons and protons. However, the contribution of protons to the observed rates is certainly negligible because their total intensity is much lower than that of electrons (Vette 1966). Moreover, the fractional width of their accepted energy range is much smaller.

As the wheel turns, the field of view sweeps out a circular band at an elevation of 15 degrees with respect to the plane of the wheel. The wheel rotation period is divided electronically into 256 equal time intervals corresponding to 256 fixed intervals of azimuth. The start of the first interval is synchronized with a pulse generated by a sun sensor by day and an inertial sensor by night. The pulses are accumulated in 256 memory registers ("bins") corresponding to the 256 equal fixed intervals of azimuth. The accumulation time between each readout is 190.1 seconds, during which the satellite moves about 1800 km. Thus

each accumulated count represents an average rate over a range of positions in space and directions in geomagnetic coordinates.

### ANALYSIS

Microfilm displays of data recorded between 7 October 1971 and 10 January 1972 were comprehensively scanned for encounters with trapped radiation. These displays were plots of the number of counts accumulated in each azimuth bin during 190.1 seconds versus the bin number. The trapped radiation generally appears as two symmetric peaks centered at the azimuths of the two intersections of the small circle scanned by the detector and the great circle at 90 degrees from the direction of the magnetic field that controls the motion of the particles. The two peaks are separated in azimuth by a number of bins which is a function of the relative orientations of the magnetic field and the spin axis of the satellite. An example of one such encounter is shown in Figure 1.

As we scanned the data, we noted the orbital positions where one or the other of the following criteria was met:

1. the peaks due to trapped radiation were just significantly (10 counts/bin) above the background.
2. the high voltage was turned off by the monitor counter (cutoff at approximately 250 counts/bin).

The first criterion is met when the peak directional intensity of electron in the accepted energy range ( $\sim 50$  to  $60$  keV) and perpendicular to the field exceeds approximately  $62$  particles/ $\text{cm}^2\text{-sec-str}$ ; the second criterion is met when the peak intensity exceeds approximately  $1480$  particles/ $\text{cm}^2\text{-sec-str}$ .

### Pitch Angle Distribution

In general the angle between the directions of the spin axis and the magnetic field changes by a substantial amount during one 3-minute accumulation period. Occasionally, however, the change is small compared to the inherent width of the pitch angle distribution in which case the shape of a peak in the azimuth distribution caused by trapped radiation reflects rather directly the pitch angle distribution of the particles. A typical distribution for such a period is shown in Figure 2. The pitch angle of 90 degrees (perpendicular to the field) was assigned to the bin with the highest number of counts; the pitch angles of other bins were calculated from the separation in bin numbers from this peak bin and data on the spin axis and magnetic field direction. The azimuth distribution can be fitted by a Gaussian function with a FWHM of 28 degrees. We have used this fact to translate the two detection criteria given above into corresponding values for the omni-directional particle intensities. These are listed in Table 1 together with the peak directional intensities.

### B-L Plots

Encounters with trapped radiation were divided into two classes according to the level of magnetic activity. Days with planetary amplitudes  $A_p \leq 10$  (in units of two gamma) are classed as magnetically quiet; days with  $10 < A_p < 45$  are classed as magnetically disturbed. During quiet periods, the geographic distribution of encounters was constant and successive

observations at a particular position yielded nearly identical values of intensity. We found in general that after a magnetic disturbance it takes about three days for the increased intensities to settle down to their quiescent values. We therefore excluded from our quiet time data all data obtained within three days after any such disturbances. The disturbed times are actually periods of only moderate magnetic activity (large magnetic storms are  $A_p > 80$ ). During the three months of our survey the ratio of quiet time to disturbed time was about 2:3.

Figure 3 shows the positions of encounters with trapped particles in the B-L coordinate system of McIlwain (1961). In this system each point in B-L space corresponds to a ring around the earth in geographic space. The data show high intensities at low values of B (magnetic field strength) corresponding to the expected increase in particle flux with altitude. During disturbed times, high intensities are encountered at larger values of B corresponding to a penetration of trapped radiation to lower altitudes.

#### Geographic Distribution

Figures 4a to 4f show the distributions of encounters with trapped particles in geographic coordinates within three altitude ranges. In the quiet time plots (Figures 4a to 4c), the contours were drawn to include all positions where trapped radiation was consistently observed (over several days); the

uncertainty in these contours is about 5 degrees of longitude and latitude. The exact extent of the contours during disturbed conditions (Figures 4d to 4f) depends upon the specific level of magnetic activity; the contours roughly indicate the area of the majority of the encounters. Since the intensity increases monotonically with altitude in our range of observation (as substantiated by the B-L plots), one can assume that all points within a contour have intensities equal to or greater than the contour intensity. The plots confirm that in general the particle intensity increases with increasing altitude and with increasing magnetic activity.

We compared these results with the predictions for electrons with energies  $\geq 500$  keV by Stassinopoulos (1971) who used the Vette electron model AE2 (Vette et al. 1966) extrapolated to 1974. His estimates of the regions in B-L and geographic spaces populated by trapped electrons with energies  $\geq 500$  keV are consistent with our measurements for  $\sim 55$  keV electrons in quiet times.

TABLE 1

Peak and omni-directional flux limits for electrons with  
energies in the range from 50 to 60 keV

	$J_{\text{peak}}$	$J_{\text{omni}}$
	(electrons/cm <sup>2</sup> -sec-ster-keV)	(electrons/cm <sup>2</sup> -sec-keV)
lower limit (10 counts)	6.2 ± 3.4	18
cutoff (240 counts)	148 ± 10	410

## References

- Bostrom, C.O., D.S. Beall and J.C. Armstrong, "Time history of the inner radiation zone", Models of the Trapped Radiation Environment, Vol. VII: Long-Term Variations, NASA SP-3024, 1971.
- Clark, G.W., Bradt, H.V., Lewin, W.H.G., Markert, T., Schnopper, H.W., and Sprott, G.F., "Observation of Taurus X-1 by the 1-60 keV X-Ray Detector on the OSO-7", Ap. J., 179, 263, 1973.
- McIlwain, C.E., "Coordinates for mapping the distribution of magnetically trapped particles", J. Geophy. Res., 66, p. 3681, 1961.
- Pfitzer, K.A., and J.R. Winkler, "Experimental observation of a large addition to the electron inner radiation belt after a solar flare event", J. Geophy. Res., 73, P. 5792, 1968.
- Rosen, A., and N.L. Sanders, "Loss and replenishment of electrons in the inner zone", 1965-1967, J. Geophy. Res., 76, p. 110, 1971.
- Stassinopoulos, E.G., "Expected electron and proton environment for the cosmic X-ray experiment aboard the OSO-I and OSO-H", Preprint X-641-71-293 of Goddard Space Flight Center, July 1971.
- Vette, I., Lucero, B., and Wright, A., "Models of the trapped radiation environment. Vol. II: Inner and outer zone electrons", NASA SP-3024, 1966.

### Figure Captions

- Figure 1. Computer plot of counts versus azimuth bin number showing an encounter with trapped radiation which produced a characteristic double peak. The slight increase just to the left of the second peak is caused by solar X-rays scattered into the collimator.
- Figure 2. Pitch angle distribution of the trapped electrons with energies in the range from 50 to 60 keV. Directional intensity is plotted versus pitch angle, and the horizontal dashed line indicates the background level. The horizontal error indicator shows the spread in angle of each data point.
- Figure 3. Distribution in B-L coordinates of encounters with trapped radiation for quiet and disturbed times. The solid line is the locus of points on the magnetic equator. Each dot is the position of an encounter with trapped particles at an intensity between the lower limit of detection and cutoff; each triangle is a position where the intensity exceeded the cutoff intensity. (a) quiet time,  $A_p < 10$ ; (b) disturbed time,  $10 \leq A_p < 45$ .
- Figure 4. Geographic distributions of encounters with trapped particles for quiet and disturbed times. a, b and c are for quiet times; d, e and f are for disturbed times. The dot and triangles have the same meaning as in Figure 2. The light dashed line defines the boundary for electron intensities between the lower limit and cutoff; the heavy dashed line delineates the area of

Figure 4. (continued)

electron intensities greater than the cutoff intensity. The solid lines connecting the triangles are the satellite's paths during the times when the high voltage was turned off by the radiation monitor counter. The occurrence of triangles in the midst of the high intensity regions means that during the cutoff the satellite moved from a lower to a higher altitude range.

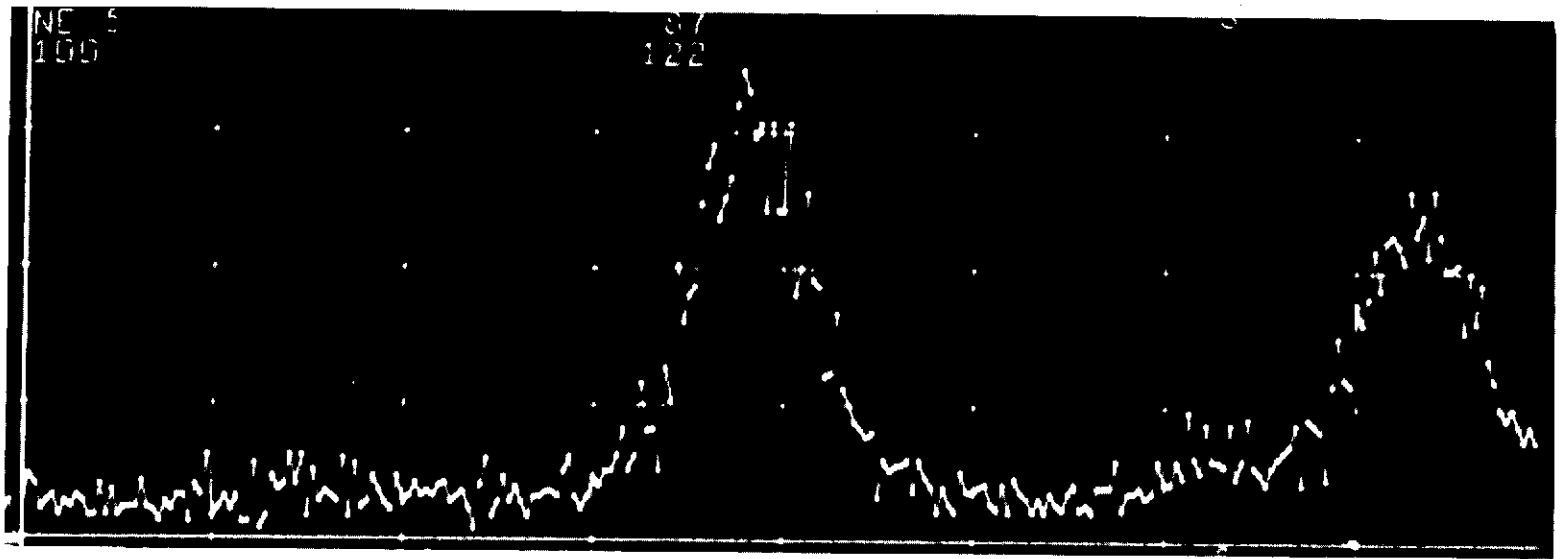


Fig. 1

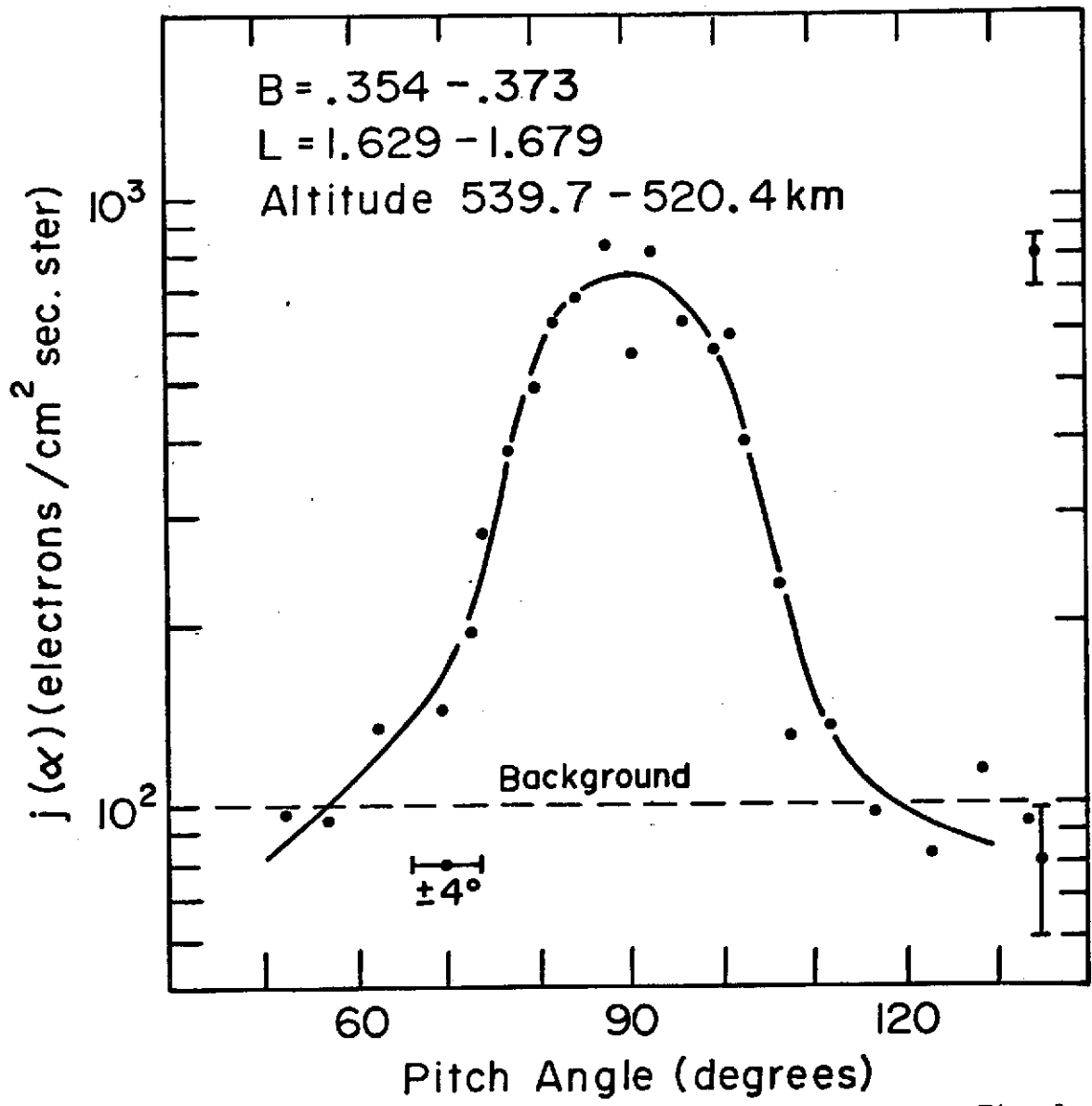


Fig. 2

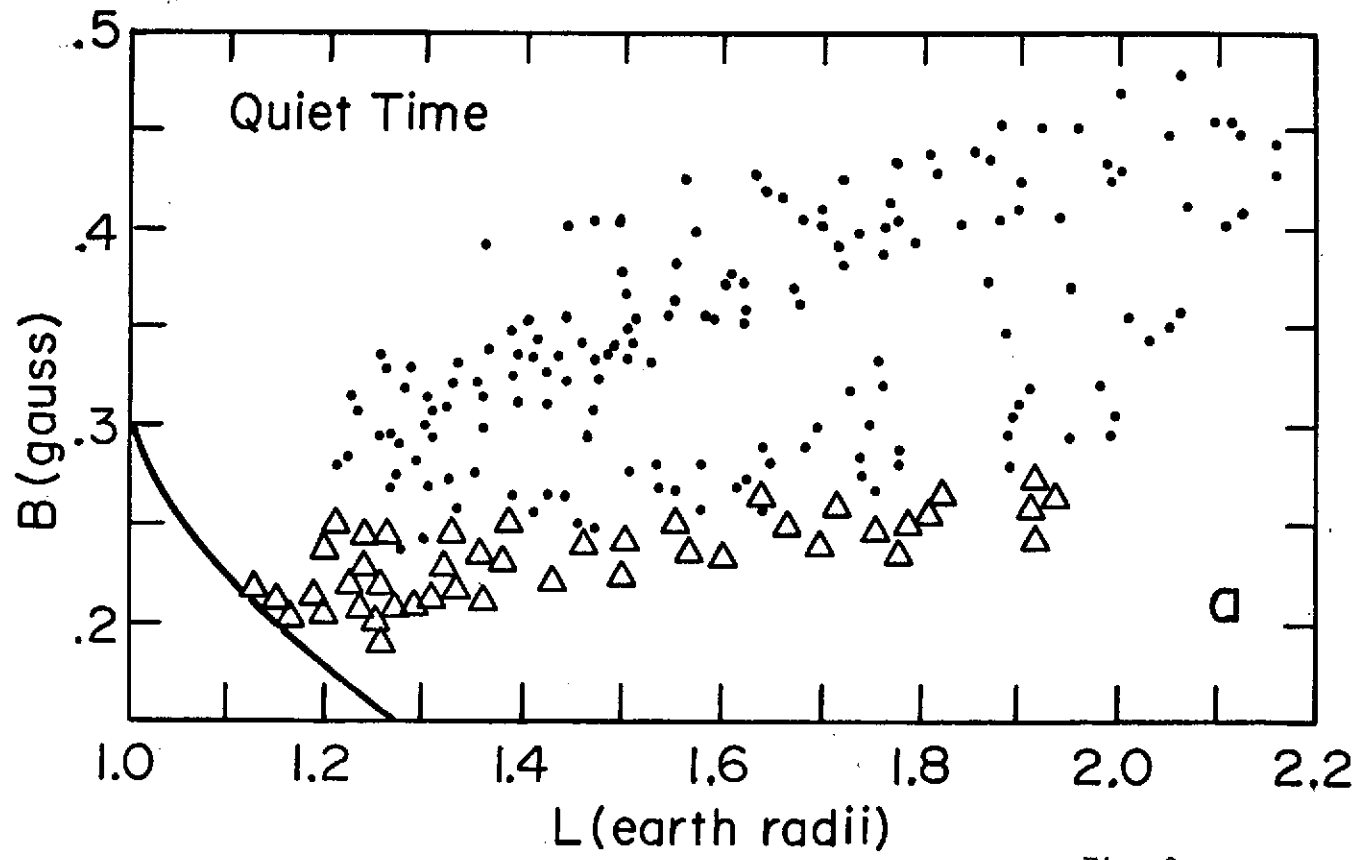


Fig. 3a

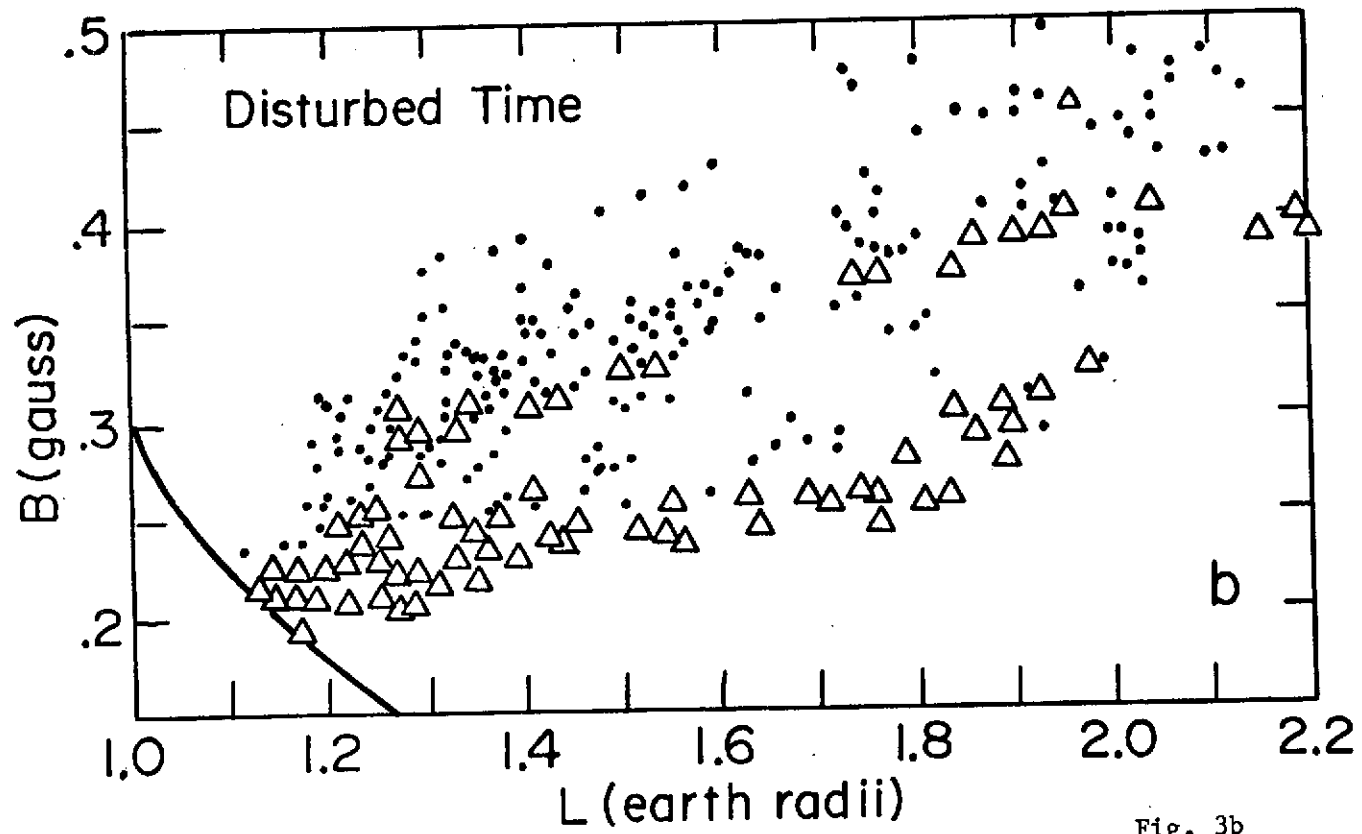


Fig. 3b

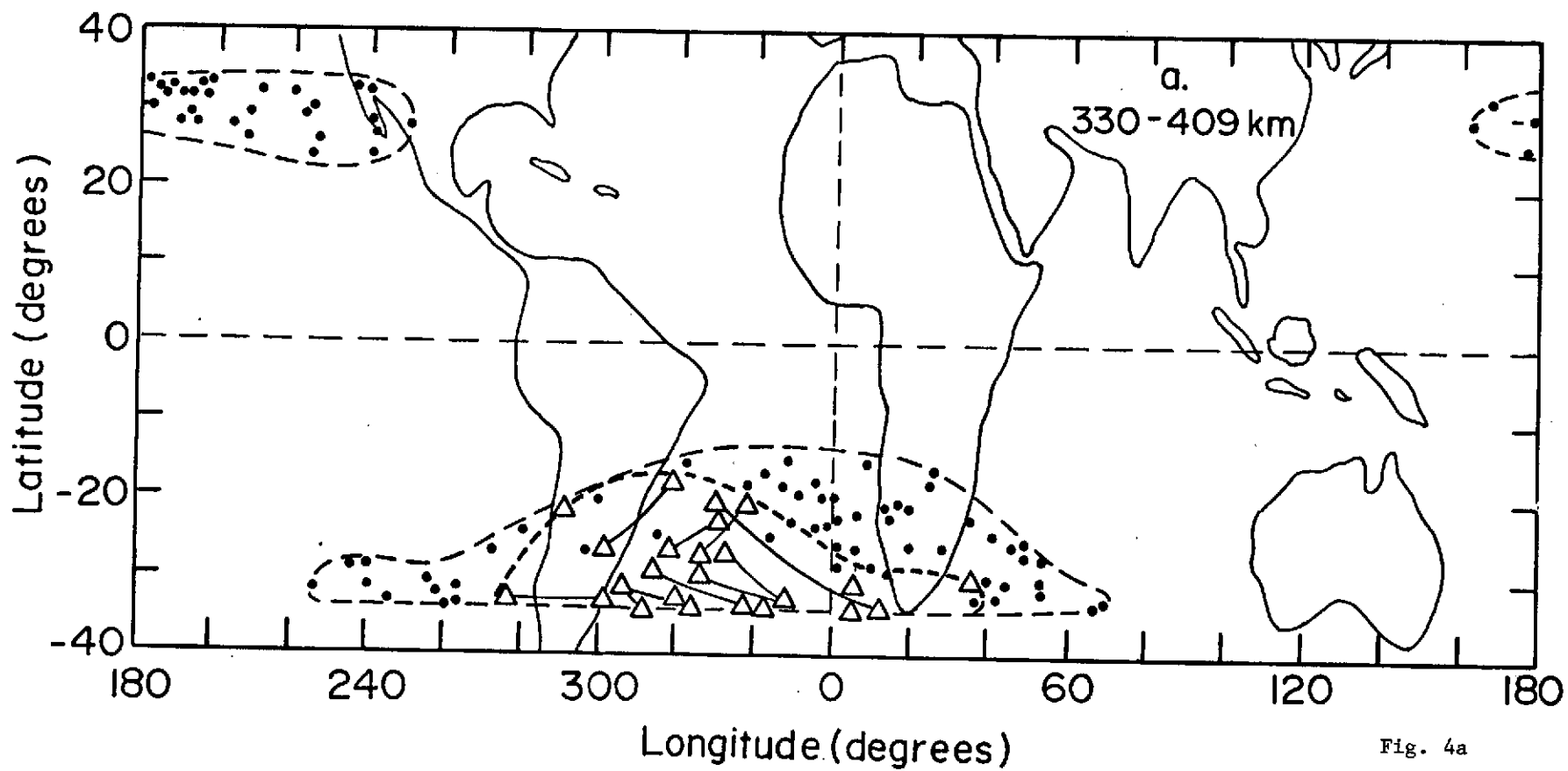


Fig. 4a

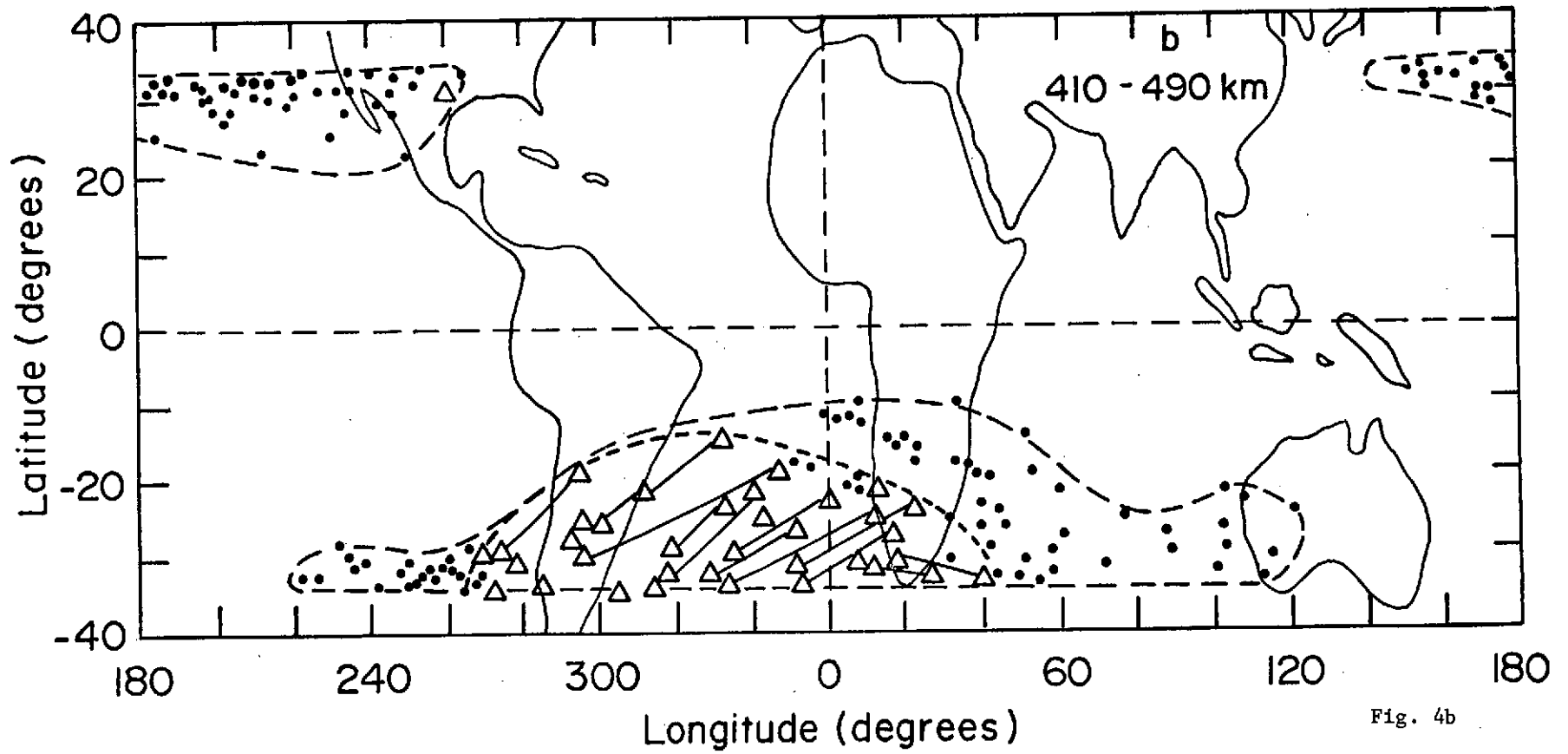


Fig. 4b

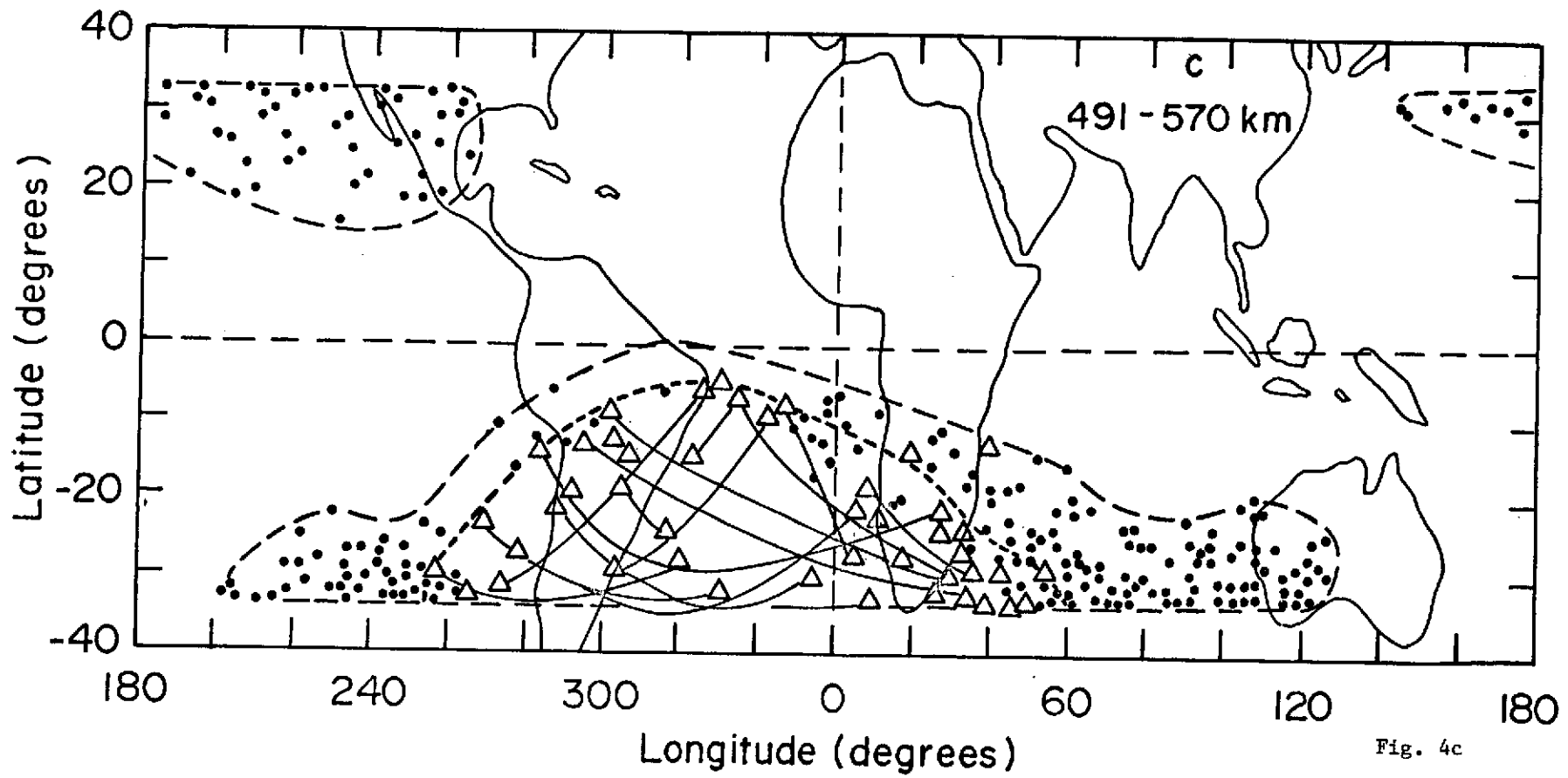


Fig. 4c

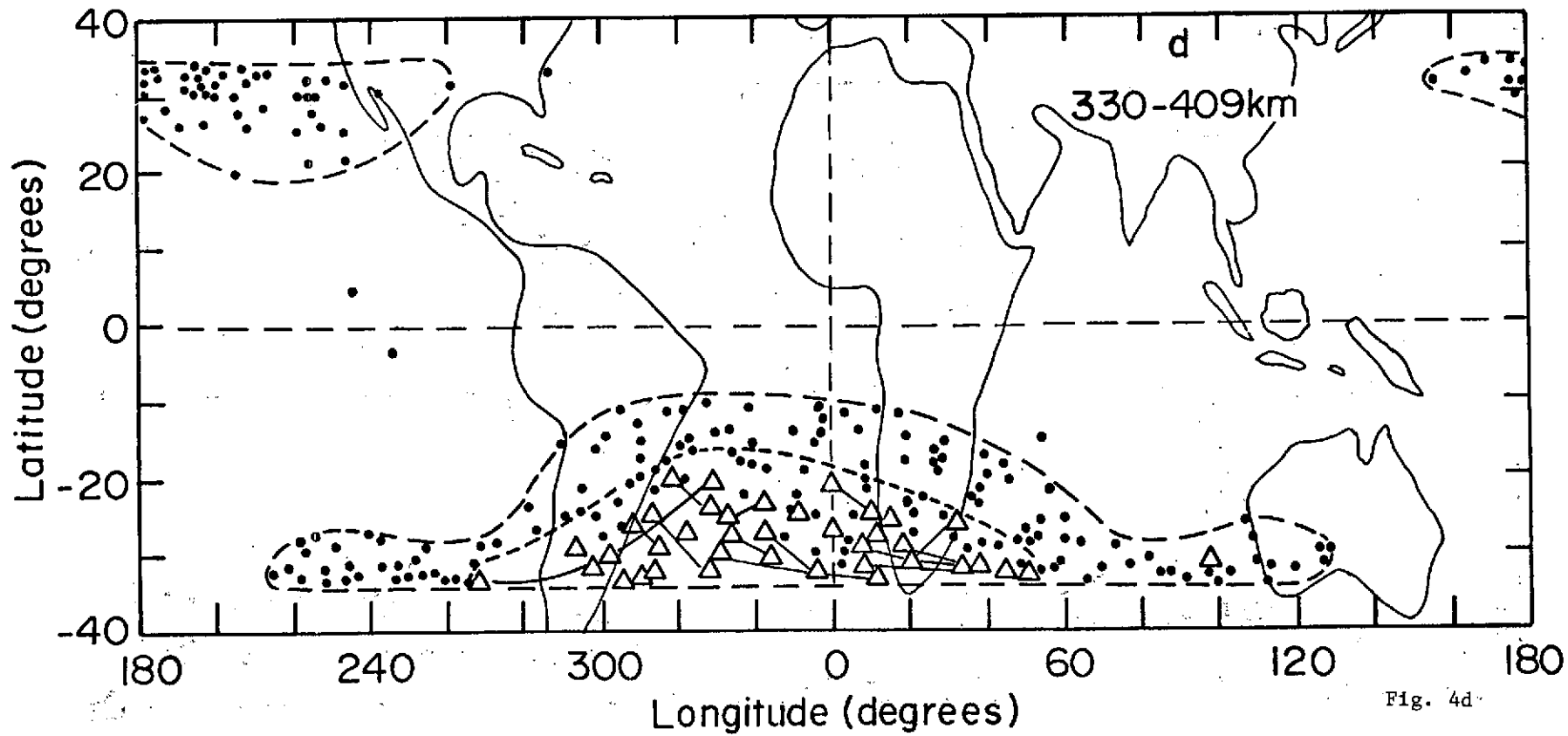


Fig. 4d

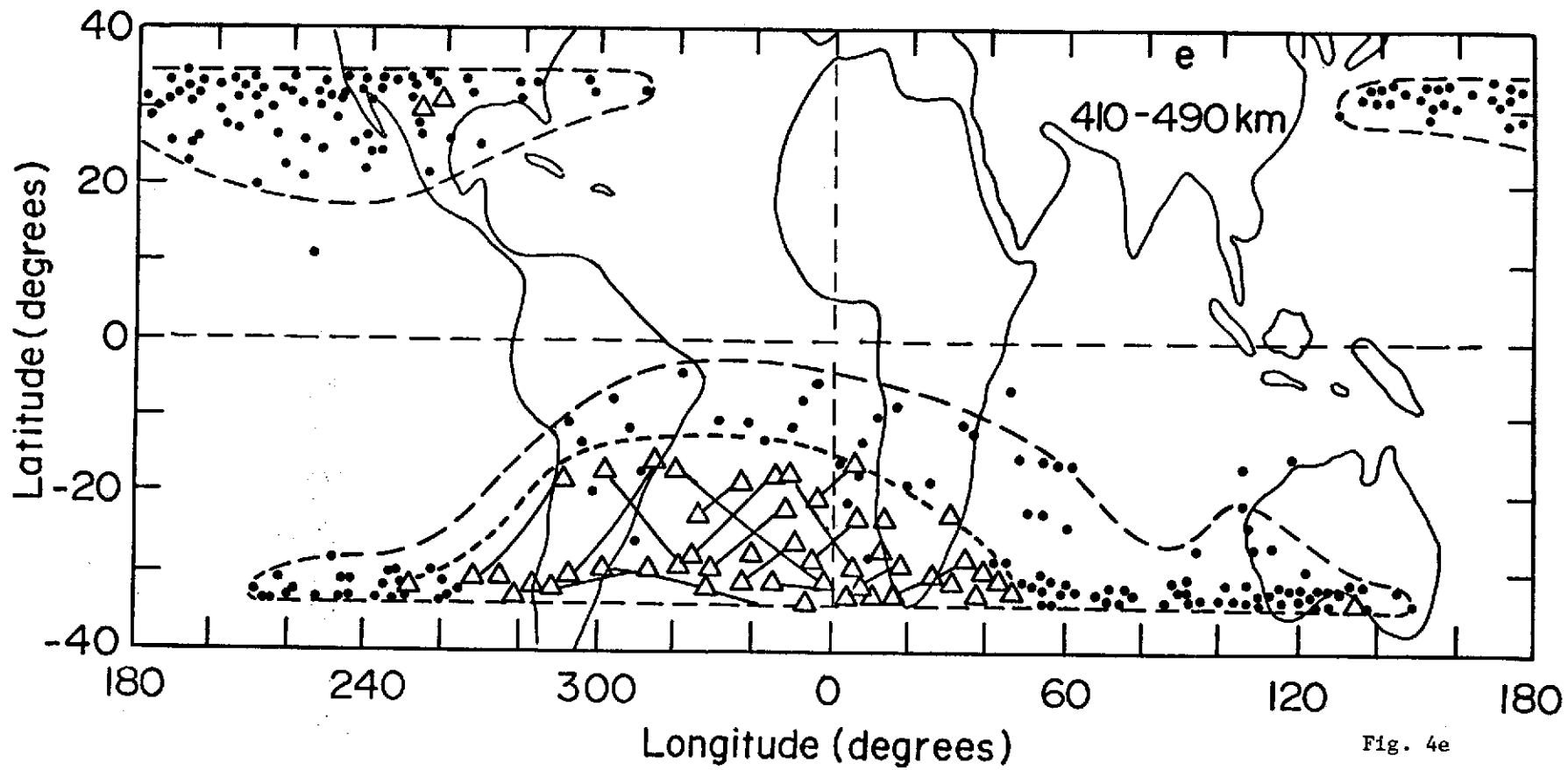


Fig. 4e

